OAK RIDGE
NATIONAL LABORATORY

MANAGED BY UT-BATTELLE
FOR THE DEPARTMENT OF ENERGY

NFE-10-02696

Research Accelerator

CRADA Final Report
For
CRADA Number NFE-10-02696

Development of Long Length, Flexible, Vacuum-Jacketed Cryostats

Jonathan Demko
Oak Ridge National Laboratory

Patricia Huber; Daniel George; Shawn Rhodes; John Ryan and Juan Valencia
Concurrent Technologies Corporation

Prepared by
Oak Ridge National Laboratory
Oak Ridge, TN 37831
managed by
UT-BATTELLE, LLC
for the
U.S. Department of Energy
under contract DE-AC05-00OR22725

PROTECTED CRADA INFORMATION

This report contains protected CRADA information which was produced on December 2011, under CRADA No. NFE-10-02696 and is not to be further disclosed for a period of five years from the date it was produced except as expressly provided for in the CRADA.

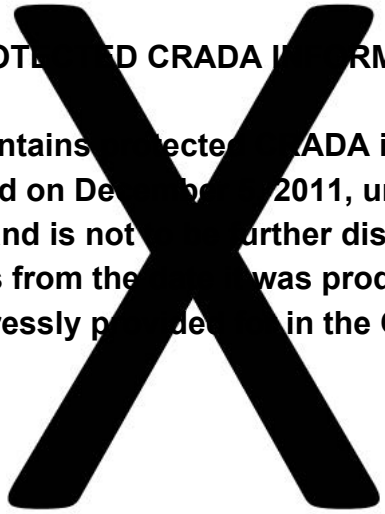

UT-BATTELLE

ORNL-27 (4-00)

TR No. 11-5725

Development of Long Length, Flexible, Vacuum-Jacketed Cryostats
S2304

Final Report

Prepared by
Ms. Patricia Huber, Concurrent Technologies Corporation, 814-269-2509, huberp@ctc.com
Mr. Daniel George, Concurrent Technologies Corporation, 814-269-6426, georged@ctc.com
Mr. Shawn Rhodes, Concurrent Technologies Corporation, 814-269-2882, rhodess@ctc.com
Mr. John Ryan, Concurrent Technologies Corporation, 814-269-2525, ryan@ctc.com
Dr. Juan Valencia, Concurrent Technologies Corporation, 814-269-2552, valencia@ctc.com

December 5, 2011
Resubmitted 22 February 2012

Project Team

Mr. Brian Fowler, Concurrent Technologies Corporation, 814-248-7628, fowlerb@ctc.com
Mr. Brian Fitzpatrick, Naval Surface Warfare Center, 215-897-8473, brian.fitzpatrick@navy.mil
Mr. Jacob Kephart, Naval Surface Warfare Center, 215-897-8474, jacob.kephart@navy.mil
Mr. David Knoll, Southwire Company, 770-832-5860, dave_knoll@southwire.com
Mr. Jonathan A. Demko, Oak Ridge National Laboratory, 865-574-1469, demkoja@ornl.gov
Mr. James E. Fesmire, NASA Cryogenics Test Laboratory, 321-867-7557,
james.e.fesmire@nasa.gov
Mr. Barry Meneghelli, ASRC Aerospace Corporation, 321-867-4011,
barry.j.meneghelli@nasa.gov
Mr. George F. Stimak, Office of Naval Research, Code 331, 703-588-0616,
george.stimak@navy.mil

Navy Metalworking Center
Operated by
Concurrent Technologies Corporation
100 CTC Drive, Johnstown, PA 15904-1935

ACKNOWLEDGMENTS

This work was conducted by the Navy Metalworking Center, operated by Concurrent Technologies Corporation under Contract No. N00014-06-D-0048 to the Office of Naval Research as part of the U.S. Navy Manufacturing Technology Program.

NMC is pleased to acknowledge the technical input provided by the integrated project team, and other contributing organizations and key personnel including the following:

- Office of Naval Research (ONR): Gregory Woods, John Carney
- LCS Program Office, PMS 501: Anthony Smith, Thomas Owen, Lloyd English and Kathleen Ryan
- Department of Homeland Security: Sarah Mahmood, Rosa Reyes and Angela Blair
- Department of Energy: Debbie Haught
- NASA Kennedy Space Center: Wesley Johnson and Jonathan (Drew) Smith
- nkt cables: Dag Willen
- Southwire Company: David Lindsay (formerly of), Donald Murphy and Axel Schlumberger

PDH/jmm

EXECUTIVE SUMMARY

The Navy intends to employ High Temperature Superconductors (HTS) for degaussing (DG) cables on future Navy platforms. The Littoral Combat Ship (LCS) is the first Navy platform targeted for this technology. The objective of this project was to reduce cost and address cryostat configuration and manufacturing issues associated with fabricating long-length, flexible, vacuum-jacketed cryostats that meet Navy shipboard performance requirements. Ultimately, a U.S. manufacturing capability was to be developed by adapting processing techniques at an existing facility for manufacturing electrical conduit.

The project was completed without meeting all the technical objectives for the project; a U.S. manufacturing capability was not developed. Southwire Company, the industry partner that was targeted as a U.S. supplier of these cryostats, returned a No-go decision to commit the capital needed to upgrade their manufacturing facility. However, the project did realize the following technical accomplishments:

1. A baseline cryostat insulation system was developed and validated via thermal performance testing.
2. The use of double aluminized Mylar® and polyester net for the reflector and spacer materials of the cryostat insulation system were shown to perform better than double aluminized Mylar® and polyester (non-woven) fabric.
3. Current technology available from an existing vendor has been identified for forming, welding and corrugating stainless steel sheet of the desired thickness ranges for the manufacture of HTSDG cryostats. Analyses have shown the technology will be able to produce corrugated tubing that meets application requirements.
4. Lessons learned during burst testing of commercially available corrugated tubing will improve upon future test specimen design and burst testing of actual HTSDG cryostats to demonstrate required performance metrics.

A follow-on project with another industry partner could easily leverage this work to its logical conclusion of a U.S. manufacturing capability for long-length cryostats. This project was

developed as an upgrade for HTSDG cryostats focused on cost reduction and does not impact the availability of the HTSDG system to future LCS hulls.

TABLE OF CONTENTS

LIST OF FIGURES

Page

LIST OF TABLES

1.0 BACKGROUND / PROBLEM STATEMENT

High Temperature Superconductors (HTS) are conductors that operate with zero electrical resistance, resulting in low transmission loss and high current density. In order to operate in a superconducting state, these conductors must be maintained at a cryogenic temperature. This is accomplished through the use of extremely effective thermal insulation used in conjunction with a high vacuum in a double-walled vessel commonly called a cryostat. The Navy intends to employ HTS technology for degaussing (DG) cables on future Navy platforms. A mock-up of a typical HTSDG cable is shown in Figure 1-1.

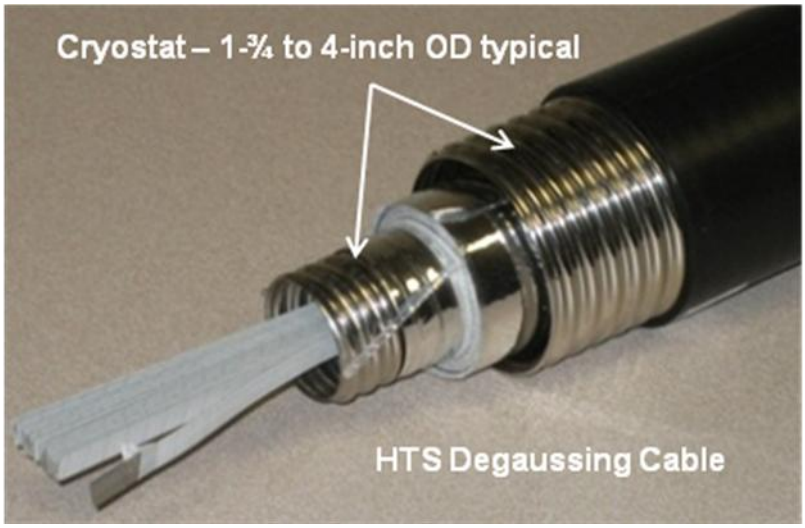

Figure 1-1. Mock-up of HTSDG cable (*Courtesy ONR Program Code 33*).

The benefits of transitioning to HTS technology for shipboard degaussing systems are significant. The increased efficiency of these superconductors results in increased power density; fewer cables are needed for the application. Fewer cables translate to lower weight, allowing increased mission payload, as well as reducing overall labor costs for system installation. Figure 2 visually compares the transition from copper conductors to HTS degaussing system cables.

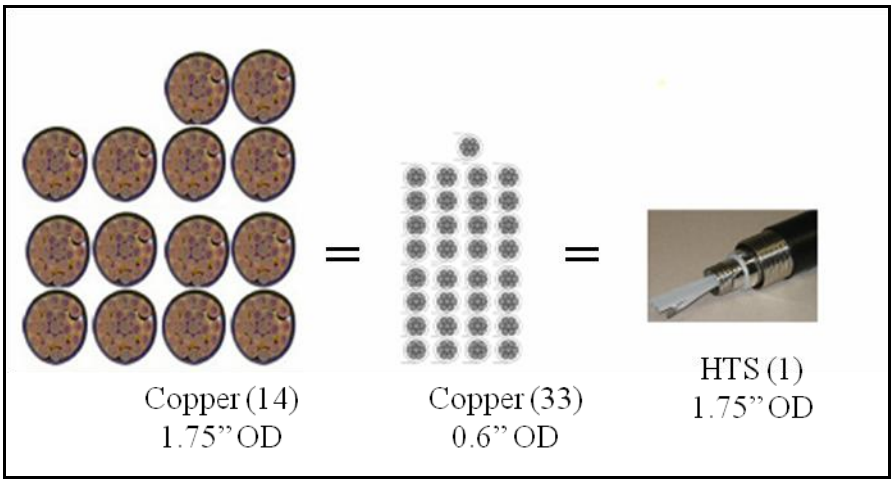

Figure 1-2. Comparison of copper and HTS degaussing system cables.

The Freedom Class Littoral Combat Ship (LCS) is the first Navy platform targeted for transition to HTS cables for the degaussing system. For LCS HTSDG cables, the cryostat runs the entire length of the HTSDG cable, in a configuration with an outside diameter of 44 mm; continuous cryostat lengths of at least 100 meters are required. Currently, the only worldwide manufacturer that can successfully manufacture cryostats in these lengths is Nexans[1], a French company that produces cryostats in its facility in Germany. At this time, all work related to HTSDG is export-controlled. While the cryostats can and have been procured through Nexans, the process is time consuming and results in increased costs to the Navy HTSDG system supplier. With the successful anticipated adoption of HTSDG for LCS, and the future expansion of HTSDG throughout the Navy surface fleet, order requirements of cryostats are estimated to be over 7,000 meters yearly. The establishment of a U.S. manufacturing capability for these long-length cryostats would result in a substantial cost savings to the Navy.

2.0 OBJECTIVE(S)

Per the project plan [1], the objective of this project was to address cryostat configuration and manufacturing issues associated with fabricating long-length, flexible, vacuum-jacketed cryostats that meet Navy shipboard performance requirements. Ultimately, a U.S. manufacturing

[1] Nexans, Group Headquarters, 8, rue du Général Foy, 75008 Paris, France

capability was to be developed by adapting processing techniques at an existing facility for manufacturing electrical conduit.

The project was completed without meeting all the technical objectives for the project; a U.S. manufacturing capability was not developed. Southwire Company, the industry partner that was targeted as a U.S. supplier of these cryostats, returned a No-go decision in Task 3 of the project. Circumstances that led to this decision are discussed further in Section 6, Implementation. The project did realize the following technical accomplishments.

1. A baseline cryostat insulation system was developed and validated via thermal performance testing.
2. The use of double aluminized Mylar® and polyester net for the reflector and spacer materials of the cryostat insulation system were shown to perform better than double aluminized Mylar® and polyester (non-woven) fabric.
3. Current technology available from an existing vendor has been identified for forming, welding and corrugating stainless steel sheet of the desired thickness ranges for the manufacture of HTSDG cryostats. Analyses have shown the technology will be able to produce corrugated tubing that meets application requirements.
4. Lessons learned during burst testing of commercially available corrugated tubing will improve upon future test specimen design and burst testing of actual HTSDG cryostats to demonstrate required performance metrics.

3.0 TECHNICAL APPROACH

The general components that make up an HTSDG cryostat are shown in Figure 3-1. The schematic shows one quarter of the circular cross-section of a representative cryostat configuration. A cryostat consists of an inner and outer corrugated tube, between which is an annular space that is held at a vacuum. The inner tube is surrounded by a multilayer insulation (MLI) system within the annular space. The MLI system is normally comprised of spiral wound pairs of thin reflector and spacer materials in combination with one or more pairs of spacer rods for structural support during bending. The MLI materials typically include double-aluminized Mylar® (DAM) as the reflector layers and polyester fabric or cloth as the spacer layers. The

cryostat assembly has a protective outer coating (cable jacket). The superconducting cable is located inside the inner tube along with the cryogenic mass, usually liquid nitrogen, liquid helium or helium gas.

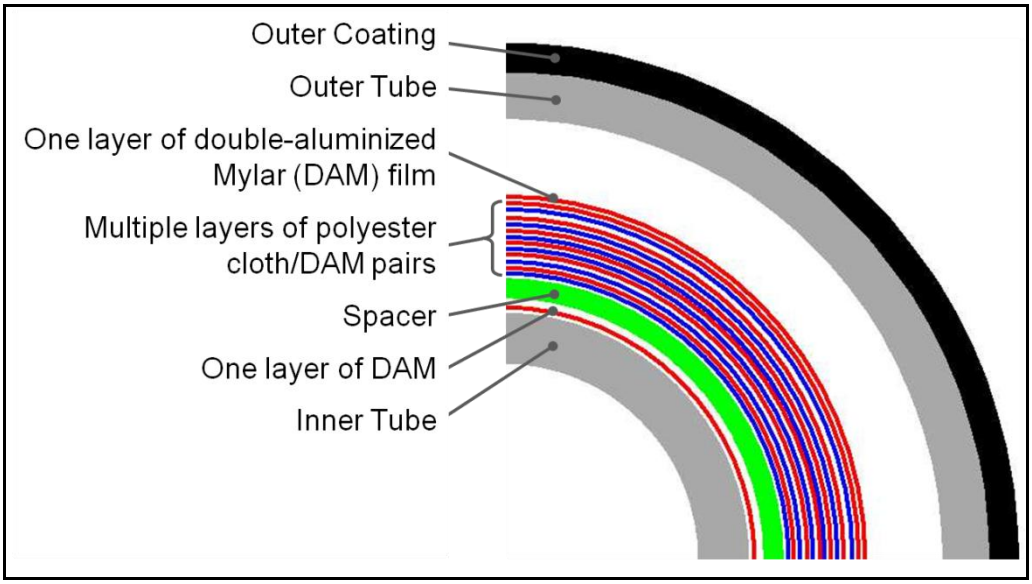

Figure 3-1. Cryostat schematic.

The project tasking was formulated to address four issues: 1) develop a complete cryostat insulation system that would meet Navy shipboard performance requirements; 2) address manufacturing issues related specifically to forming, welding and corrugating the inner and outer tubes of the cryostat; 3) develop a U.S. manufacturing capability for long-length cryostats; and 4) manufacture and test long-length cryostat prototypes against system requirements. In order to adequately address these issues, a multi-faceted integrated project team (IPT) was assembled with expertise in manufacturing processes, wire and conduit manufacturing, and cryogenic applications and testing. The IPT consisted of Naval Sea Systems Command (NAVSEA), Naval Surface Warfare Center, Carderock Division (NSWCCD), Southwire Company (Southwire), Oak Ridge National Laboratory (ORNL), ASRC Aerospace, the National Aeronautics and Space Administration (NASA) Kennedy Space Center (KSC) and the Navy Metalworking Center (NMC). The following sections present the physical and operational requirements for the HTSDG cryostats, and the technical approach for the manufacturing and insulation system assessments that were completed during the project.

3.1 CRYOSTAT REQUIREMENTS

While the project is primarily focused on HTSDG cryostats, there is also interest in utilizing HTS cables in the future for naval power systems. Each application requires a different size, or class, of cryostat: HTSDG cables require 1.75-inch class cryostats, and HTS power cables require 2.75-inch class cryostats. Sections 3.1.1 through 3.1.7 outline the physical and operational requirements for each class of cryostats as provided by NSWCCD. Additional guidance from relevant industry standards is also discussed.

3.1.1 PHYSICAL CONFIGURATIONS

The cryostat size requirements were given as:

1.75 Class Cryostat:

- The inner diameter of the inner corrugated tube shall be greater than 0.8″
- The outer diameter of the outer corrugated tube shall be less than 1.75″

2.75 Class Cryostat:

- The inner diameter of the inner corrugated tube shall be greater than 1.5″
- The outer diameter of the outer corrugated tube shall be less than 2.75″.

3.1.2 COATINGS

The coating requirements were given as:

- Must meet requirements (MIL-C-24643/5 and MIL-C-24643/20) of existing degaussing cables for coatings and bending
- Smoke index less than 25
- Tensile strength of jacket, 1300 psi minimum; elongation 160% minimum
- Flame propagation: No failure.

3.1.3 BENDING PERFORMANCE

The minimum bending capability for the cryostats was given as:

- Cryostat must be able to bend in a diameter of 13 times the cable diameter to an arc of 170 degrees while at -20 °C (ambient temperature) without cracking the outer jacket or failing the cryostat
- A minimum threshold of 5 bends and an objective of 15 bends were assumed.

3.1.4 WEIGHT

The weight requirements were given as:

1.75 Class Cryostat:

- Weight shall be less than 0.75 lb/ft

2.75 Class Cryostat:

- Weight shall be less than 1.25 lb/ft

3.1.5 HEAT LEAK

The maximum heat leak rates were given as:

1.75 Class Cryostat:

- Less than 1 Watt/meter (0.6 W/ft) at 77 K at the ID and at 300 K on the OD.

2.75 Class Cryostat:

- Less than 2 Watt/meter (0.6 W/ft) at 77 K at the ID and at 300 K on the OD.

There shall be no external icing or condensation along the cryostat.

Maximum heat leak rate shall be maintained for 25 years. Provisions to regenerate vacuum and reestablish heat leak rate to extend life to 50 years shall be available.

3.1.6 OPERATING TEMPERATURE

The operating temperature requirements were given as:

- Cryostat must have a designed operating range of 30 K to 305 K.

3.1.7 OPERATING PRESSURE

The operating pressure requirements were given as:

- Cryostat must have a designed operating pressure of 300 psi over the design temperature range
- Cryostat burst pressure at room temperature shall exceed 1000 psi.

3.1.8 OTHER RELEVANT REQUIREMENTS AND STANDARDS

ASME Codes B31.1 (Power Piping) [2] and B31.3 (Process Piping) [3] were also reviewed for applicable cryostat requirements. The IPT determined that B31.3 does apply to cryogenic piping; however, it pertains specifically to straight (smooth-walled) pipe and provides

limited design guidance for corrugated piping. Appendix X in B31.3 provides requirements for metallic bellows expansion joints which are similar to corrugated piping in several aspects. The following relevant metallic expansion joint bellows requirements are given:

- Design should be in accordance with Expansion Joint Manufacturers Association (EJMA) standards [4] except as modified by Appendix F of EJMA
- Factor of safety on squirm pressure shall be 2.25
- Factor of safety on ultimate rupture pressure shall be not less than 3.0
- Stresses at design pressure shall not result in permanent deformation of convolutes.

The EJMA standard provides methods for calculating bellows stresses due to small relative deflections, small bend angles and internal pressure. The requirements listed above and the EJMA handbook-style calculation methods were all used as guidance in the final design of the long-length flexible cryostat corrugation profiles.

3.2 MANUFACTURING ASSESSMENT

3.2.1 CORRUGATED TUBING SURVEY

In order to provide baseline characteristics of existing technology, examinations of a commercially-produced flexible cryostat sample and also a commercially-produced flexible stainless steel pipe sample were made.

3.2.1.1 Characterization of Nexans Cryostat Sample

One sample of Nexans flexible cryostat approximately 2.15 inches long was available for study. The average overall diameter of the sample was approximately 1.87 inches. An end-on view of the specimen is shown in Figure 3-2 and a side view is shown in Figure 3-3.

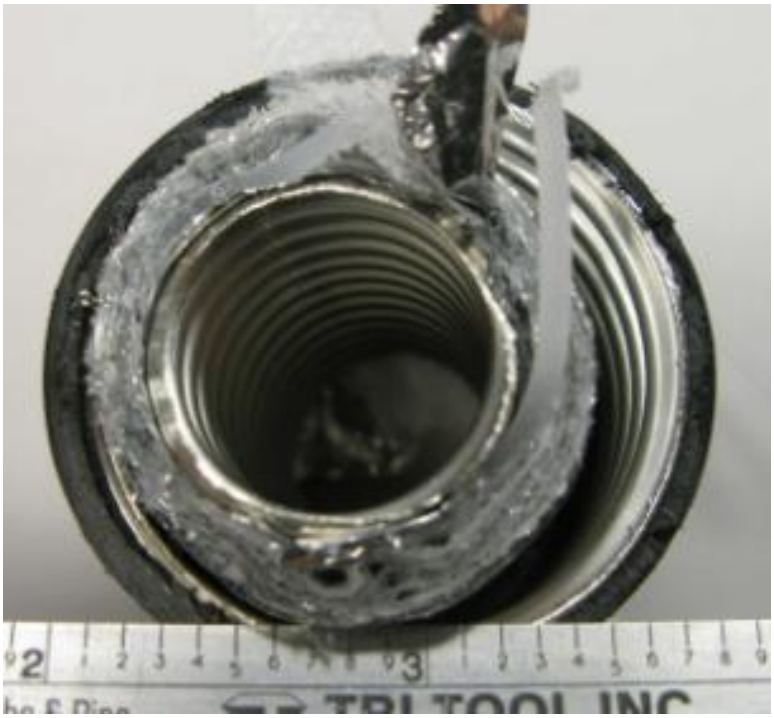

Figure 3-2. Flexible cryostat assembly, end view.

Figure 3-3. Flexible cryostat assembly, side view.

The cryostat consists of an outer tube, MLI, and an inner tube, as previously described in Figure 3-1. A plastic coating covers the metallic corrugated outer tube, which is formed from welded stainless steel tubing. Inside the outer tube is a composite MLI stack-up including two plastic spacer rods, which wrap around the inner tube in counter-rotating helixes. The inner tube is also a corrugated welded stainless steel tube, similar to the outer tube. The components of the cryostat assembly were examined starting from the outer plastic cover and finishing at the inner tube.

Outer Coating

A black plastic coating, visible in Figure 3-2 and Figure 3-3, covers the corrugated outer tube, conforming somewhat to the corrugations of the tube. A cross-section of the outer coating and outer tube is shown in Figure 3-4. This coating was examined to determine its thickness and the extent to which it would contribute to the stiffness of the cryostat assembly by filling in the voids between the outer tube corrugations.

Outer Tube

The outer tube was formed by corrugating welded stainless steel tubing using a right-handed helical spiral, single-start configuration. A photograph of the outer tube with the outer coating on it and the inside weld seam visible is shown in Figure 3-4.

Figure 3-4. Outer tube, inside view.

Characterization of the outer tube consisted of measurement of the finished dimensions, as well as the following metrics:

- Corrugation profile, to generate inputs for a finite-element model of the tube for analyses of flexibility, strength, etc.
- Surface finish, to provide information for the estimation of radiant heat transfer across the tube
- Weld and base material microstructures, to determine the welding method used and provide ductility and strength information
- Determination of the alloy used to make the tube.

Multi-Layer Insulation

The MLI consisted of several layers of DAM alternating with a polyester cloth material, and plastic spacer rods. The insulation system, as removed from the outermost layer to the final layer at the inner tube, consisted of:

1) One layer of DAM film
2) Six layers of polyester cloth/DAM pairs (DAM to the outside of the cloth)
3) Two counter-rotating, helically wrapped spacer rods
4) One layer of DAM wrapped tightly around the inner tube.

The MLI was characterized to provide inputs to estimate the heat leak of the finished cryostat.

Inner tube

The inner tube was formed by corrugating welded stainless steel tubing using a right-handed helical spiral, single-start configuration. A photograph of the inner tube with the inside weld seam visible is shown in Figure 3-5, and the outside surface with weld seam visible is shown in Figure 3-6. The inner tube was examined in the same manner as the outer tube.

Figure 3-5. Inner tube, inside view.

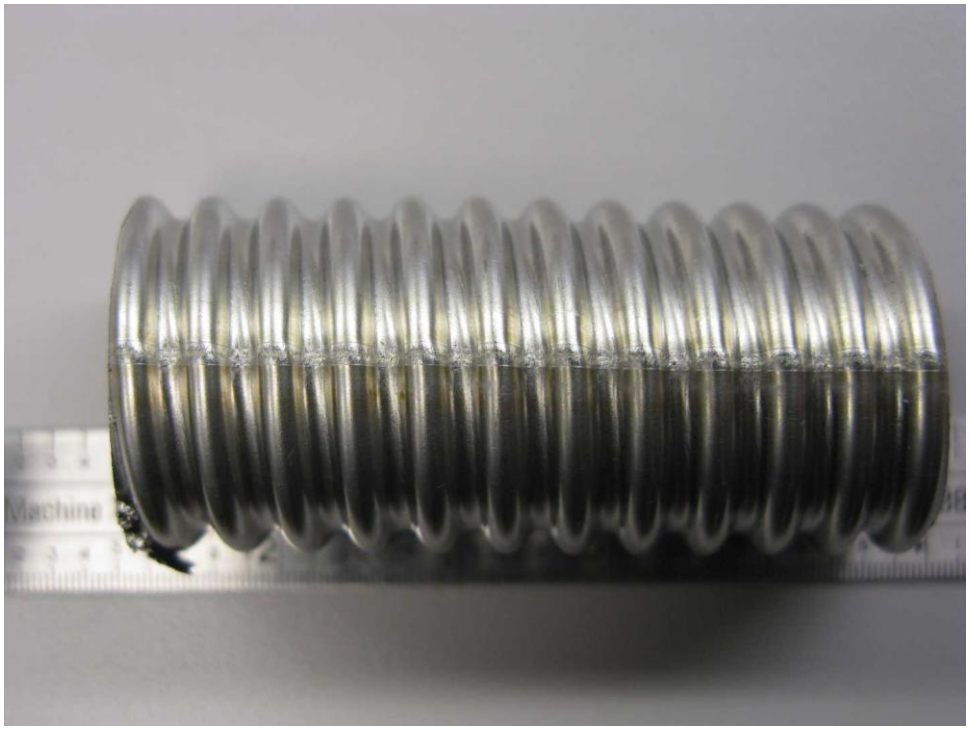

Figure 3-6. Inner tube, outside view.

3.2.1.2 Characterization of Flexible Pipe

To assist in evaluating the Nexans cryostat sample, a sample of a commercially-produced metallic corrugated flexible pipe was also examined. The flex pipe was made from welded tubing using a similar alloy and material thickness as the cryostat, except the corrugations were annular instead of helical. By examining the cross-section of the flex pipe, a correlation between the starting tube wall thickness and the finishing wall thickness after the corrugating process can be established, since the starting tube wall thickness for the flex pipe was known. A photograph of the flex pipe appears as Figure 3-7, and a closer view of the welded seam is shown in Figure 3-8.

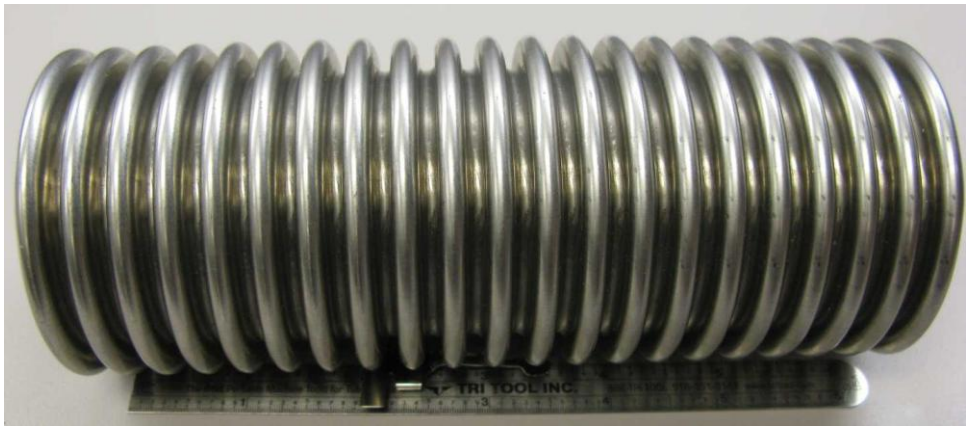

Figure 3-7. Flex pipe side view.

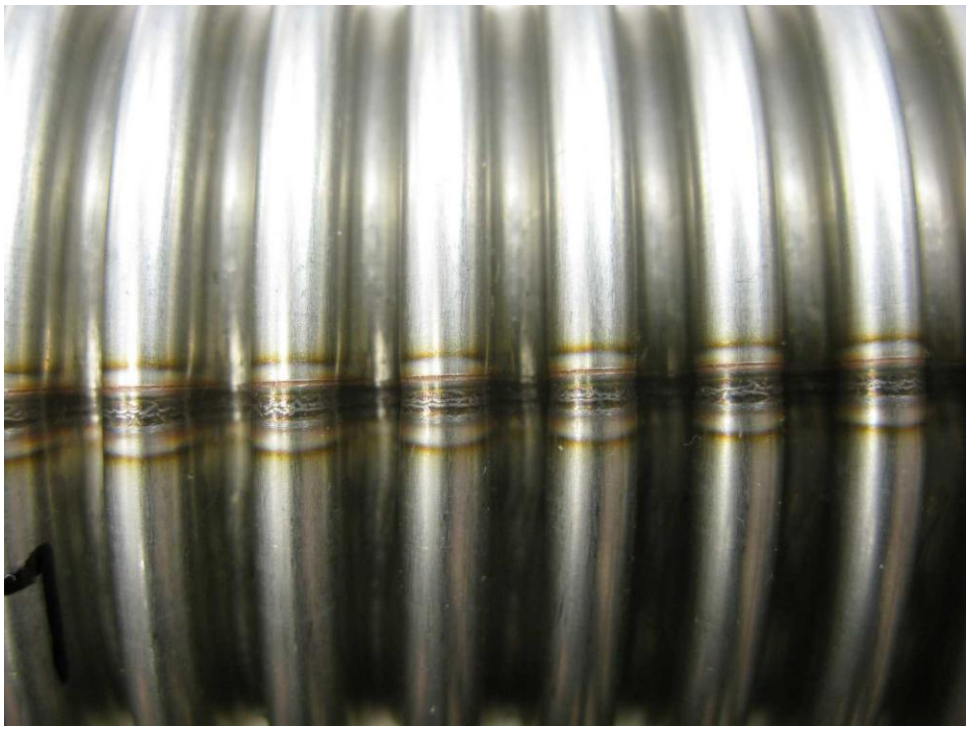

Figure 3-8. Flex pipe weld seam.

3.2.2 SITE ASSESSMENTS AT SOUTHWIRE

Southwire Company, headquartered in Carrolton, Georgia, is North America's leading manufacturer of wire and cable used in the distribution and transmission of electricity. Southwire has extensive experience in wire and conduit manufacturing, as well as significant manufacturing capability already installed. In assessing their current manufacturing capabilities,

Southwire proposed modifying an existing copper and aluminum sheathing line at their Heflin, Alabama facility to allow production of stainless steel cryostats. NMC conducted several site assessments to evaluate the feasibility of modifying the existing equipment for forming, welding and corrugating Type 316L stainless steel sheet. Weber & Scher (W&S), an industry consultant with extensive experience in designing and outfitting cable and wire producing lines, also completed a third party assessment.

3.2.3 CRYOSTAT CORRUGATION PROFILE DEVELOPMENT

The cryostat corrugation profile was developed to minimize strain resulting from the forming operation while also minimizing the cyclic bending strain resulting from handling and installation. This balanced approach of minimizing the overall cumulative strain (forming + bending) will result in a cryostat design with the best possible overall performance given the other required performance parameters (pressure, temperature, etc.) and the material and size constraints.

Finite element analysis (FEA) has been utilized to numerically analyze forming simulations based on the W&S manufacturing process. Additionally, cryostat bending models have been developed and analyzed to establish cyclic bending strain amplitudes. Material flexibility limits (number of permissible bends to cryostat failure) have been established through correlation of low cycle fatigue (LCF) test data from welded and non-welded thin plate specimens with the numerical results. The corrugation profile was also developed to meet geometric, pressure load, and handling load requirements as detailed in Section 3.1.

To obtain material properties such as tensile strength, elongation, modulus and other stress/strain behavior needed for the FEA, baseline tensile testing on 316L annealed sheet material was performed. Tensile testing was performed according to ASTM E8 [5] on annealed Type 316L sheet material in 0.015-inch thickness. Longitudinal and transverse specimens were machined using standard ASTM E8 geometry with a gauge section width of 0.25 inch. Stress/strain data were gathered until specimen failure. The specimens were tested at room temperature using a quasi-static strain rate.

In order to complete LCF testing, material properties were needed to provide information to choose fatigue testing parameters. To supply this, tensile testing was performed according to ASTM E8 on annealed Type 316L sheet material in 3/16-inch thickness. Longitudinal and

transverse specimens were machined using standard ASTM E8 geometry with a gauge section width of 0.25 inch. The specimens were tested at room temperature using a quasi-static strain rate.

Fatigue testing was then completed using baseline annealed specimens and specimens with various degrees of pre-strain. In addition, welded specimens were also tested transverse to the weld direction to observe the effects of welding on the fatigue life. Axial fatigue testing was conducted per ASTM E606 [6] at an external laboratory.

3.2.4 FRACTURE ANALYSIS OF LCF SPECIMENS

After fatigue testing, some specimens were selected for evaluation of their microstructure and fatigue fractures. The microstructural analysis was conducted using light optical microscopy (LOM) on metallographically polished and chemical etched samples. A dilute aqua-regia solution of H_2O+ HNO_3+ HCL for approximately 4–10 minutes was used to reveal the microstructure. The fracture analysis was conducted using a CAM-SCAN scanning electron microscope (SEM).

3.2.5 CRYOSTAT BURST TESTING

Hydrostatic burst testing was performed to evaluate the performance of the corrugated tubing during over pressure conditions. The testing utilized the Meridonial Yield-Rupture test method described in paragraph 7.3.3 of the EJMA standards for guidance. There were four main goals to the test program:

- To discover the mode of failure of the corrugated tubing
- To determine the burst pressure of the tubing used for the 5-meter prototype cryostats (see Section 3.3.2, Fabrication and Testing of 5-meter Prototype Cryostats)
- To validate the FEA models generated to predict the hydrostatic failure point of corrugated tubing
- To establish the factor of safety that exists between the rated pressure of commercially available corrugated tubing and the actual rupture pressure.

Testing was performed by attaching short, 4 corrugation (4 peaks, 3 valleys) segments of tubing to end pieces that would serve to fixture the specimens and also to introduce the hydrostatic pressure. Specimens were constructed using the same corrugated tubing that was

used to manufacture the 5-meter prototype cryostats discussed in Section 3.3.2. Complete details of specimen design and fabrication are included in Appendix B. Both the inner and outer tubing sizes were tested in two different loading arrangements: fixed-length and free end. Figure 3-9 shows the test fixture configured for fixed-length testing with an outer tube specimen installed.

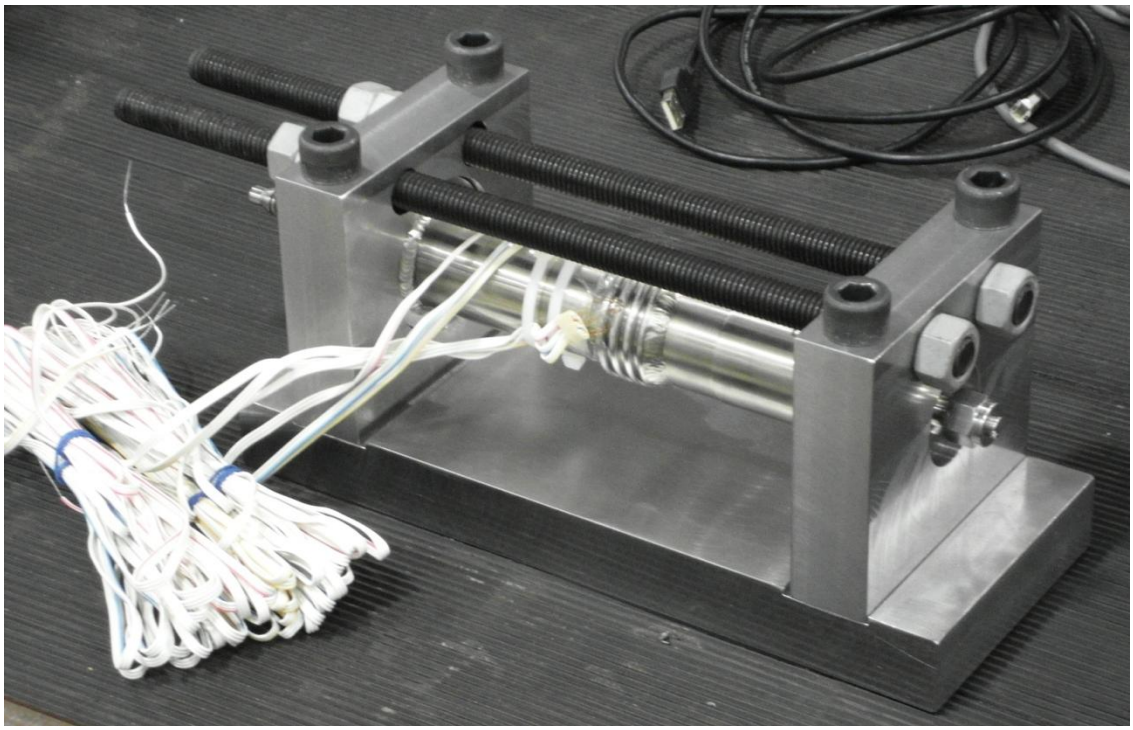

Figure 3-9. Hydrostatic burst test setup.

Pressure and specimen displacement data were gathered electronically using a PC-based data acquisition system. The specimens were instrumented with rectangular strain gauge rosettes fixed to a corrugation peak and also with a transducer that measured circumferential growth of the specimen at a valley. Figure 3-10 shows the strain gauge mounted to an outer tube specimen. The electronic data could then be compared to the predictions of the FEA model to determine its validity.

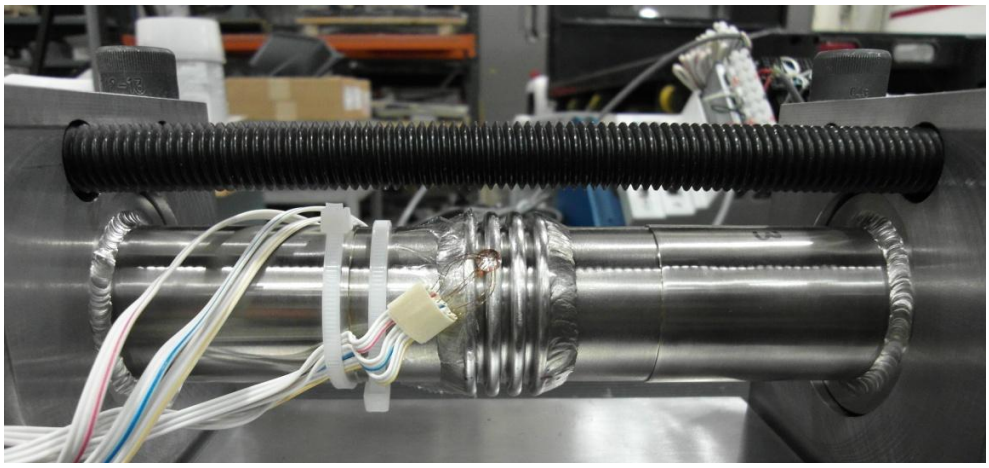

Figure 3-10. Typical strain gauge location.

3.3 INSULATION SYSTEM ASSESSMENT

While the Navy is interested in two classes of cryostats, 1.75-inch (44 mm) and 2.75-inch (70 mm), these thermal performance investigations were primarily focused on the 1.75-inch class of cryostats specific to the LCS HTSDG system. The effectiveness of the thermal insulation system is a key function of the cryostat. That is, heat leakage rates must be reduced to very low levels so that the cryogen can be preserved and controlled as a coolant for the electrical cable. The required maximum heat leakage rate (heat leak) for the HTSDG cryostat was defined as 1 W/m. The corresponding boundary temperatures are 77 K (near the cold inner tube surface) and 300 K (near the warm outer tube surface). Per NSWCCD, the required heat leak shall be maintained for 25 years, and the life of the product must be extendable to up 50 years with vacuum regeneration (planned maintenance).

The capabilities and expertise of both ORNL and the Cryogenics Test Laboratory at KSC included testing and development of thermal insulation systems. As such, these team members were tasked to: 1) develop the optimum number of MLI layers and stack-up for the 1.75-inch class cryostat and 2) evaluate the thermal performance of representative prototype cryostats. The following sections detail the technical approach for these investigations.

3.3.1 CRYOSTAT 100 TESTING

Two separate series of tests were completed at KSC using an insulation test instrument designated as Cryostat-100; the KSC reports of this testing are provided in Appendices C and D.

These tests were completed to evaluate various insulation system configurations against the HTSDG cryostat requirements, and were specifically focused on establishing the optimum MLI and spacer rod configuration.

However, in addition to the MLI and spacer rods, the thermal insulation also includes getter and desiccant packs to assist with long-life vacuum retention. Getter packs are typically palladium oxide (PdO) packets in wire mesh material fastened on the warm side of the MLI (nearest the inner surface of the outer tube). Getter packs are often preferentially located near the termination(s) of the cryostat for ease of installation and future replacement possibilities. Desiccant packs consisting of molecular sieve material in foil packages are also preferentially located at the terminations for ease of installation. Desiccant packs can typically be regenerated by heating up to approximately 200 °F. Investigation into appropriate getter and desiccant materials and quantities and their optimum distribution throughout the long length cryostats has not been addressed within this project tasking.

As stated previously, the required maximum heat leak for the 1.75-inch class cryostat was given as 1 W/m. This heat leak requirement is valid only for a specific diameter cryostat; in this case, 1.75 inches. The Cryostat-100 test instrument utilizes a cylindrical cold mass that is 40 inches (1-meter) long and 6.6 inches (167 mm) in diameter. In order to compare the thermal performance of different insulation systems it is essential that the heat flux (heat leakage rate per unit area) be used. The maximum allowable heat flux as calculated from the 1 W/m heat leak requirement for the 1.75-inch class cryostat is 5.8 W/m^2.

For the 1.75-inch class cryostat, there is a nominal 7 mm gap between the outer diameter of the inner tube and the inner diameter of the outer tube that is available for the insulation system. The target MLI thickness for each test article was 6.5 mm. Figure 3-11 shows the Cryostat-100 during testing, and Figure 3-12 shows a simplified schematic of the test rig. For all tests, the cold boundary temperature (CBT) was approximately 78 K. The warm boundary temperature (WBT), maintained by a heater shroud assembly inside the vacuum can, was approximately 300 K. An additional heater system (not shown) internal to the vacuum chamber was used for control of the warm boundary temperature. The cold vacuum pressure (CVP) was maintained in the range of 10^{-6} torr by active vacuum pumping for high vacuum testing. The principle of power measurement was the boil-off calorimetry method using liquid nitrogen. Cooldown, stabilization, and testing were performed in accordance with the standard KSC lab

procedure. Primary thermal performance data reported for each test article included heat flux and the effective thermal conductivity.

Figure 3-11. Cryostat-100.

Surface Temperature Measurement	
Sensor	**Location**
VC1, VC2, VC3	Vacuum Can Temperature
T11, T12, T13	Warm Boundary Temperature (WBT)
T4 – T10	Insulation Layer Temperatures
T1, T2, T3	Cold Boundary Temperature (CBT)
CM1, CM2	Cold Mass Temperature

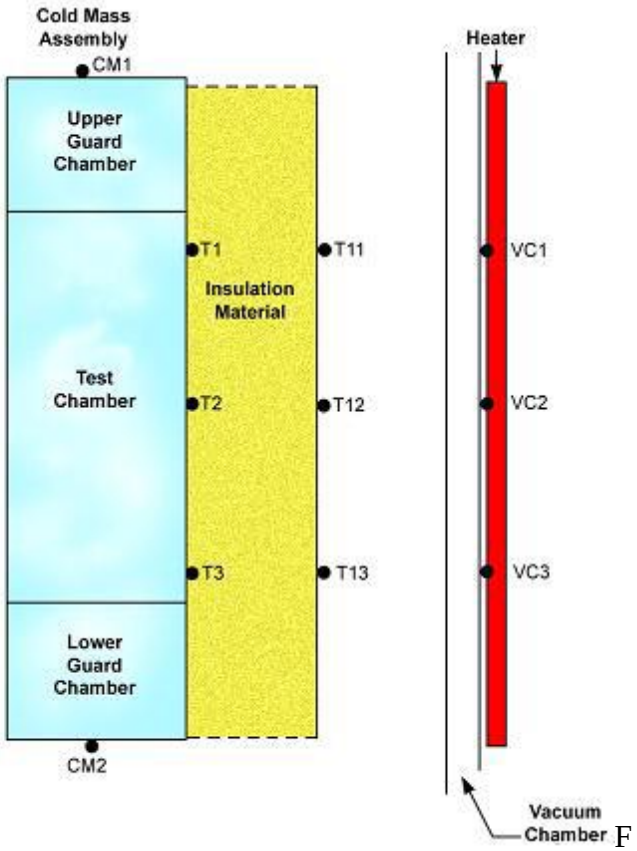

Figure 3-12. Simplified schematic of insulation test.

3.3.1.1 Initial Cryostat-100 Testing

The MLI used for these initial Cryostat-100 tests consisted of alternating thin layers of reflector and spacer material. The reflector material used in this series of tests was DAM in thicknesses of 0.0007 inches (18 μm) and 0.002 inches (51 μm). The spacer material was a non-woven polyester fabric with a thickness of 0.005 inches (127 μm). These layer pairs (layers) would normally be built up in a spiral, overlapping fashion on the outer surface of the inner tube. For these tests, the layers were applied by hand as individual blanket layers ('cigarette-style'), with an approximate 25 mm overlap at the layer seam and a 120° stagger between subsequent layer seams.

Stack-ups of two possible MLI designs for the 1.75-inch class cryostat, as well as a baseline, or control configuration, were tested.

- Baseline (A145): This test article provided basic MLI reference data to link with prior (historical) MLI data and analysis. Design: nine layer pairs, one outer protective layer pair (10 layer pairs total).
- Design 1 (A146): Starting from the inner tube: one layer pair, spacer rod helical pair, eight layer pairs, outer protective layer pair (10 layer pairs total).
- Design 2 (A147): Starting from the inner tube: one layer pair, first spacer rod helical pair, two layer pairs, second spacer rod helical pair, six layer pairs, outer protective layer pair (10 layer pairs total).

Temperature sensors were placed between the blanket layers in accordance with

Table 3-1. These sensors were used to obtain a layer temperature profile as a function of distance from the cold mass. Circumference measurements were made for each blanket layer that was applied to the cold mass. The thermocouple locations (distances) were then calculated based on the installed final thickness of the total MLI system.

Table 3-1. Temperature Sensor Placement for Initial Cryostat-100 Testing

Temperature Sensor Designation	MLI Baseline (A145)	MLI Design #1 (A146)	MLI Design #2 (A147)
T1,T2, T3[1]	Cold mass	Cold mass	Cold mass
T4	Layer 1	Layer 1	Layer 1
T5	Layer 2	Layer 2	Layer 2
T6	Layer 3	Layer 3	Layer 3
T7	Layer 4	Layer 4	Layer 4
T8	Layer 5	Layer 5	Layer 5
T9	Layer 6	Layer 6	Layer 6
T10	Layer 7	Layer 7	Layer 7
T23	Layer 8	Layer 8	Layer 8
T24	Layer 9	Layer 9	Layer 9
T11,T12,T13[2]	Layer 10	Layer 10	Layer 10

[1] T1, T2, T3 are on the cold boundary surface (underneath the zero layer of DAM).
[2] T11, T12, T13 are on the warm boundary surface (on top of the outermost layer of DAM).

The spacer devices were either one or two pairs of opposing helically-wound spacer rods. The purpose of the spacer rods was to minimize the local compression of the MLI layers and the resultant increase in heat transfer due to bending in the long flexible cryostat. The spacer rods were manufactured by Southwire using Ultem, a very low thermal conductivity polymer. The rods were extruded as a circular cross-section with a diameter of 0.080 inch (2.0 mm). Figure 3-13 shows the helically wrapped spacer rod pair on the Design 1 test article. The spacer rods were wrapped with a 3 to 4 inch spacing at an approximate 20° angle over the entire 40-inch length of the cold mass. The baseline test article with the ten layer pairs of MLI is shown in Figure 3-14, ready for insertion in the Cryostat-100 vacuum chamber.

Figure 3-13. Design 1 test article with helically wrapped spacer rods.

Figure 3-14. Completed baseline test article outside of vacuum chamber.

3.3.1.2 Follow-on Cryostat-100 Testing

The initial Cryostat-100 testing utilized MLI test articles comprised of DAM as the reflector material and polyester fabric as the spacer material. Within the sequence of project tasking, two 5-meter-long prototype cryostat assemblies were then built and tested as discussed in Section 3.3.2. The two prototypes were fabricated to directly compare tightly wrapped versus loosely wrapped insulation. The MLI for both prototypes was comprised of perforated DAM as the reflector material and polyester net as the spacer material. Based on the overall prototype performance results, new baseline testing of the MLI system was needed to better understand the effect of layer density and total thickness on thermal performance. MLI test articles were

subsequently constructed using materials similar to those used in the 5-meter-long prototypes and tested using the Cryostat-100.

The MLI test articles for the second series of tests were constructed from sheets of DAM and polyester net. These materials were essentially the same as those used for the two prototype cryostats, with the exception that the reflector layers were not perforated. This was not deemed an issue, however, as continuous vacuum pumping is standard practice with the Cryostat-100, and evacuation of the blanket-wrapped MLI layers takes place readily through the seams and edges of each layer. All test articles were similarly constructed and instrumented as for the initial Cryostat-100 testing.

Three test articles with MLI of 10, 15 and 20 layers were tested (no spacer rods were included). Based on the as-built configuration and performance of the 5-meter prototypes, the target layer density range was from 2.8 layers/mm to 2.0 layers/mm, with the preference towards the higher end of the range. The physical parameters of the test articles are given in Table 3-2. Also included in the table is the baseline test article (A145) from the initial Cryostat-100 testing for reference. The 20 layer test article (A152) was constructed and tested first. The next test article (A153) was prepared by removing the outer 5 layers from the previous test. The third and final test article (A154) was similarly prepared by removing 5 layers from the previous test. The layer densities of all test articles were well within the target range of 2.0 to 2.8 layers/mm.

Table 3-2. Physical Parameters of MLI Test Articles

Test Series	Number of Layers	Layer Density (layers/mm)	Thickness[1] (mm)	Mean Area[2] (m^2)
A145	10	1.57	6.38	0.316
A152	20	2.52	7.95	0.319
A153	15	2.28	6.57	0.316
A154	10	2.05	4.87	0.313

[1] Thickness is based on measurements of the final installed circumferences.
[2] Mean area is the mean heat transfer area for the cylindrical blanket.

3.3.2 FABRICATION AND TESTING OF 5-METER PROTOTYPE CRYOSTATS

Project tasking included the fabrication of representative cryostat prototypes to determine the effects of manufacturing and handling on thermal performance. Two 5-meter long test articles were fabricated and tested to directly compare tightly wrapped versus loosely wrapped

insulation as well as to gain the additional fabrication experience. The prototypes were fabricated by hand at KSC following the design approach and guidelines established by the project team. Liquid nitrogen boil-off thermal performance testing was conducted at KSC. A report detailing fabrication of the prototype cryostats and testing at KSC is included in Appendix B. Following the tests at KSC, liquid nitrogen (LN2) flow-through (dynamic) thermal performance testing was performed at ORNL; the report of this testing is included in Appendix E.

The inner and outer tubes were commercially available, welded, stainless steel corrugated tube. Nominal inner and outer tube diameters were 16 mm and 32 mm, respectively. The annular corrugation profiles of the selected tubing resulted in a gap space of approximately 6.6 mm, which is relatively close to the targeted 7 mm gap for the HTSDG cryostat.

The results from the initial Cryostat-100 testing established the thermal insulation system design for the prototypes. The MLI system consisted of double-aluminized polyester film (perforated, 2-mm-diameter holes on a 50-mm-square pattern) and polyester tulle (netting) on 2.5-inch (64-mm) wide collated rolls. The polyester film was 6-micron thick and the polyester tulle weighed approximately 7.5 grams per square meter. The installation sequence was as follows: one layer pair of helically wrapped MLI, one pair of helically wrapped spacer rods, and nine layer pairs of MLI (10 layer pairs total). The overlap of the MLI was no more than about 50%. The spacer rods were 0.060-inch (1.5 mm) diameter Ultem spacer rods applied at a spacing of approximately 64 mm.

Two 5-meter long prototypes were fabricated; both units were essentially identical except for the difference in the layer density of the MLI. Of the two prototypes, the first (designated "Tiger") was wrapped in a tight fashion, with a total MLI thickness of 3.6 mm for a layer density of 2.8 layers/mm. The second prototype (designated "Fluffy") was wrapped very loosely with a total thickness of 6 mm for a layer density of 1.7 layers/mm. Specific details regarding fabrication of the prototypes, including design and fabrication of the end termination assemblies, assembly of the inner line to the outer line, welding of the end termination assemblies, and initial evacuation and mass spectrometer leak testing of the completed prototype units can be found in Appendix B. Figure 3-15 visually documents some aspects from the fabrication process. Discussion of the test set-up, apparatus and method are included in Appendices B and E for testing completed at KSC and ORNL, respectively.

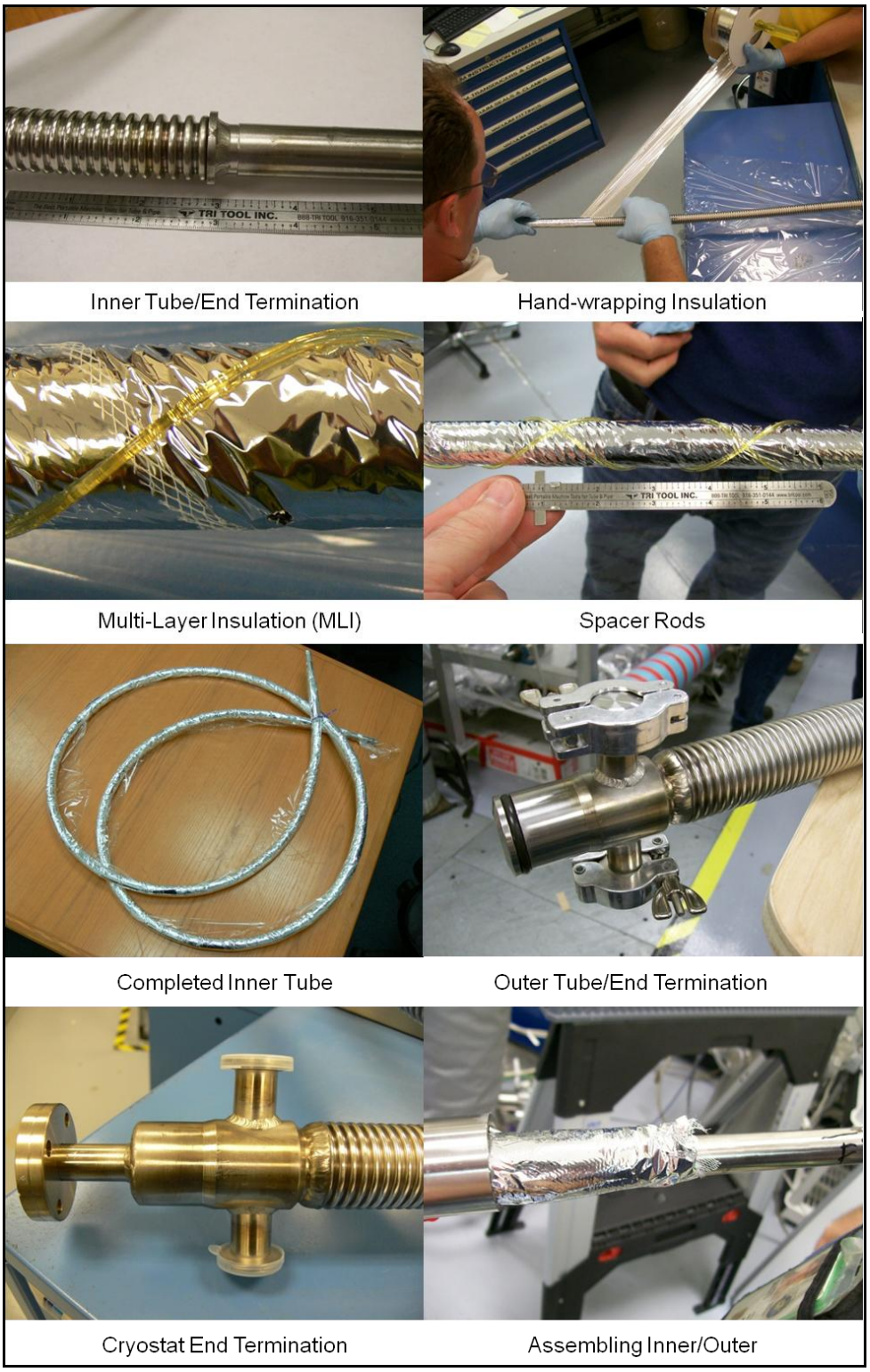

Figure 3-15. Fabrication of the 5-meter prototype cryostats.

4.0 RESULTS AND DISCUSSIONS

As stated in Section 2, Objectives, the project has completed without meeting all the technical objectives for the project; specifically, a U.S. manufacturing capability was not developed. Southwire Company, the industry partner that was targeted as a U.S. supplier of these cryostats, returned a No-go decision to commit the capital needed to upgrade their manufacturing facility. Circumstances that led to this decision are discussed further in Section 6, Implementation. Table 4-1 identifies the goals and metrics as set forth in the project plan. The listed technical metrics were derived from the HTSDG cryostat requirements provided by NSWCCD. These requirements were the basis for the manufacturing and insulation assessments completed on the project. However, physical testing of cryostat prototypes manufactured by a U.S. supplier was not completed due to the No-go decision by Southwire.

Table 4-1. Goals and Metrics

Process Goal	Metric	Baseline	Threshold	Target	Actual
Cost Savings Per Shipset	% Reduction	Based on foreign supplier cost history, $400/meter	30%	50%	Preliminary business case for Southwire predicted $350/meter price for the cryostat; Southwire No-go decision returned.
Cryostat Heat Leak	Heat Leak (Watts/meter @ 77 K / 300 K) for nominal 1.75″ OD	None	Heat Leak < 1.0 W/m	Heat Leak < 0.5 W/m	N/A: Project exited due to Southwire No-go decision. However, prototype testing met < 1.0 W/m threshold.

Process Goal	Metric	Baseline	Threshold	Target	Actual
Cryostat Single Bend Radius Effects	% Increase in heat leak across the bend, no loss in vacuum	None	Bend Diameter of (13 x OD); < 200% increase in heat leak across the bend	Bend Diameter of (6 x OD); < 200% increase in heat leak across the bend	N/A: Project exited due to Southwire No-go decision. However, prototype testing showed100% increase in heat leak with ~ (17 x OD) bend.
Cryostat Propagated Bend Residual Effects	% Increase in heat leak across the bend, no loss in vacuum	None	Bend Diameter of (13 x OD); < 20% increase in heat leak across the bend	Bend Diameter of (6 x OD); < 20% increase in heat leak across the bend	N/A: Project exited due to Southwire No-go decision. However, prototype testing showed100% increase in heat leak with ~ (17 x OD) bend.
Cryostat Accelerated Vacuum Life	Vacuum level; warm vacuum pressure (WVP), cold vacuum pressure (CVP)	None	Accelerated life of 25 years; WVP < 10 mTorr; CVP < 1 mTorr	Accelerated life of 50 years; WVP < 10 mTorr; CVP < 1 mTorr	N/A: Project exited due to Southwire No-go decision.
Cryostat Burst Pressure	Burst Pressure (psi)	None	Burst pressure > 500 psi; Vacuum integrity through 300 psi	Burst pressure >1000 psi; Vacuum integrity through 300 psi	N/A: Project exited due to Southwire No-go decision. However, burst testing results of commercially available corrugated tubing were well above target 1,000 psi burst pressure.

4.1 MANUFACTURING ASSESSMENT

4.1.1 CORRUGATED TUBING SURVEY

The complete results of the corrugated tubing survey are included in Appendix F. Key information from this survey was leveraged for the manufacturing and insulation assessments that followed. The physical parameters as determined for the Nexans inner and outer cryostat tubes are shown in Table 4-2.

Table 4-2. Nexans Cryostat Tube Physical Parameters

Cryostat Tube	Material	Outer Diameter (inches)	Inner Diameter (inches)	Stock Material Thickness (inches)	Surface Finish (Corrugation Peak)	Surface Finish (Corrugation Valley)	Pitch (inches)
Inner	Type 316	0.980-0.988	0.821-0.829	0.0129	57 μin Ra	Undetermined	0.181
Outer	Type 316	1.732-1.742	1.531-1.535	0.0158	24 μin Ra	57 μin Ra	0.193

The MLI consisted of 2.17 inch wide strips of double-aluminized (aluminized both sides) Mylar® film that measured 0.0007 inches in thickness. The polyester cloth strips measured 2.8 inches in width (perpendicular to the strip edge), and approximately 0.005 inches thick. The construction of the cloth was a nondirectional (non-woven) mat of individual polyester fibers. The six pairs of polyester cloth and DAM strips were applied in a right-handed helical configuration; the helix angle[2] of each pair measured approximately 60°. The cloth was slightly wider than the DAM, and each DAM strip was approximately centered on its respective cloth strip, with the cloth strip to the inside of the DAM. Due to the increase in thickness of the MLI buildup from layer to layer, the circumference of the MLI ranged from 3.6 inches at the innermost cloth/DAM pair, to 4.28 inches at the adhesive Mylar® tape. The spacer device

[2] The included angle between the centerline (or edge) of the wrapping material and the longitudinal axis of the cryostat, i.e., a longitudinal strip would have a helix angle of 0°, and an annular ring would have a helix angle of 90°.

consisted of two round plastic rods helically wrapped as a counter-rotating pair – one left-handed, and one right-handed. The diameter of the rods measured 0.081 inches. A Fourier-Transform Infrared (FTIR) analysis performed on the spacer determined that the material was most likely high-density polyethylene (HDPE).

4.1.2 SITE ASSESSMENTS AT SOUTHWIRE

4.1.2.1 NMC Site Assessments

NMC participated in three site assessments at Southwire's Heflin, Alabama manufacturing facility. The first visit consisted of an initial walk-down of the existing copper and aluminum sheathing line. For current product, the 0.090-inch-thick sheathing material is purchased to width in the form of slit-to-width coils. The cable subassembly runs through the center of a set of progressive dies into a set of rollers, around which the sheathing material is formed into a circular shape with a longitudinal seam at the 12-o'clock position. Welding is completed by autogenously melting the edges of the seam with the Gas Tungsten Arc Welding (GTAW) process. The GTAW current is proportional to the travel speed of the line; as the line speeds up, the current increases. The formability of the relatively soft copper and aluminum sheathing material easily takes the set of the dies and produces the round sheath around the cable assembly. The welded tube/cable assembly then proceeds through a clamp-type caterpillar capstan (cleat cat). The cleat cat consists of a series of shoes attached to two chains that clamp the welded tube in succession and feeds the welded tube into a corrugating unit. The corrugating machine utilizes a gear-type corrugating process for imparting the annular corrugations into the welded tube.

The second visit focused on completing forming and welding trials on 0.015-inch-thick Type 316L stainless steel sheet using the existing and/or modified production line equipment. Due to the difference in sheathing material thickness (0.015 inch versus 0.090 inch) together with the increased stiffness of the stainless steel material, a modification to the forming dies prior to the welding torch was necessary in order to maintain fit-up of the weld joint. The location of the welding torch was also moved closer to the forming dies in an attempt to compensate for spring-back of the stainless steel material after forming, and an additional fixture was built downstream of the weld zone to maintain position of the weld seam during cooling. Figure 4-1 shows some product that was welded during this trial. Even with the stated modifications, a

continuous weld seam was not achieved. This was primarily credited to the resulting vibration and general movement of the tubing caused by the cleat cat tube feeder located downstream of the welding zone that negatively affected the positioning of the weld seam relative to the torch/weld arc.

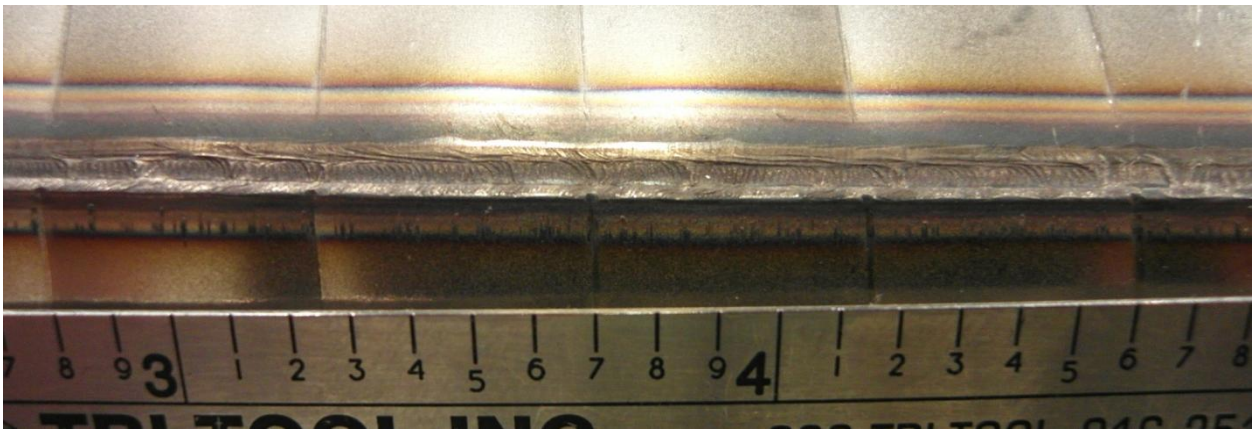

Figure 4-1. Southwire initial welding trial.

The third visit focused on evaluating alternative or modified weld processes together with additional fixturing to improve weld seam fit-up. A Thermal Arc plasma arc welding (PAW) machine was used for this evaluation. An advantage of the plasma arc process is that a well-controlled arc position height relative to the weld seam is not as critical as is the case with the GTAW process. The PAW arc is more columnar than the GTAW arc which feathers out as a cone from the electrode. Tubing welded using PAW produced a very narrow weld pool that appeared very close to the Nexans sample, as shown in Figure 4-2. However, the extreme focus of the PAW arc requires even greater accuracy in weld joint placement. Even with additional tooling changes, the overall alignment of the production line was not accurate enough to maintain the position of the weld seam for the PAW process.

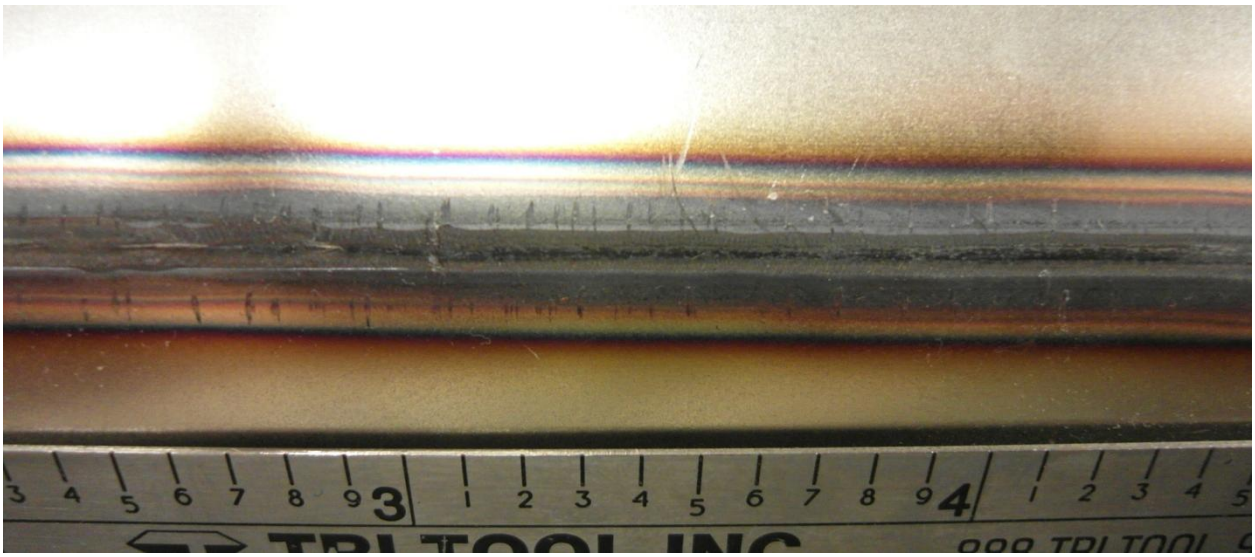

Figure 4-2. Southwire welding trial – PAW process.

Additional trials were completed during this visit using the GTAW process with the improved fixturing. The resulting welded tube was sound enough to be successfully corrugated, but it still had intermittent weld defects as shown in Figure 4-3. In general, the overall misalignment of the production line equipment, the type and placement of the forming dies, and the tube feeding equipment (cleat cat) were all significant factors that contributed to the failure in modifying the existing production equipment for manufacturing stainless steel cryostat tubing.

Figure 4-3. Southwire welding trial – GTAW process.

4.1.2.2 Weber & Scher Site Assessment

Following the NMC forming and welding trials at Southwire, W&S conducted a third party assessment of the copper and aluminum sheathing line. The evaluation focused on the feasibility of forming and welding 0.015-inch-thick Type 316L stainless steel sheet using the existing production line components. Several trials were conducted over the course of the two-day evaluation. Similarly to the assessment completed by NMC, W&S determined that the current production line design and configuration would not be suitable for forming the desired stainless steel tubing. First, the current line is designed for copper and aluminum products ranging from 2.0 inch through 6.0 inch tube diameter; the targeted HTSDG tube diameters are approximately 0.750 inches and 2.0 inches. Second, the current set-up does not take into consideration the "over-forming" that is necessary to successfully weld stainless steel sheet.

In addition, quite a few of the mainline components were observed to be out-dated or worn, and use of the cleat cat for feeding the tube into the corrugating machine was noted to contribute to slippage and misalignment of the product as it progressed through the line. W&S recommended that the cleat cat be replaced by a linear belt type caterpillar capstan. This would eliminate tube slippage and improve the consistency and quality of the welded seam and the corrugation profile. Upon inspection of the existing corrugating machine, there was also concern about the tooling wear that would result when corrugating stainless steel tubing on an ongoing production basis. Based on their expertise in the design and construction of corrugating equipment, W&S recommended an eccentric ring type corrugating technology that would provide both longer tooling life and a better overall solution for corrugating stainless steel as well as copper and aluminum tubing.

W&S provided a report detailing a two-phased approach for the production line upgrade. The first phase would allow Southwire to successfully produce the inner and outer tubes that are required for testing, evaluation and production of Navy HTSDG cryostats. The second phase would allow Southwire to expand production into other cryogenic cable markets outside of the Navy. A schematic of the complete proposed upgraded cryostat production line is shown in Figure 4-4.

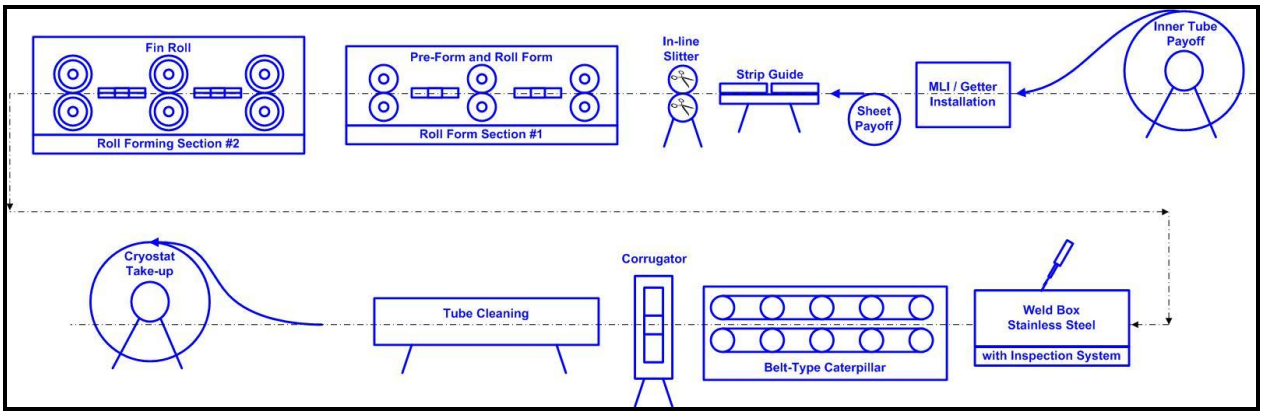

Figure 4-4. Schematic of proposed production line upgrade.

The upgrade detailed in Figure 4-4 would be used to form, weld and corrugate both the inner and outer tubes of the HTSDG cryostat. After the inner tube is complete, it would be fed back through the production line from a payoff (spool), where the MLI and spacers would be wrapped around the inner tube and the getters distributed throughout the length of tubing. The entire subassembly would then proceed through the line where the outer tube would be formed, welded and corrugated around the inner tube/MLI subassembly. Note that the manufacturing upgrade recommendations and cost estimate provided by W&S did not include any aspects of the cryostat insulation system.

4.1.3 CRYOSTAT CORRUGATION PROFILE DEVELOPMENT

The following sections provide the overall results of the various tasks that were part of the cryostat corrugation profile development effort. Additional details regarding this work can be found in the following Appendices:

- Appendix G: Numerical Analysis of the Weber & Scher Forming Process
- Appendix H: Preliminary Numerical Study to Determine Key Process Parameters
- Appendix I: Development of the Cryostat Corrugation Profile Design Bounds
- Appendix J: LCF Specimen Preparation and Test Matrix

4.1.3.1 Characterization of 316L Stainless Steel Mechanical Properties

To supply the FEA with the material data needed to perform the analyses, tensile testing was performed on annealed Type 316L sheet using two different thicknesses of material.

Engineering stress/strain plots for representative samples from this testing are shown in Figure 45. True stress/strain data were calculated from these tests, and are shown in Figure 46.

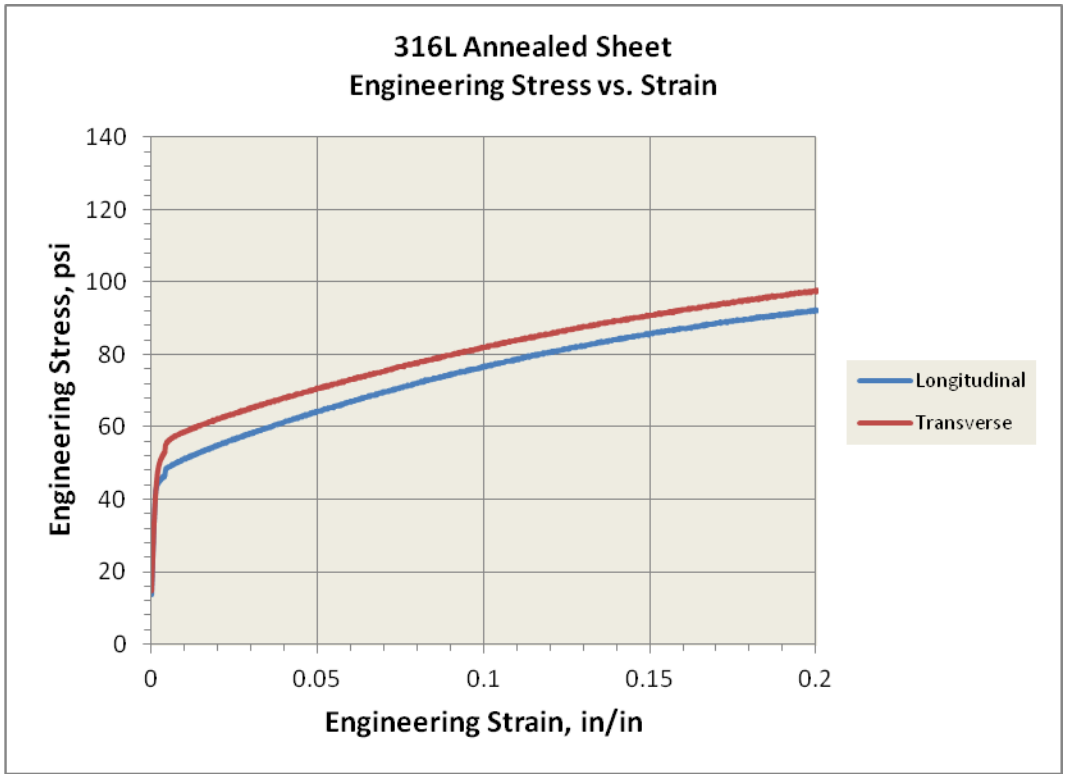

Figure 4-5. Engineering stress/strain curves for 0.015–inch-thick 316L annealed stainless steel strip, longitudinal and transverse directions.

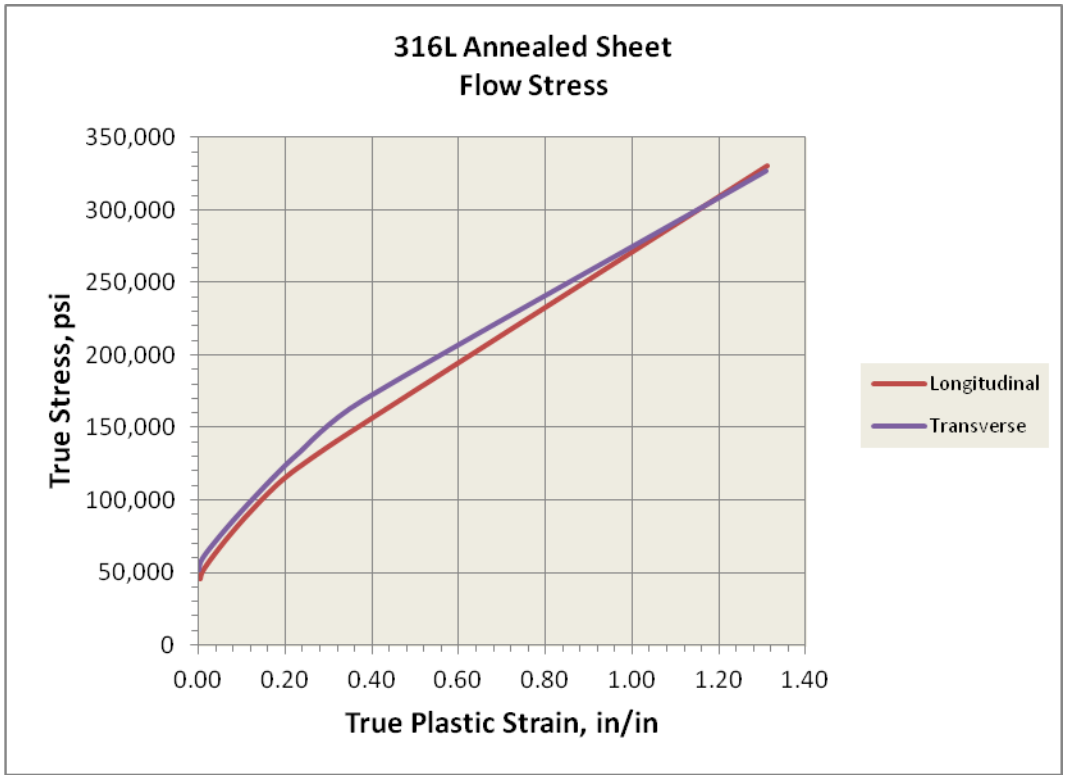

Figure 4-6. Flow stress curves for 0.015–inch-thick 316L annealed stainless steel strip, longitudinal and transverse directions.

4.1.3.2 Characterization of Low Cycle Fatigue (LCF) Specimen Material

In order to complete LCF testing, tensile testing was on annealed Type 316L sheet material in 3/16-inch thickness. Engineering stress/strain plots for representative samples from this testing are shown in Figure 4-7. Tabular results of this testing are shown in Table 4-3. True stress versus true plastic strain data were calculated from these tests and are shown in Figure 4-8. In both of these figures, Y represents the longitudinal direction and X the transverse.

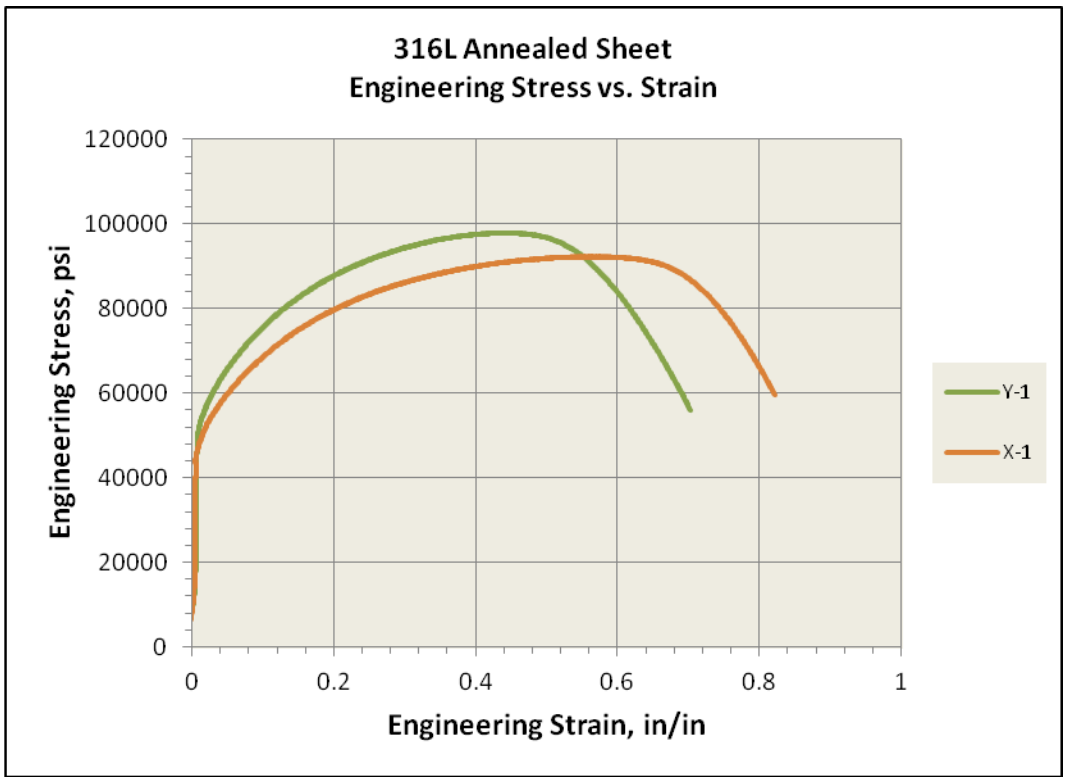

Figure 4-7. Engineering stress/strain curves for 3/16–inch-thick 316L annealed stainless steel sheet, longitudinal and transverse directions.

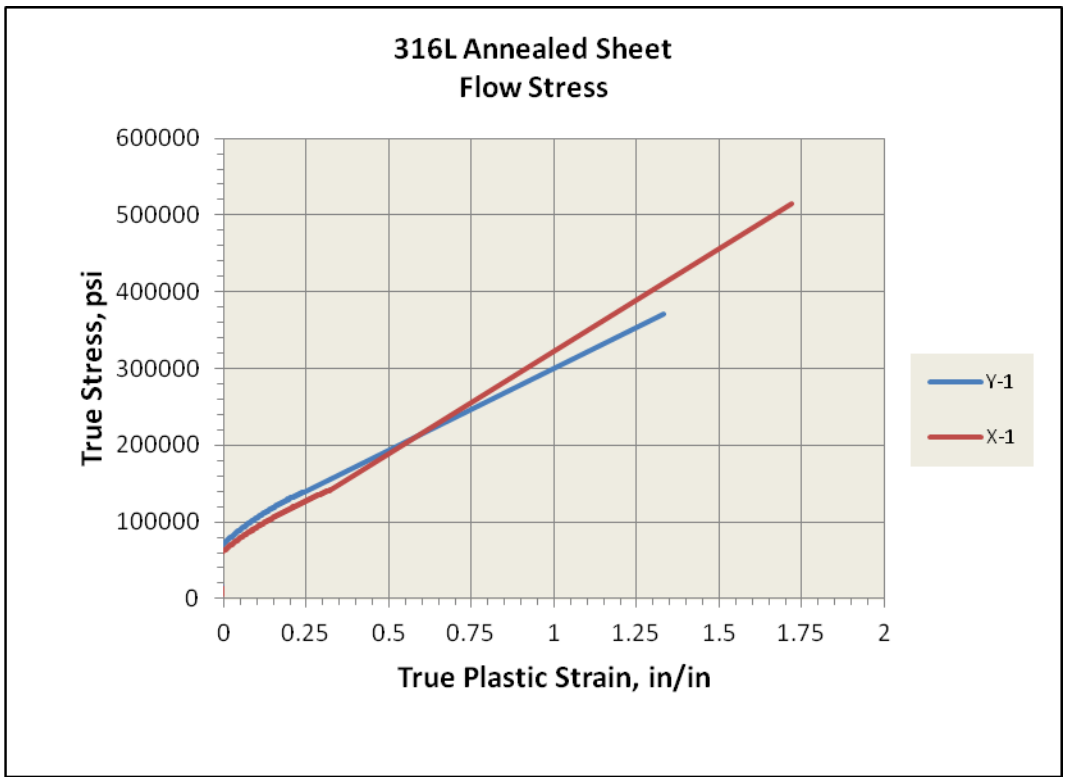

Figure 4-8. Flow stress curves for 3/16–inch-thick 316L annealed stainless steel sheet, longitudinal and transverse directions.

Table 4-3. Summary of Mechanical Properties for 3/16–inch-Thick 316L Annealed Stainless Steel Sheet, Longitudinal and Transverse Directions

Specimen Identification	Ultimate Tensile Strength	0.2% Offset Yield Strength	Elongation Increase	Reduction of Area
	(ksi)	(ksi)	(%)	(%)
X-1	94.9	44.6	80.0	82.1
X-2	95.1	42.4	80.0	82.7
X-3	95.3	44.4	78.0	82.0
Average	**95.1**	**43.8**	**79.3**	**82.3**
Y-1	100.6	49.8	70.0	73.6
Y-2	100.0	47.1	74.0	78.4
Y-3	99.5	45.7	74.0	79.8
Average	**100.0**	**47.5**	**72.7**	**77.3**

4.1.3.3 Three Roller Corrugation Concept

Initial investigations into possible corrugating processes included evaluation of an externally applied, three roller process. NMC developed a finite element model for this process which showed, like the physical trials, that the process would not produce satisfactory results. Thus, details of this analysis and the results are not included in this report as the concept was quickly dismissed.

4.1.3.4 Weber & Scher Corrugation Process

Numerical forming simulations were developed using the W&S annular corrugating die geometry and process parameters as discussed in detail in Appendix G. A baseline process model was developed using geometry based on W&S drawings. This model was validated by comparing the resulting net shape of the corrugated tube as predicted by the FEA model to a physical specimen provided by W&S. The process model accurately predicted the final net shape and the process parameters were representative of typical W&S practices. Therefore, the process model was considered valid and capable of accurately predicting the as-formed configuration for cryostat profile development.

4.1.3.5 Preliminary Numerical Study to Determine Key Process Parameters

In order to determine the important corrugation design parameters and their influence on bending and forming strain, a series of preliminary analysis studies was conducted. The following conclusions pertaining to the effect of key corrugation design parameters on the resulting bending and forming strains can be drawn based on the analyses presented in Appendix H:

- Shorter corrugation pitch results in more forming strain than longer pitch
- Shorter corrugation pitch results in less bending strain than longer pitch, but the lower bending strains may not outweigh the increase in forming strains until a significant number of bends have been reached
- The relationship between corrugation height and resulting valley plastic strain from forming is not necessarily linear. For the particular profile parameters analyzed, shallow corrugations resulted in more valley strain and deeper corrugations resulted in a more even strain distribution between the peaks and valleys.

- Deeper corrugations, even with a longer pitch, result in significantly less bending strain than shallow corrugations with a shorter pitch
- Corrugation depth has a much more significant effect on bending strain than corrugation pitch
- Because the low-density polyethylene (LDPE) coating is not bonded to the tube, both the presence of the LDPE coating and the LDPE material properties have little effect on bending strain
- There were no apparent benefits to utilizing the helical corrugation designs in flexible cryostat applications.

4.1.3.6 Development of the Cryostat Corrugation Profile Design Bounds

With an understanding of how the various corrugation profile design parameters affect the resulting strain levels and flexibility, NMC analysts determined that the most important design parameter was corrugation height. They also determined that the corrugation height was limited by two requirements: physical size and thermal performance. The physical size requirements dictated by NSWCCD impose limits on the outer diameter of the outer tube and the inner diameter of the inner tube. Thermal performance requirements dictate the amount of space required for insulation between the two tubes. A detailed discussion on the development of the cryostat corrugation profile design bounds can be found in Appendix I. The key takeaways from that discussion are:

- An insulation space of 0.25 inch (6.4 mm) should be used as the minimum space allowance for both the 2.75-inch and 1.75-inch class cryostat designs based on the thermal performance of Fluffy and Tiger (Section 3.3.2, Fabrication and Testing of 5-meter Prototype Cryostats).
- Within the corrugation height design bounds, the forming strains will generally be between 60% and 80% in the valleys and 15% and 40% in the peaks.

4.1.3.7 Low Cycle Fatigue Testing

Low cycle fatigue (LCF) testing was conducted in order to predict the cryostat fatigue life (number of bends to failure) based on the analytical results. Cyclic loading was uniaxial and

fully reversing with initial straining in the tensile direction. In order to achieve the most meaningful results, testing was conducted on the following representative material samples:

- Annealed 316L material
- Annealed 316L material with a transverse weld
- Annealed 316L material that has been subjected to similar pre-strain conditions as the cryostats
- Annealed 316L material with a transverse weld, which has been subjected to similar pre-strain conditions as the cryostats.

An in-depth discussion on specimen preparation and a detailed test matrix containing strain amplitude, cycle life and fracture locations for each specimen, as well as post-test photographs of each specimen, can be found in Appendix K.

A graphical summary of the test data is shown in Figure 4-9. The following conclusions can be drawn from the test data.

- The base metal and welded specimens in the unstrained and 15% tensile pre-strained condition exhibited little scatter.
- However, the indentation pre-strained specimens (40–60% pre-strain) showed considerable scatter. This is largely attributed to gage area skew as detailed in Appendix J.
- There is no evidence that pre-strain nor transverse weld adversely affected fatigue performance for the strain ranges tested.

These conclusions are further reinforced by similar observations found in literature references. More specifically, other researchers have shown that the effect of static pre-strain on LCF performance may only be noticeable at very low strain amplitudes [7] and that the LCF performance of weld deposited material and base metal material do not differ significantly [8].

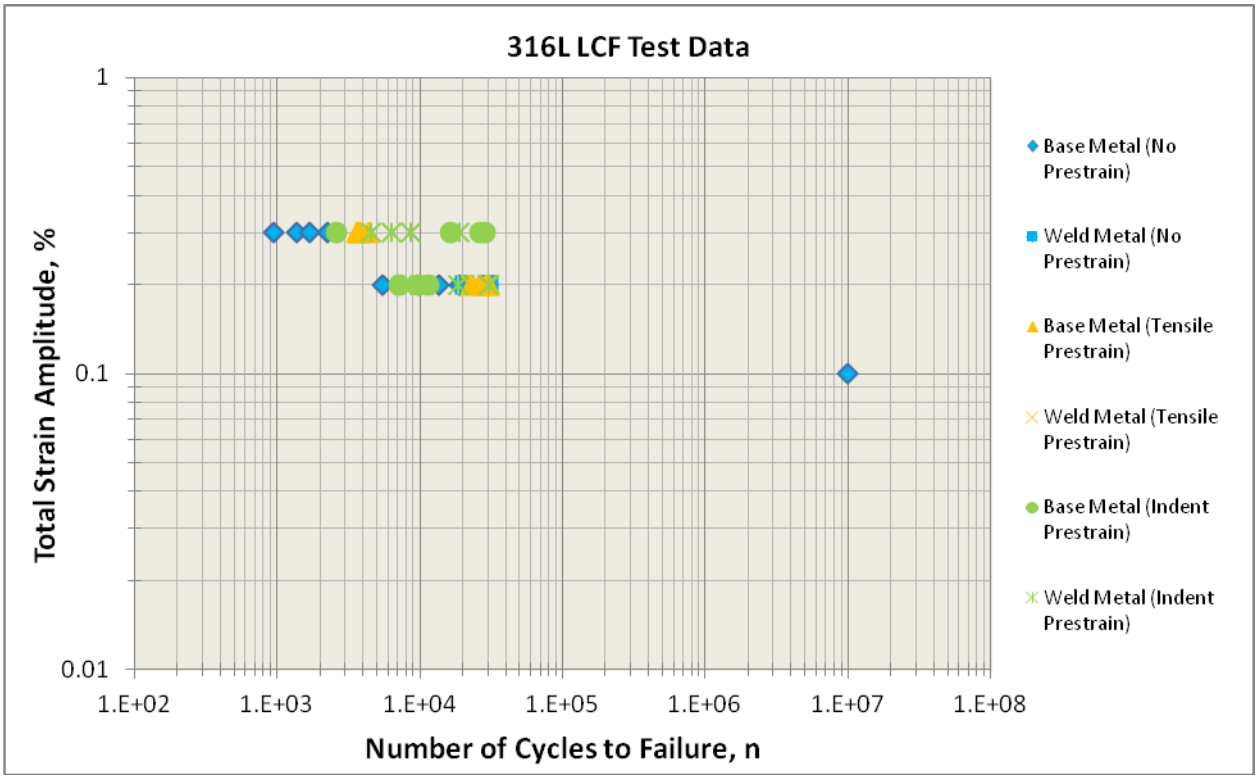

Figure 4-9. Number of cycles to failure vs. total strain amplitude for the 316L test specimens.

Rather than extrapolating the test data to the appropriate strain ranges, additional high and low cycle fatigue data were obtained from literature references. Figure 4-10 shows a combined plot that includes both the LCF and literature data. An overall best fit curve was calculated using a least squares method assuming the functional form shown in equation 1 where ε is the strain amplitude, n is the number of cycles to failure, and x, y, and z are the shape optimization parameters. The curve of best fit converged to the following x, y, and z parameters, respectively: 16.0, -0.47, and 0.10.

$$\varepsilon = xn^{y} + z \tag{1}$$

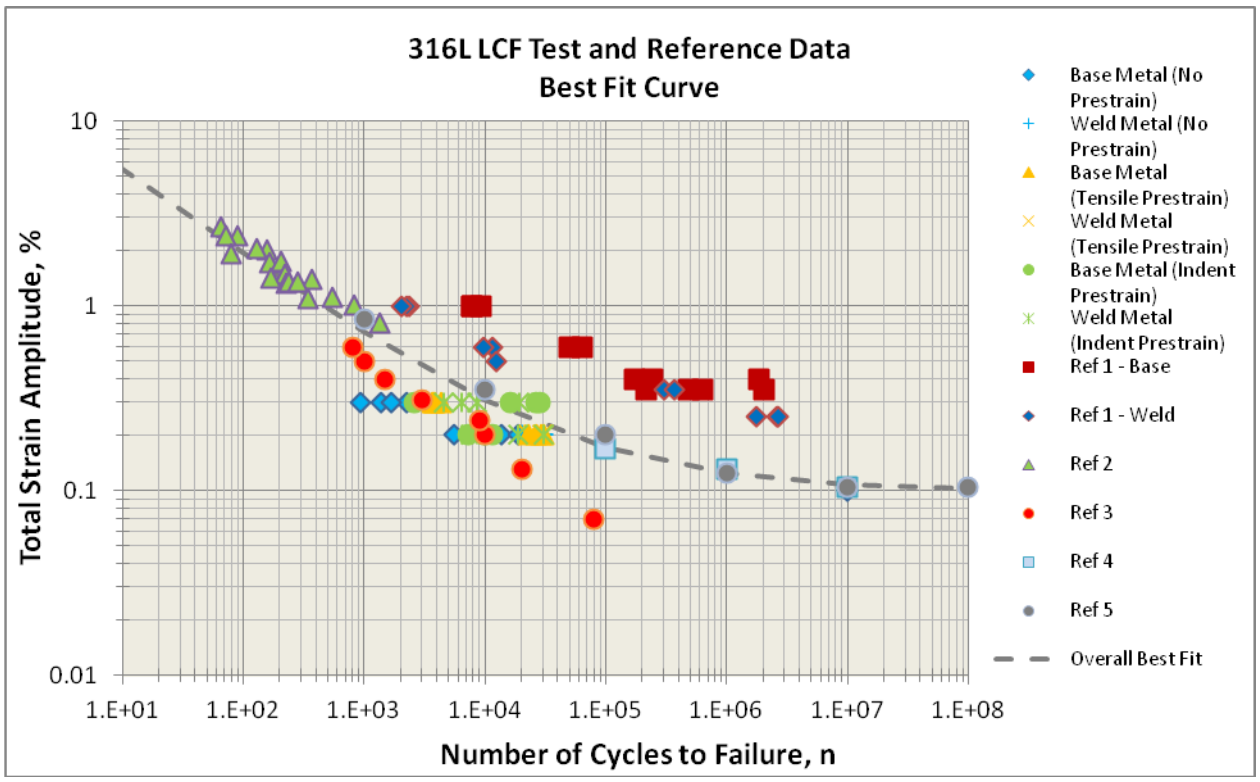

Figure 4-10. Combined plot showing test and literature fatigue data and an overall best fit curve.

Two additional best fit fatigue curves based on ASME and Argonne National Laboratory (ANL) testing were obtained from literature [9] and used for comparison as shown in Figure 4-11. Table 4-4 compares the number of cycles to failure for the three curves at various strain amplitudes. The present fatigue data are shown to be more conservative across the entire strain range.

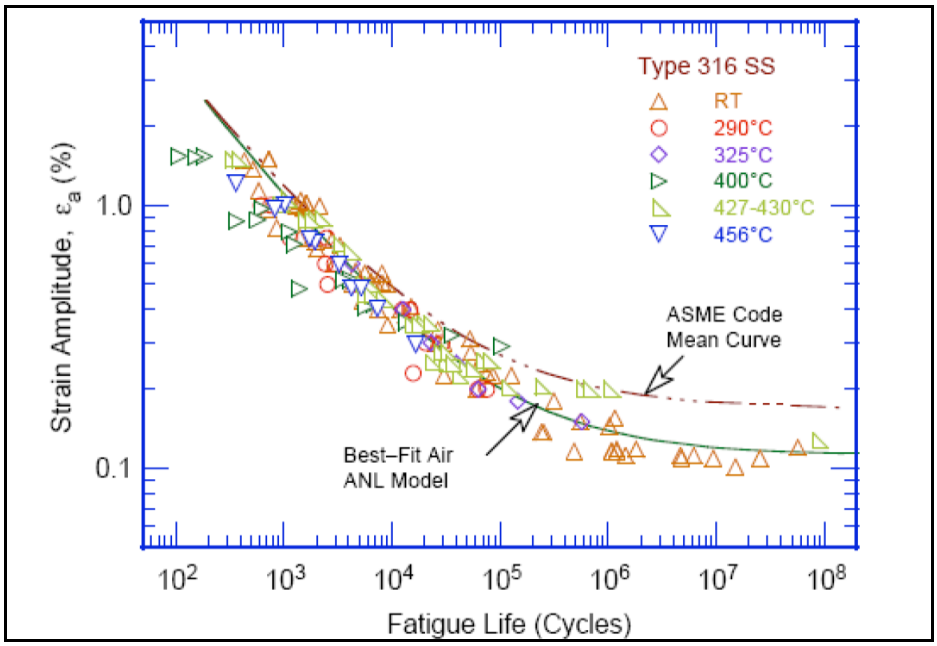

Figure 4-11. ASME and ANL fatigue design curves.

Table 4-4. Comparison of Number of Cycles to Failure for Given Strain Amplitudes of Three Fatigue Curves

Strain Amplitude	NMC Best Fit	ASME Code Mean Curve	ANL Model
5.0	12	N/A	N/A
4.0	20	80	80
3.0	38	130	130
2.0	93	300	300
1.0	456	1,100	1,300
0.75	912	2,000	3,000
0.50	2,560	6,000	10,000
0.25	20,700	55,000	170,000

4.1.3.8 Profile Optimization and Correlation with LCF Data

Based on the findings from the LCF testing, corrugation profile optimization was completed with little consideration given to minimizing forming strains. Instead, the primary design objective was to minimize cyclic bending strain while staying within the given design requirements outlined in Section 3.1, Cryostat Requirements. A series of iterative FEA

simulations was conducted and the resulting optimized profile dimensions are summarized in Table 4-5. Figure 412 and Figure 413 visually present the optimized corrugation profiles.

Table 4-5. Optimized Corrugation Profile Dimensions (inches)

		2.75-inch Class	1.75-inch Class
Required Insulation Thickness		0.25	0.25
Required Coating Thickness		0.075	0.075
Outer Tube	Required Cryostat OD	2.75	1.75
	Tube OD	2.600	1.600
	Tube ID	2.225	1.400
	Tube Wall Thickness	0.0164	0.0149
	Corrugation Height	0.188	0.100
	Corrugation Pitch	0.375	0.180
	Corrugation Radii	0.102	0.053
Inner Tube	Required Cryostat ID	1.50	0.80
	Tube OD	1.725	0.900
	Tube ID	1.500	0.800
	Tube Wall Thickness	0.0149	0.0097
	Corrugation Height	0.1125	0.0500
	Corrugation Pitch	0.260	0.120
	Corrugation Radii	0.075	0.038

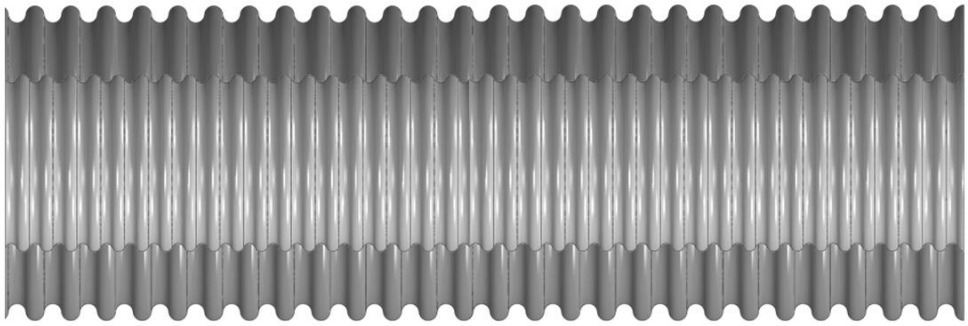

Figure 4-12. Optimized 1.75-inch class cryostat profile.

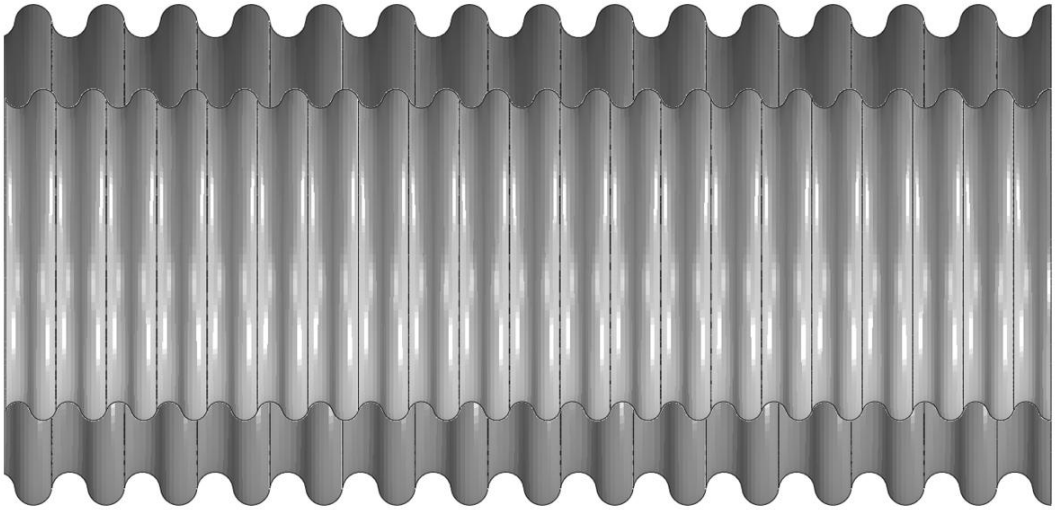

Figure 4-13. Optimized 2.75-inch class cryostat profile.

The contour plots of the optimized profiles showing plastic strain amplitude are shown in Figure 414 and Figure 4-15. At the minimum required bend radius, the maximum predicted bending strains for the 2.75-inch and 1.75-inch class cryostats were 1.9% (2.75-inch class) and 4.4% (1.75-inch class). Based on the LCF best fit curve, these strain amplitudes result in 104 and 16 bends to failure for the 2.75-inch and 1.75-inch class cryostats at the minimum required bend radius, respectively. These bends to failure for each class cryostat meet the 15 bend objective for the HTS cryostat. One bend is defined as starting from the initially straight position, bending up to the specified bend radius, and then back down to the straight position.

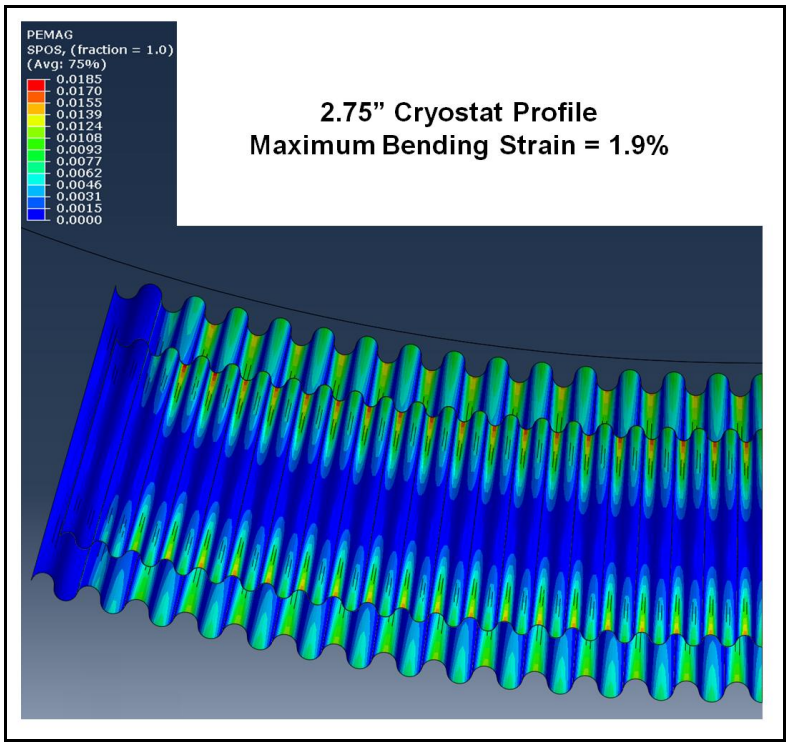

Figure 4-14. Contour plot of plastic strain amplitude at the minimum specified bend radius, 2.75-inch class cryostat.

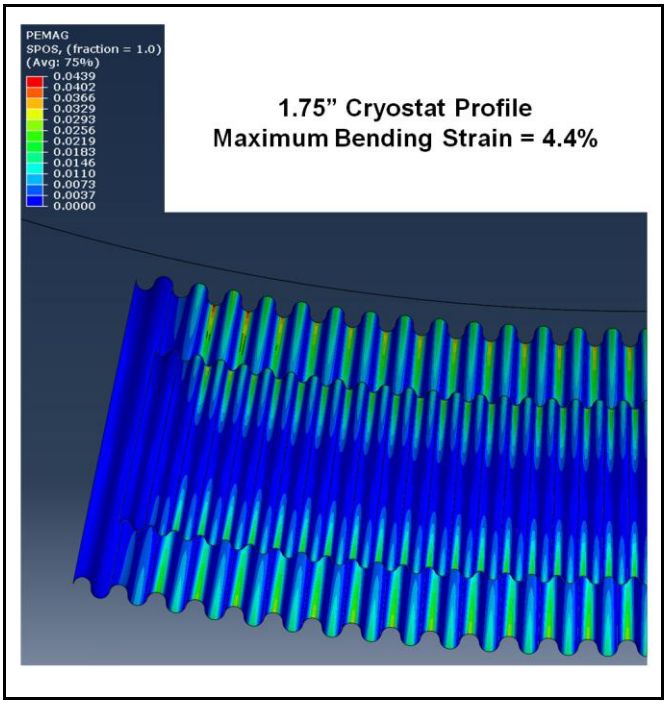

Figure 4-15. Contour plot of plastic strain amplitude at the minimum specified bend radius, 1.75-inch class cryostat.

4.1.3.9 Verification of Operating and Burst Pressure

As a final check, a pressure analysis was conducted on the optimized corrugation profiles. Both the operating and burst pressures were evaluated. For the operating pressure, 300 psi was applied to the inner tube and the resulting stresses were compared to the room temperature yield strength for annealed Type 316L stainless steel. The burst pressure was evaluated by first subjecting the tube to one bend cycle followed by pressurization until failure. Table 4-6 summarizes the operating pressure and burst pressure safety factors for both cryostat classes.

Table 4-6. Operating and Burst Pressure Safety Factors

	2.75-inch Class	1.75-inch Class
Material Yield Stress (ksi) [10]	26	26
Stress from Internal Pressure (ksi)	13.9	11.2
Safety Factor (yield/predicted)	**1.9**	**2.3**
Specified Minimum Burst Pressure (psi)	1000	1000
Predicted Burst Pressure (psi)	1846	2193
Safety Factor (predicted/allowable)	**1.8**	**2.2**

4.1.3.10 Cryostat Weight Estimates

The inner and outer corrugated tube weight estimates are given below. Final weight estimates will be dependent on the down-selected MLI materials and stack-up geometry.

- 2.75-inch Class = 0.5 lb/ft (only two tubes, no plastic coating, insulation, etc.)
  Target ≤ 1.25 lb/ft
- 1.75-inch class = 0.24 lb/ft (only two tubes, no plastic coating, insulation, etc.)
  Target ≤ 0.75 lb/ft

4.1.4 FRACTURE ANALYSIS OF LCF SPECIMENS

Fatigue failure is usually initiated at regions with a high level of stress when the component is subjected to cyclic stresses of sufficient magnitude. Microscopically, the nucleation of cracks is the most important feature that occurs under the influence of reverse

stresses that exceed the flow stress of the material. Once the cracks are nucleated, they grow at the slip bands and grain boundaries and propagate by a series of cyclic opening and closing motions at the crack tip perpendicular to the direction of the crack growth. Based on this sequence of events, three stages for fatigue failure are universally characterized: 1) crack nucleation by initial fatigue damage, 2) progressive cyclic growth (beach marks), and 3) un-sustained load that leads to sudden fracture (fast shear fracture). Another factor that is very important to fatigue life is the state of residual stresses in the component. In the present case, the tensile and compressive stresses that develop during corrugation of the Type 316L welded tube will play an important role in the LCF life of the cryostat.

Plastic strain is of paramount importance in cyclic fatigue and has a major influence in the number of cycles to failure. In low cycle fatigue, the plastic component of strain dominates the material behavior. This indicates that the level of pre-strain (compression or tension) and ductility of the material will have a direct influence on the low cycle fatigue. Therefore, the objective of this work was to qualitatively analyze the magnitude of the effect of pre-strain on the fatigue life of representative baseline and welded Type 316L stainless steel sheet specimens, as well as to characterize their fractures and microstructures after testing.

Table 4-7 shows the specimens that were selected for fracture and microstructural analyses. The table also identifies the level of pre-strain (tensile and compressive) of each specimen, the strain amplitude, the number of cycles to failure and LCF frequency. The results for the Type 316L base metal and weldment analyses are summarized in the following sections.

Table 4-7. Fatigue Specimens Used for Fracture and Microstructural Analyses

Specimen ID	Material Condition	Orient.	Actual Pre-strain	Strain Amplitude	No. Cycles	Test Freq (Hz)	Comments
B1	Base Metal No Pre-strain	L	0%	0.1%	10,000	1.00	Run out, no fracture
B3		L	0%	0.2%	13,630	0.50	Fracture in gage length
B4		L	0%	0.3%	942	0.33	Fracture at edge of gage length
B13	Base Metal w/Tensile Pre-strain	L	15%	0.2%	29,412	0.50	Fracture at edge of gage length
B16		L	15%	0.2%	30,800	1.00	Run out, no fracture
B17		L	15%	0.3%	3,813	1.00	Fracture at edge of gage length
L6	Base Metal w/Compressive Pre-strain	L	41%	0.3%	2,631	1.00	Fracture at edge of gage length
L7		L	59%	0.3%	28,748	1.00	Fracture in gage length
W15	Welded No Pre-strain	T	0%	0.2%	30,800	0.50	Run out, no fracture
W16		T	0%	0.2%	20,480	0.50	Fracture in gage length
W17	Welded w/Tensile Pre-strain	T	15%	0.2%	30,000	1.00	Run out, no fracture
W18		T	15%	0.2%	25,092	1.00	Fracture in gage length
W3	Welded w/Compressive Pre-strain	T	40%	0.2%	7,665	1.00	Fracture in gage length
W4		T	41%	0.2%	18,714	1.00	Fracture at edge of gage length
W5		T	39%	0.2%	30,800	1.00	Run out, no fracture
W7		T	57%	0.3%	19,111	1.00	Fracture in gage length
W9		T	59%	0.3%	4,512	1.00	Fracture at edge of gage length

4.1.4.1 Base Metal Specimens, No Pre-Strain

All specimens were to be tested for 10,000 cycles or until failure. Those specimens that survived 10,000 cycles without failure have been highlighted in pink in Table 4-7. Figure 4-16(a) shows the run-out specimen for the base metal specimen without pre-strain. Multiple

crack initiation sites are present at the surface of the sheet. The cracks were initiated primarily at surface gashes and other deep irregularities on the surface. However, in this case the crack initiation sites were not formed at the machining or grinding marks that run perpendicular to the crack initiation fatigue lines.

For the other base metal specimens without pre-strain, the fatigue fracture occurred in a ductile mode. The crack propagation rate was dependant on the strain amplitude. The presence of multiple beach marks was characteristic of the slow fatigue crack growth observed in the material with the low strain amplitude (Figure 4-16(b)). Fewer or no beach marks were observed in the material with higher strain amplitude (Figure 4-16(c)). In each instance, a shear-like crack propagated quickly once the material could not sustain the applied load.

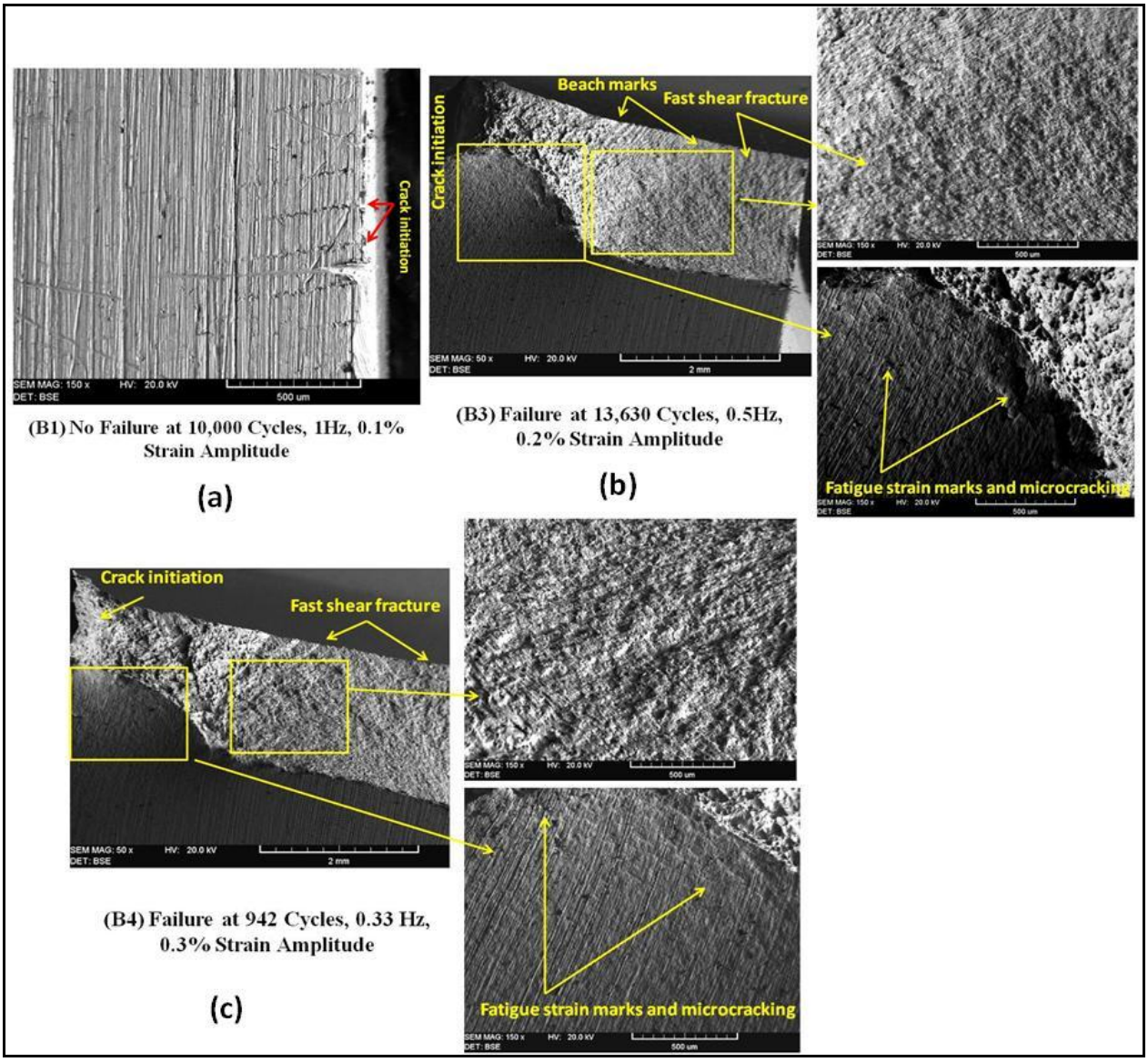

Figure 4-16. SEM of LCF specimens; base metal, no pre-strain.

4.1.4.2 Base Metal Specimens, 15% Tensile Pre-Strain

Figure 4-17 shows the effect of 15% tensile pre-strain on the LCF fracture of the base metal material. Similar to the material without pre-strain, the cracks were initiated at the deep surface gashes and fracture also occurred in a ductile mode. However, the pre-strained material showed the presence of a surface texture with microscopic hairline cracks. This can be observed in the run-out specimen shown in Figure 4-17(a). This effect was induced by the combination of the tensile pre-strain and shear stresses induced by the cyclic fatigue stresses.

Figure 4-17(b) shows that the pre-strained specimen tested at 0.2% strain amplitude had wider beach marks than those observed in the material without pre-strain. Increasing the strain amplitude to 0.3% decreased the number of cycles to failure; however, the fracture initiation site appeared to occur towards the center of the sample as shown in Figure 4-17(c).

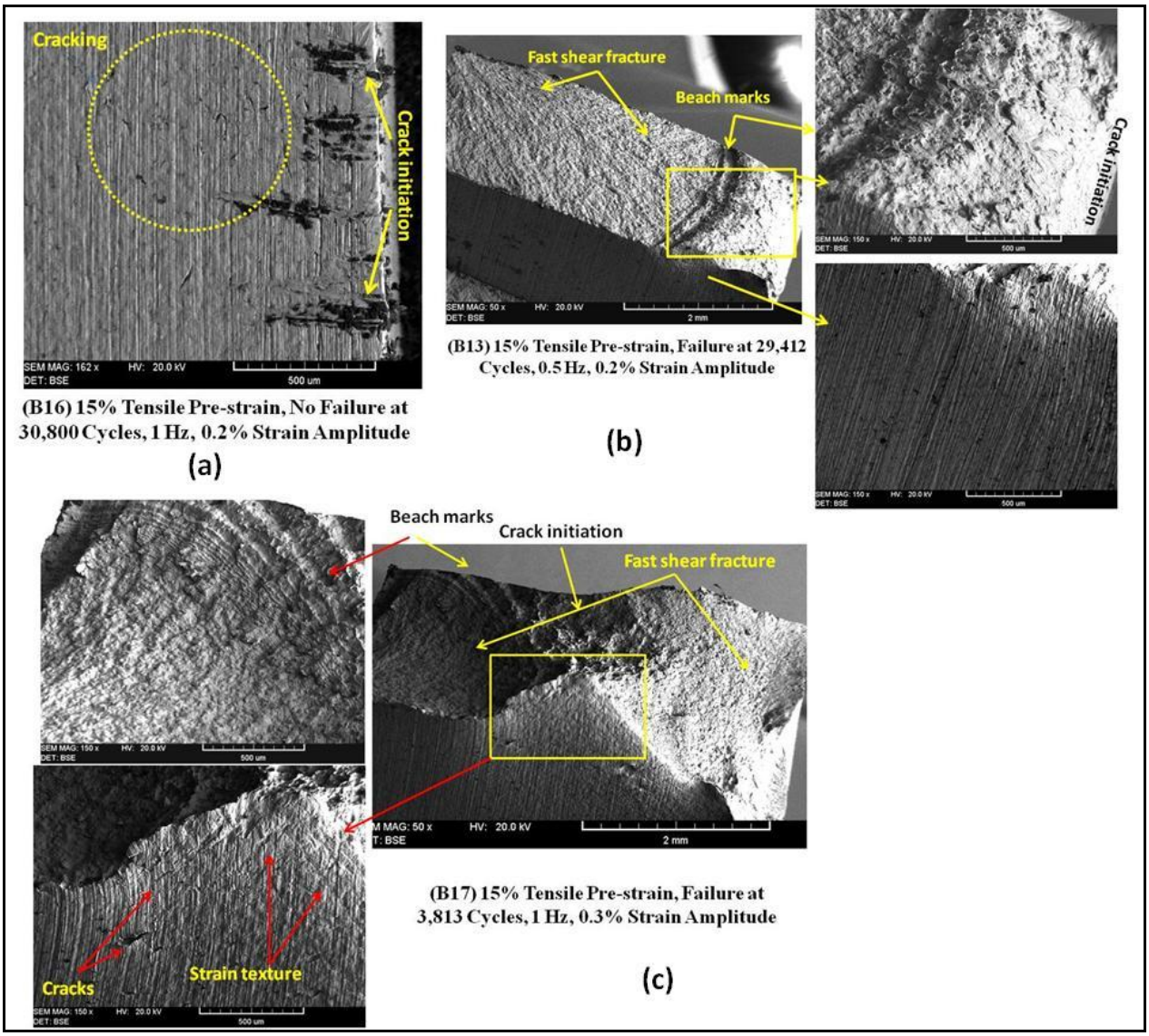

Figure 4-17. SEM of LCF specimens; base metal, 15% tensile pre-strain.

4.1.4.3 Base Metal Specimens, 41% and 59% Compressive Pre-Strain

The LCF fracture behavior of 41% and 59% compressive pre-strain, base metal specimens was also of a ductile mode. However, no correlation was found between the number of cycles to failure and the amount of pre-strain and strain amplitude. The fracture appearance was irregular as illustrated in Figure 4-18. These samples were tested at a strain amplitude of 0.3% with pre-strains of 41% and 59%. The sample with lower pre-strain had the lowest number of cycles to failure (Figure 4-18 (b)). Interestingly, the sample with 59% pre-strain had the highest number of cycles to failure of the entire group, and the fatigue marks showed localized

cyclic shear bands indicating slow crack growth at the surface (Figure 4-18 (a)). The sample with 41% pre-strain had a larger number of microcracks and fatigue strain marks at the surface of the sample, as well as a well-defined region of tensile ductile-like dimples towards the center of the sample. This region was surrounded by a very fine shear appearance indicating that the fracture occurred relatively quickly.

The irregular fracture behavior of the compressive pre-strain material indicates that the samples had an irregular distribution of stresses that were produced during the indentation forming process. This effect is also responsible for the large variation in the number of cycles to failure for a given strain amplitude observed in this type of pre-strained material. However, the LCF life of the compressive pre-strain (indented) material improved slightly over the LCF of the base metal without pre-strain (Figure 4-16).

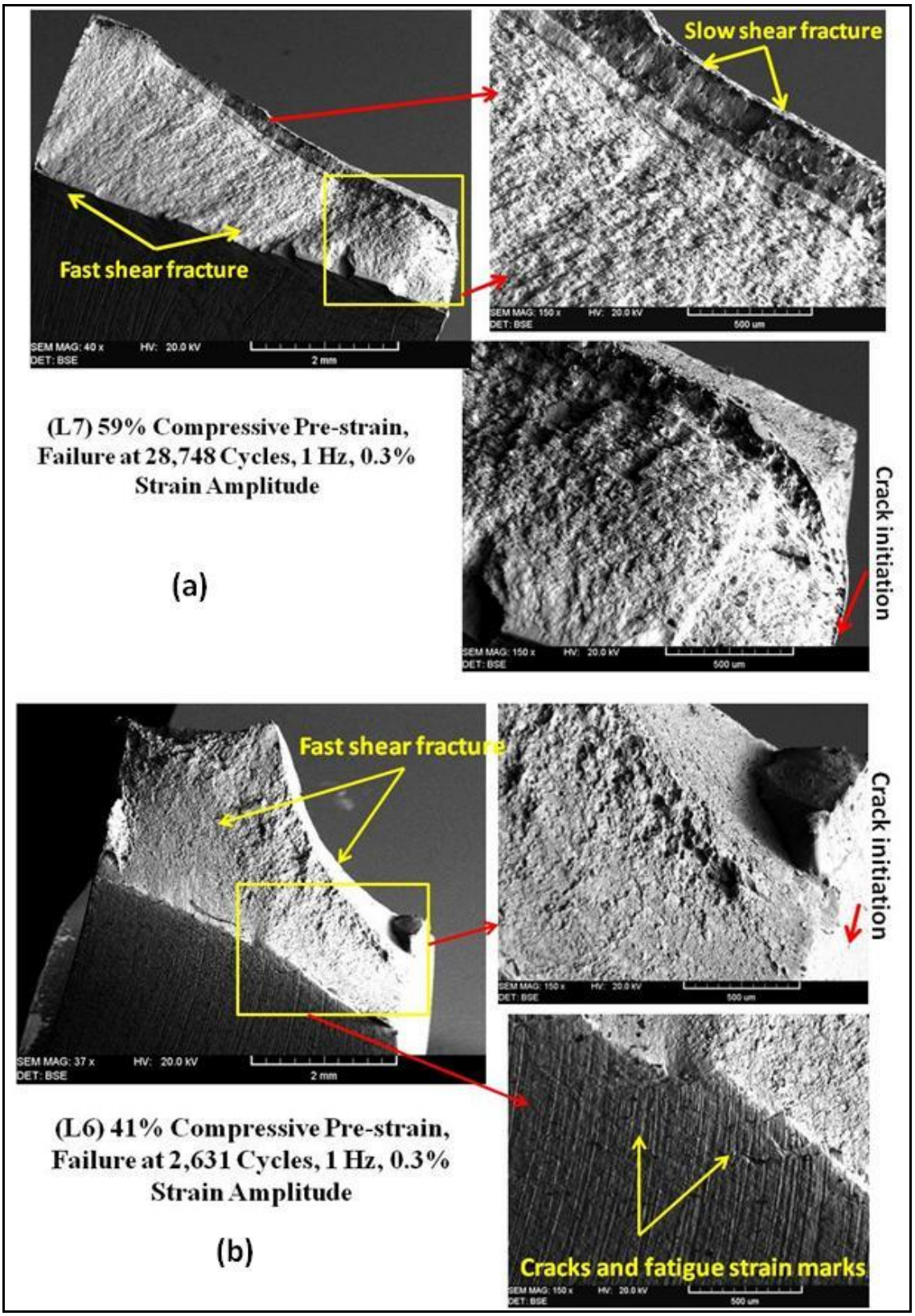

Figure 4-18. SEM of LCF specimens; base metal, 41% and 59% compressive pre-strain.

4.1.4.4 Weldment, No Pre-Strain

Figure 4-19(a) shows the surface crack initiation site of the run-out weldment fatigue specimen. Although the specimen was cycled to 30,800 cycles, the specimen did not fracture; however, the presence of periodically spaced hairline cracks was observed. The other weldment, also cycled at 2% strain amplitude, fractured at 20,480 cycles. In this case, the heavy and irregular deformation pattern at the crack initiation site seen in Figure 4-19(b) indicates that the crack initiated at the heat affected zone (HAZ) and propagated in an irregular manner through the weld metal.

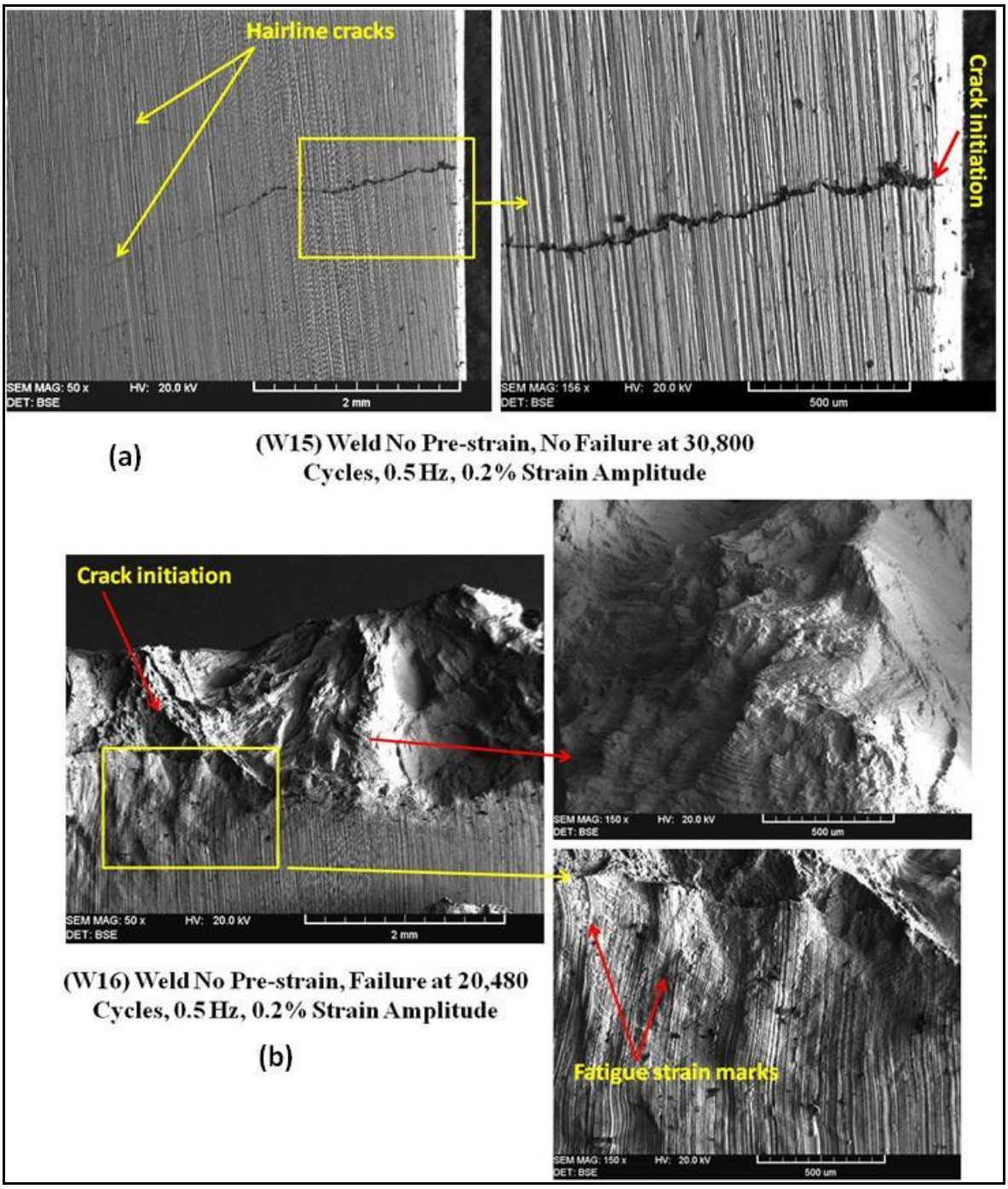

Figure 4-19. SEM of LCF specimens; weldment, no pre-strain.

4.1.4.5 Weldment, 15% Tensile Pre-Strain

Figure 4-20 shows the fatigue crack behavior of specimens with 15% tensile pre-strain cycled at 0.2% of strain amplitude. The run-out specimen shows that the crack initiated at gashes on the surface (Figure 4-20(a)). However, the presence of very irregular regions of deformation at the weld is clearly seen on the surface. This irregular strain texture is due to the "as-cast structure" of the weld; i.e., there is not a preferential crystal orientation as seen in the base metal (Figure 4-17). The pre-strain contributed to the periodic and extensive cracking of the surface seen in Figure 4-20(b) for the sample that fractured at 25,092 cycles. Also, in this case the fracture has multiple initiation sites and is predominantly shear-like but ductile.

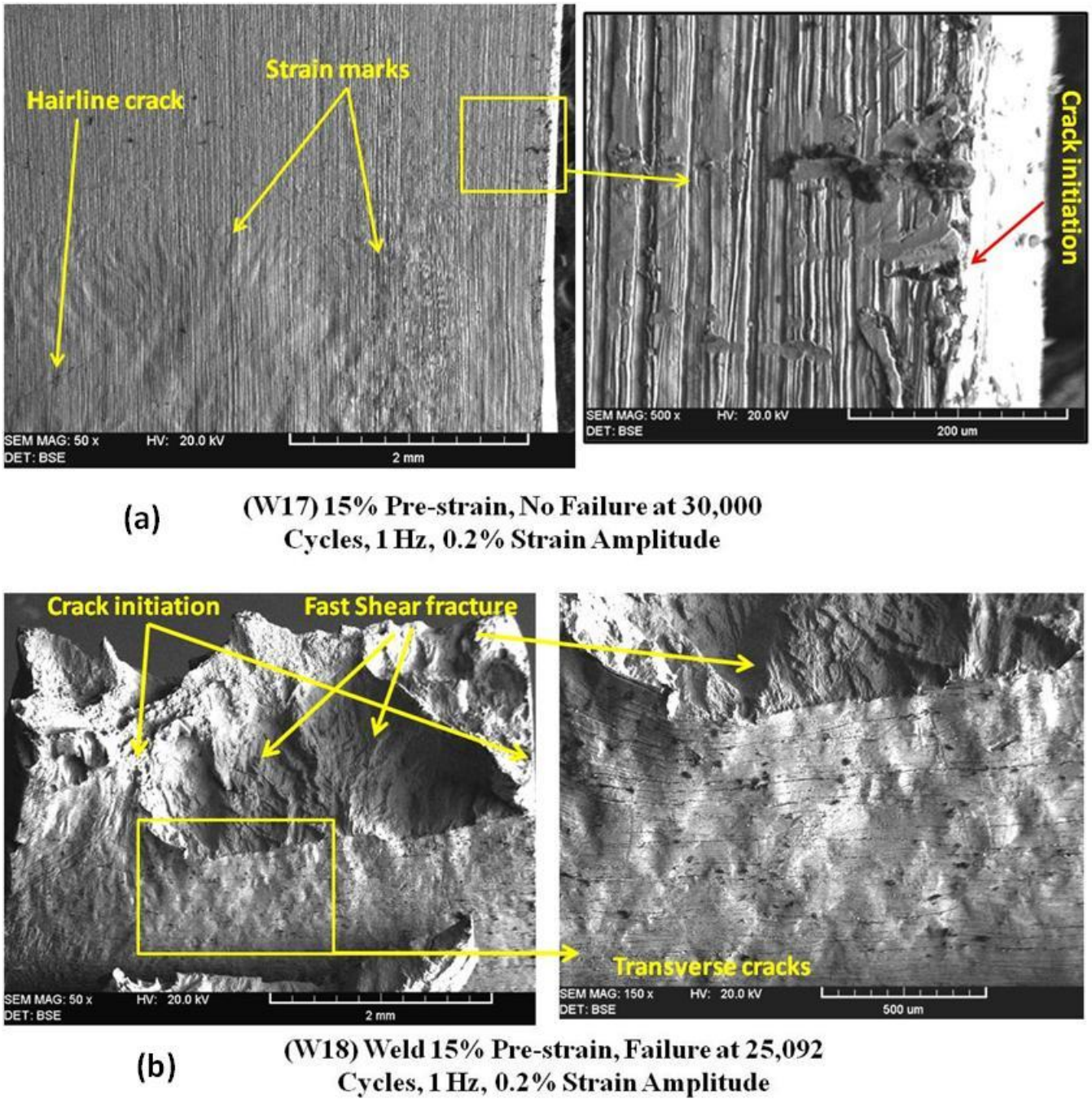

Figure 4-20. SEM of LCF specimens; weldment, 15% tensile pre-strain.

4.1.4.6 Weldment, 35–59% Compressive Pre-Strain

Figure 4-21 and Figure 4-22 show the LCF specimens tested at 0.2% and 0.3% strain amplitude, respectively. Figure 4-21(a) shows that the run-out specimen with a pre-strain of 39% did not appear to have any surface strain marks at the weld region after 30,800 cycles, but microscopic or hairline cracks started to appear on the surface, possibly at the HAZ region in the base metal. However, the weldment with 40% pre-strain tested at the same 0.2% strain amplitude fractured at 7,665 cycles. This sample had multiple initiation sites and showed irregular crack propagation through the weld metal as seen in Figure 4-21(b). Extensive strain marks were also observed closer to the fracture surface. The large difference in fatigue life may be attributed to defects in the weld that were exacerbated by the indentation process used to pre-strain the specimen.

When tested at 0.3% strain amplitude levels, multiple crack initiation sites and very irregular crack propagation through the weld metal were observed. Figures 4-22(a) and (b) show the two specimens pre-strained at 57% and 59% that fractured at 19,111 cycles and 4,512 cycles, respectively. The large difference in fatigue life for the two samples may be attributed to internal and surface imperfections in the weld.

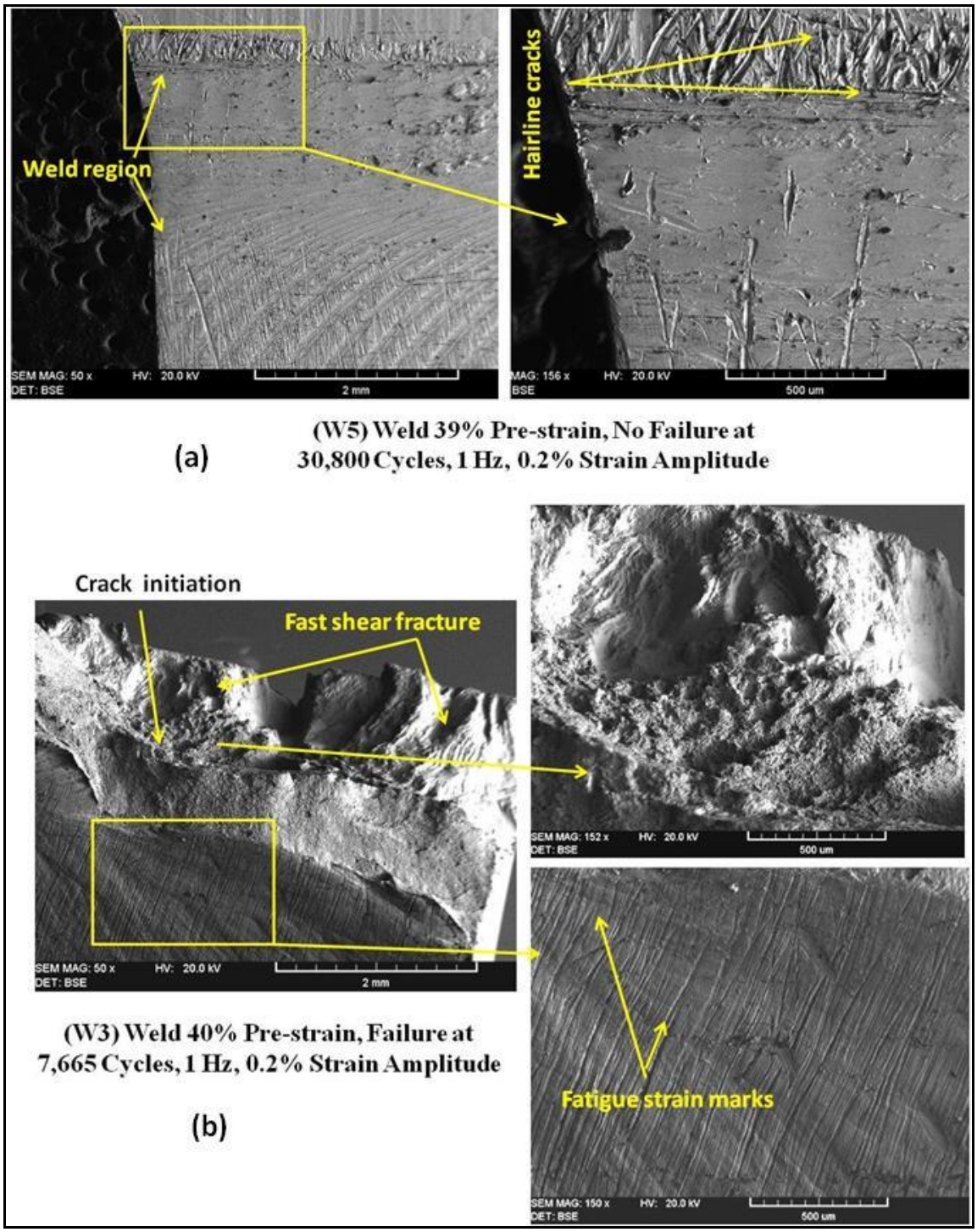

Figure 4-21. SEM of LCF specimens; weldment, compression pre-strain, 0.2% strain amplitude.

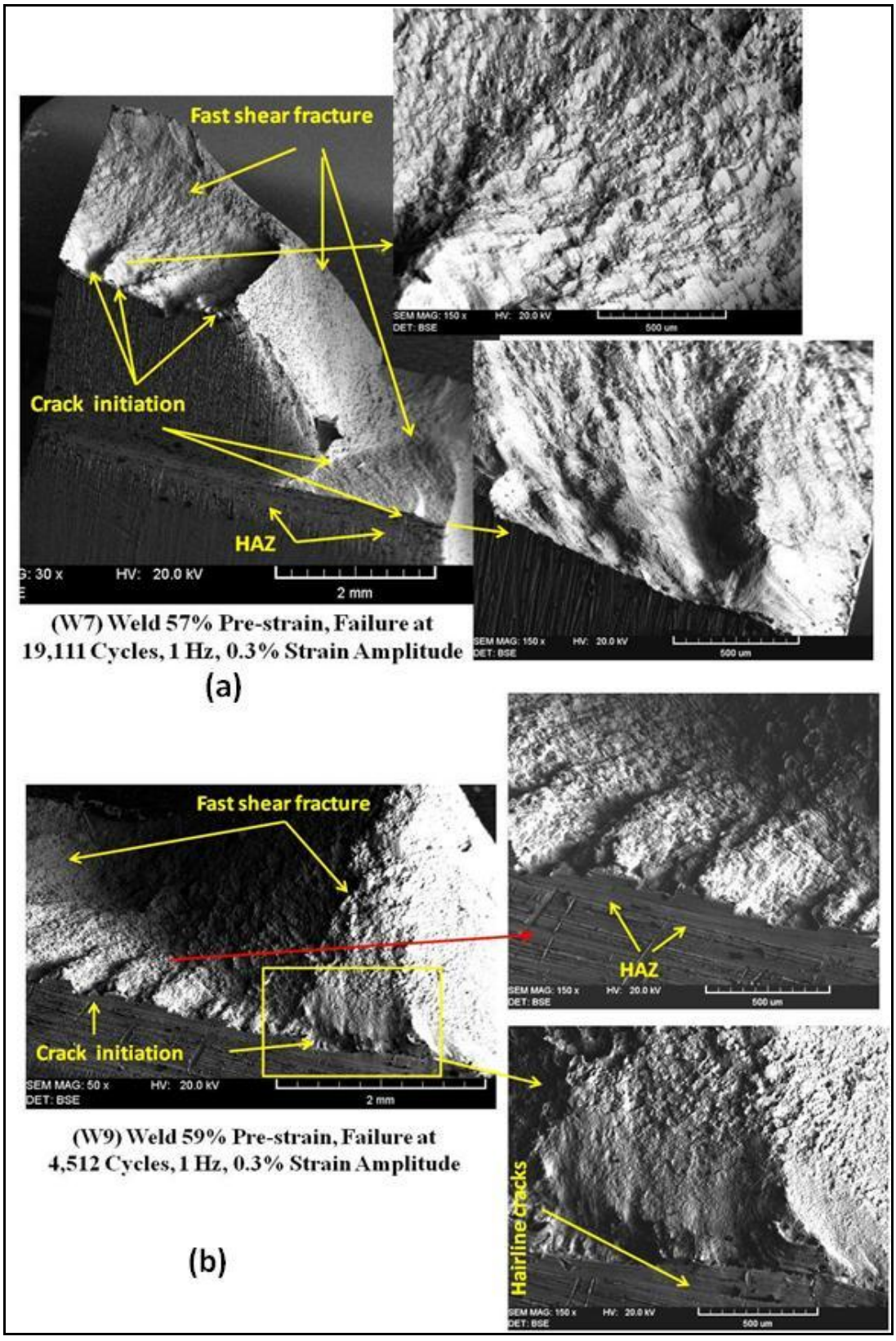

Figure 4-22. SEM of LCF specimens; weldment, pre-strain, 0.3% strain amplitude.

4.1.4.7 Fracture Analysis Summary

The results of the fracture analysis indicated that the level of tensile or compressive pre-strain had a direct influence on the LCF fracture behavior of the Type 316L base metal and weldments. In the case of the base metal specimens without pre-strain, the cracks were primarily initiated at deep surface gashes and a ductile mode of failure was observed. The specimens with tensile pre-strain also showed a ductile mode failure but the crack initiation most often occurred at the interior of the sample. In addition, failure occurred at a slightly higher number of cycles than was observed in the base metal. The compressive pre-strained specimens also showed a ductile failure mode. The irregular fracture behavior observed was primarily attributed to the irregular distribution of stresses produced by the indentation forming (pre-strain) process. Nevertheless, the LCF life of the compressive pre-strain specimens improved slightly over that of the unstrained base metal.

The weld metal without pre-strain showed a heavy and irregular deformation pattern at the crack initiation site with indications that cracking was initiated at the HAZ and propagated in an irregular manner through the weld metal. However, the LCF failure of these samples was ductile and very consistent. Also, this group of samples had the largest number of cycles without failure of all samples tested both with and without pre-strain. The weld samples with tensile pre-strain had very irregular regions of deformation due to the as-cast structure of the weld. The tensile pre-strain contributed to the periodic and extensive cracking of the surface where the cracks were initiated and propagated in a shear ductile manner. In the case of the samples with compressive pre-strain, the LCF the fracture was also ductile but the failure occurred from multiple initiation sites and showed irregular crack propagation through the weld metal. The large difference in fatigue life may be attributed to imperfections in the weld that were exacerbated by the indentation process used to pre-strain the specimen.

The findings in this work in conjunction with the FEA analysis indicate that the tensile and compressive stresses that develop during corrugation of the Type 316L welded tube will play an important role in the LCF life of the cryostat. In this case, either tensile or compressive stresses could produce variability in the LCF expectancy and failures would occur at high strain amplitudes. However, the LCF failures observed occurred at significantly higher number of cycles than those required for the HTSDG cryostat.

4.1.5 CRYOSTAT BURST TESTING

Burst testing was completed on the same inner and outer tubes used to fabricate the 5-meter prototype cryostats. The tubing was commercially available, welded, stainless steel corrugated tubing of sizes similar to those anticipated for use for the HTSDG cryostat. The rated pressures of the inner tube (DN 16) and outer tube (DN 32) were 8 bar (116 psi) and 3 bar (44 psi), respectively. Three specimens of each size were tested with fixed ends, and three of each size with free ends.

Pressure was supplied using a hydraulic hand pump that provided pressurized hydraulic oil to one side of a double acting hydraulic cylinder. The other end of the cylinder was filled with water and connected to the test specimen. The cylinder rod was free to move as pressure was applied by the pump. In this way, the specimens were tested hydrostatically using water as the pressurizing medium.

Connected to the water side of the apparatus were two electronic pressure transducers, one of 0–5,000 psi and one of 0–15,000 psi capacity. During testing, all transducer outputs agreed to within 0.5% of the maximum range of the 5 ksi transducer, so only data from this transducer are presented.

One 120 Ω strain gauge rectangular (0°, 45º, 90°) rosette (Omega model KFG-1-120-D17-11L3M3S) was mounted to the peak of a corrugation on each specimen. For redundancy, one DN 16 and one DN 32 specimen were instrumented with a second rosette 180º around the circumference from the first, but on the same corrugation. The strain gauges were oriented in the longitudinal/circumferential plane.

A string potentiometer (Celesco model SP3-4) was also attached to a wire running around the circumference of the specimen in the center corrugation valley. As the circumference of the specimen expanded, the wire would extend the string pot, recording the amount of growth.

The EJMA testing method recommends pressurizing the specimen in steps, returning to zero after every step, up to at least twice the yield pressure, using a step size <10% of the yield pressure. However, due to the use of a manual pump and the extremely low yield pressures of the thin-wall corrugated tubing, maintaining fine control of the pressure was very difficult; therefore, this procedure was not followed precisely. Also, due to pump internal check-valve leakage, pressure drops were experienced every time the pump handle was cycled for another stroke.

4.1.5.1 Fixed-End Testing

The first three specimens of each size were tested using a fixture to constrain the ends of the specimens and prevent motion. Data plots for the fixed-end specimens are shown in Figure 4-23 through Figure 4-28.

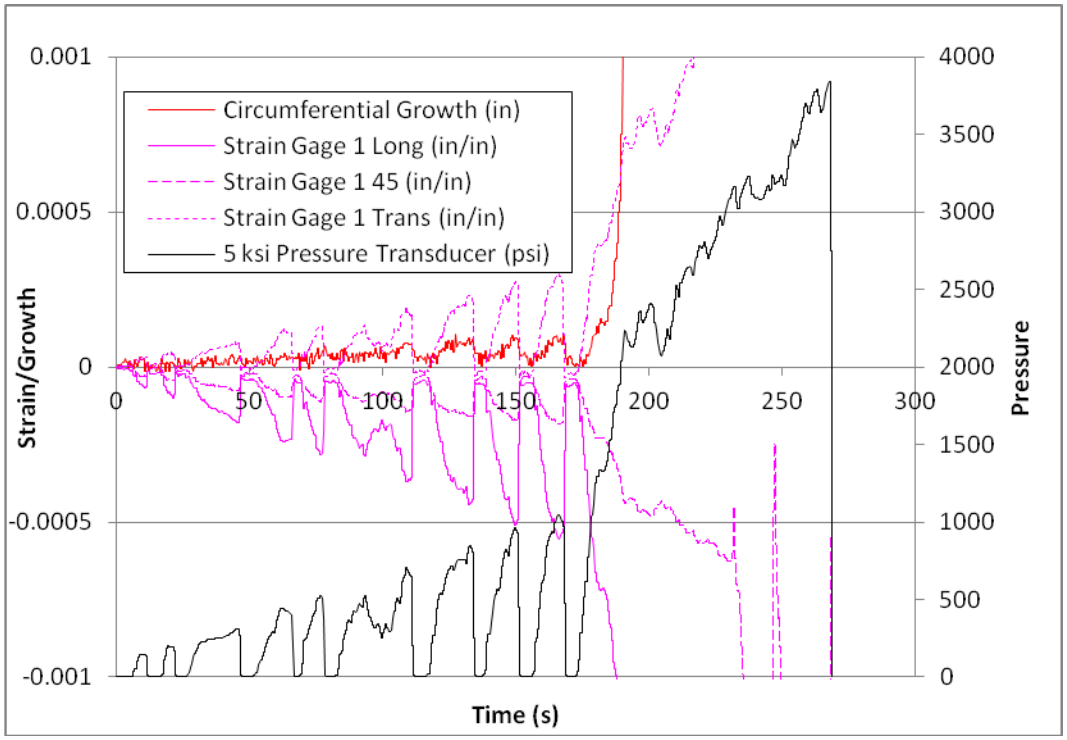

Figure 4-23. Fixed-end chart, DN 16 sample #1.

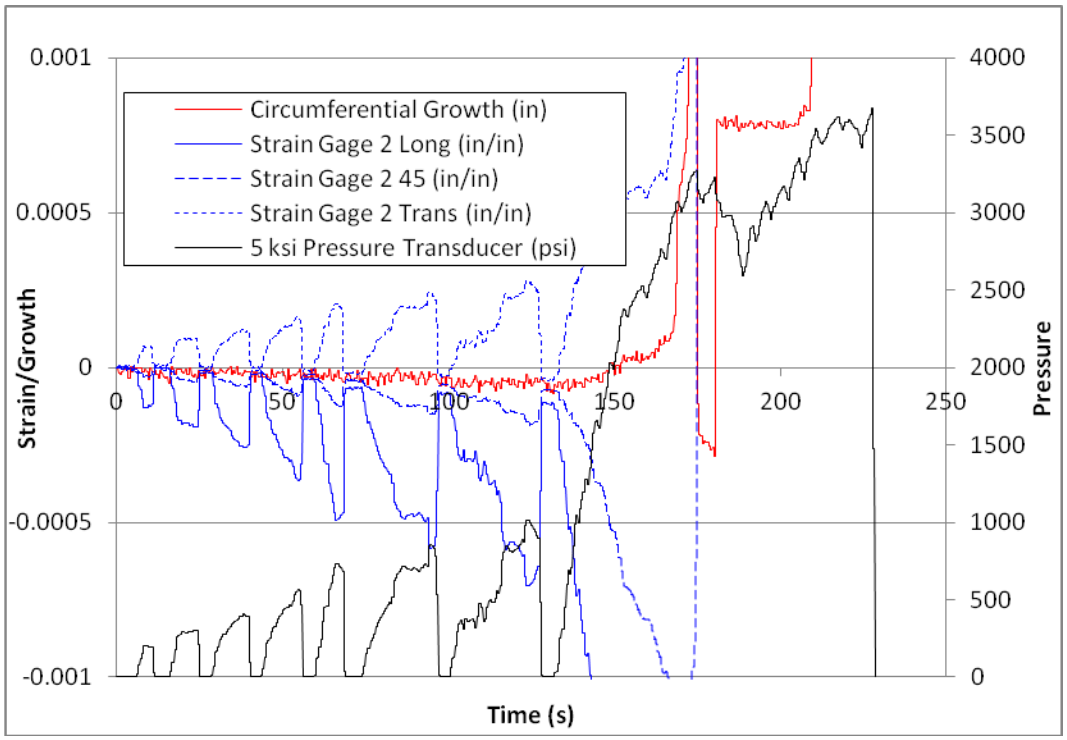

Figure 4-24. Fixed-end chart, DN 16 sample #2

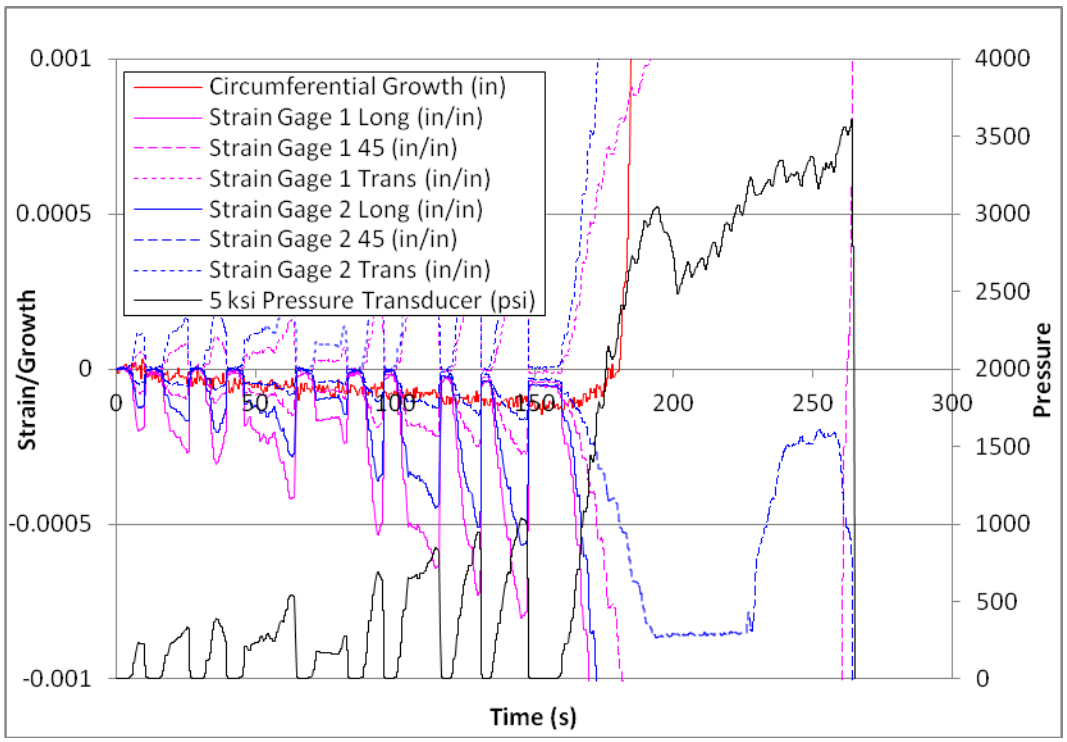

Figure 4-25. Fixed-end chart, DN 16 sample #3

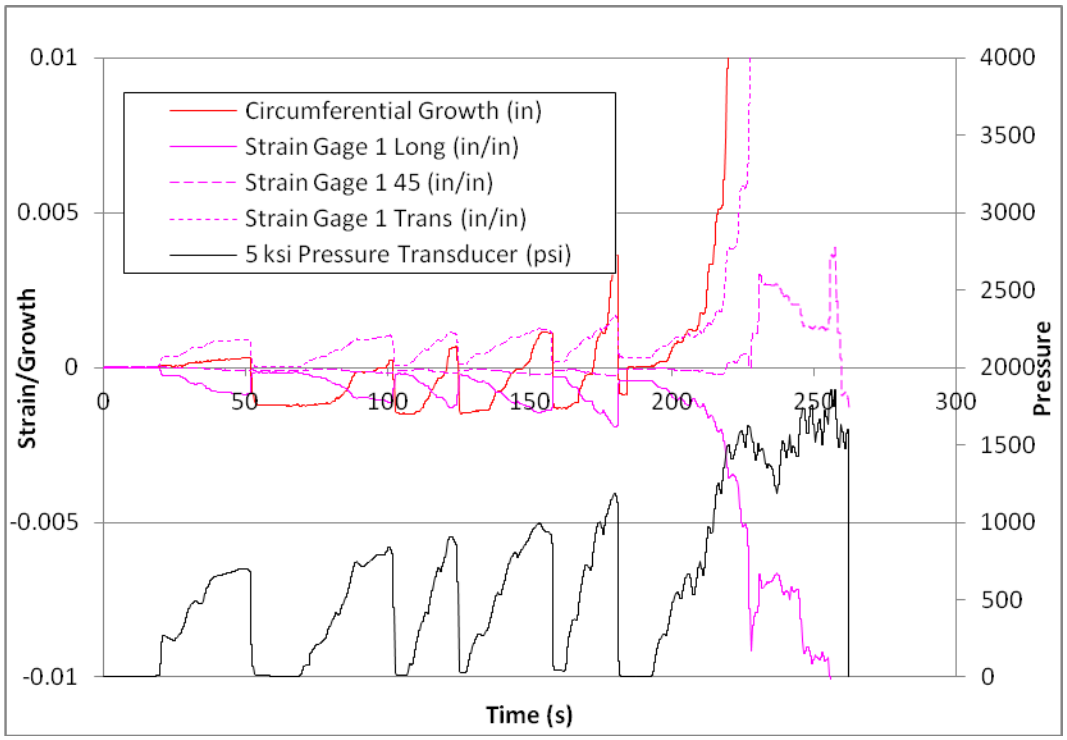

Figure 4-26. Fixed-end chart, DN 32 sample #1.

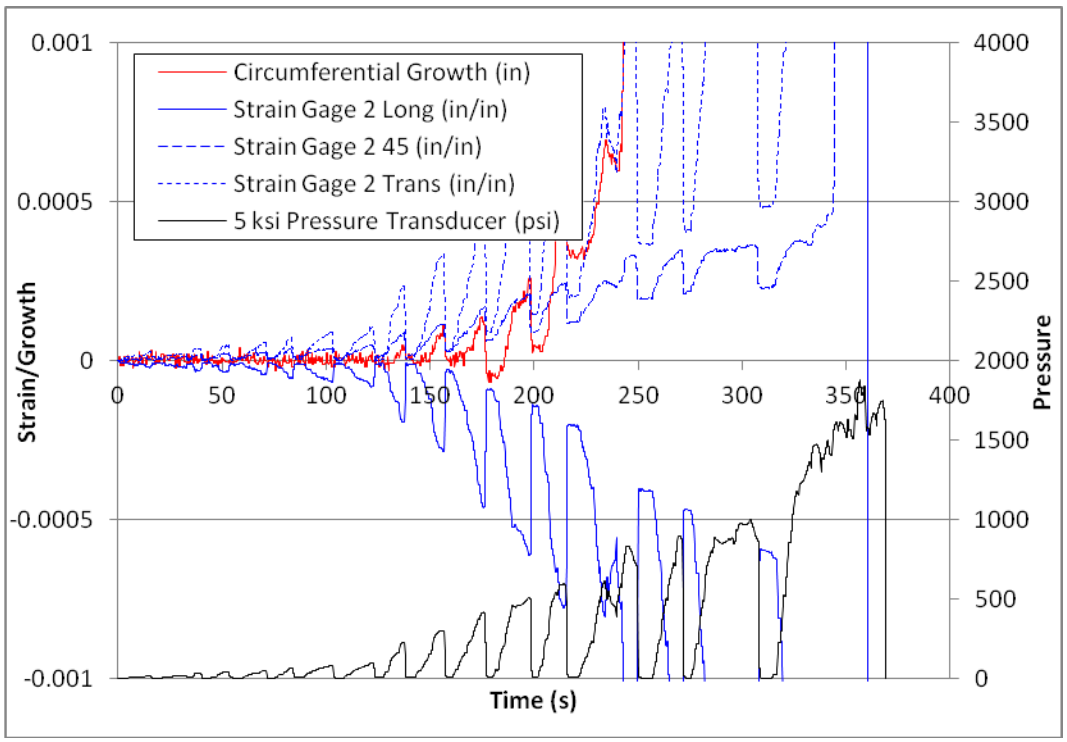

Figure 4-27. Fixed-end chart, DN 32 sample #2.

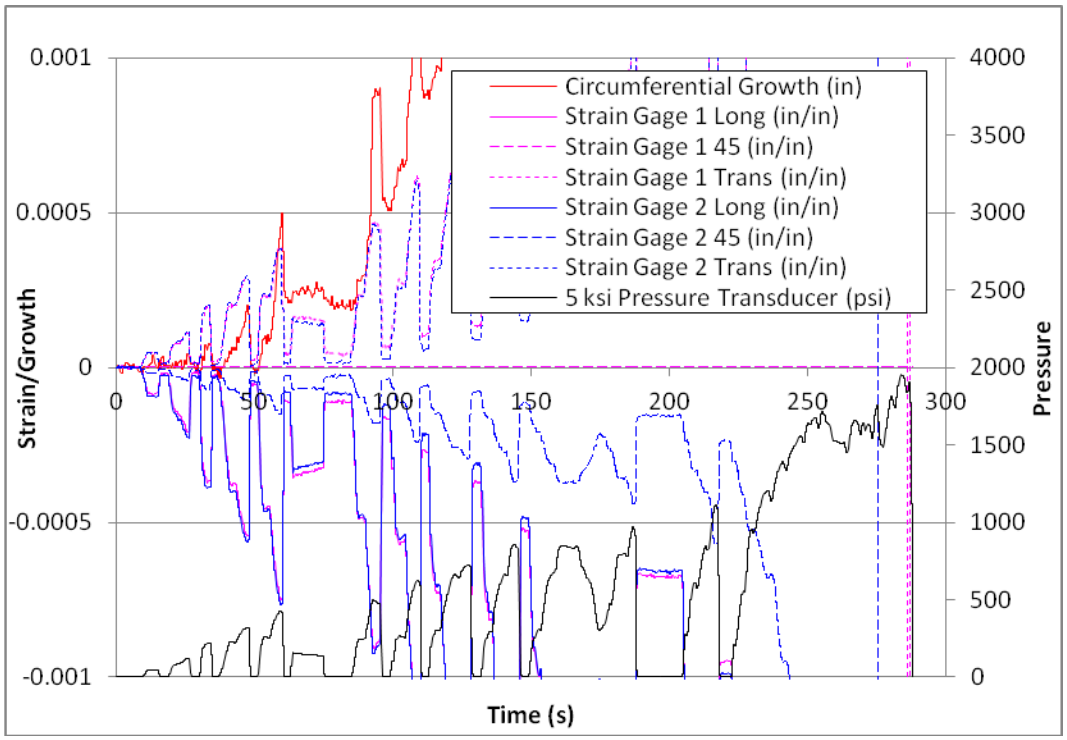

Figure 4-28. Fixed-end chart, DN 32 sample #3.

Unfortunately, due to the severe deformation of the convolutions at even low pressures, the strain gauge data collected were not useful except at very low pressures. However, using the loading steps, the strain gauge data can provide a rough indication of the onset of plastic deformation by noting the pressure peak after which the strain gauges no longer return to zero as the pressure is released, and then by recording the previous pressure peak. In accordance with this methodology, Table 4-8 shows the minimum pressures at which yield (permanent plastic deformation) occurs in the specimens where this value was available.

Table 4-8. Minimum Yield Pressure

Size	Specimen ID	Pressure (psi)
DIN 16	1	185
	2	202
	3	393
	Average	**260**
DIN 32	1	NA[1]
	2	101
	3	319
	Average	**210**
[1] First pressurization exceeded yield pressure.		

Due to hydrostatic squirm (the tendency of a pressurized tube with fixed ends to behave as a column at its critical buckling load), the failure mode of these specimens was buckling, followed by the inversion of one or more convolutes, followed by rupture of the tube walls. Due to the buckling of the center corrugations, the string pot wire was pinched by adjacent corrugations, and so the data from this transducer are considered unreliable. In five of the six specimens, failure occurred by rupture at the tubing seam weld. Photographs of the failed specimens are shown in Figure 4-29. Red dots mark the locations of the weld seams.

	DN 16	DN 32
Sample 1	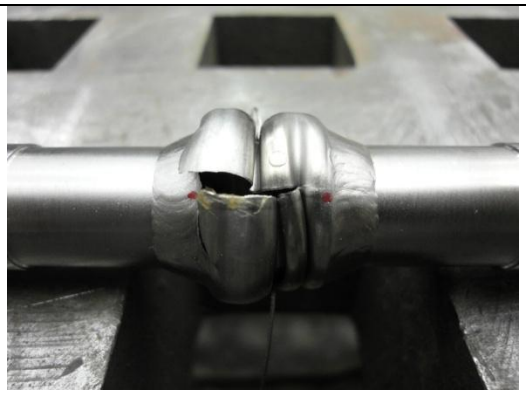	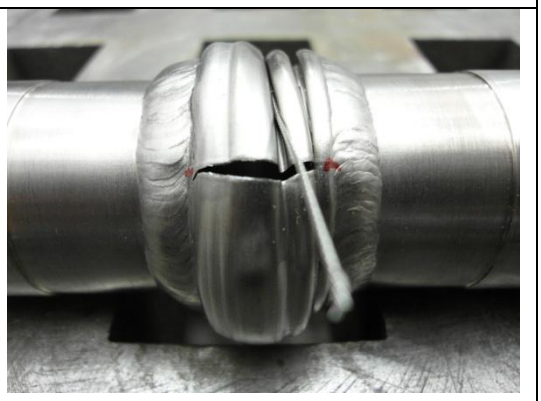
Sample 2	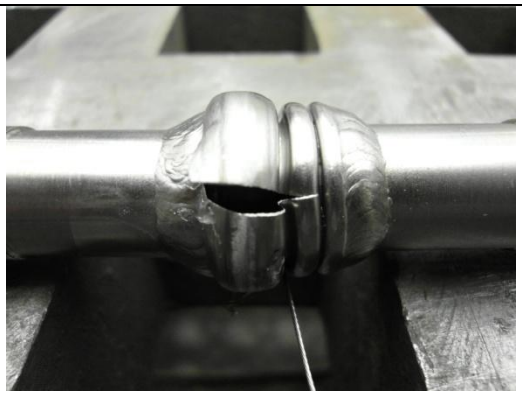	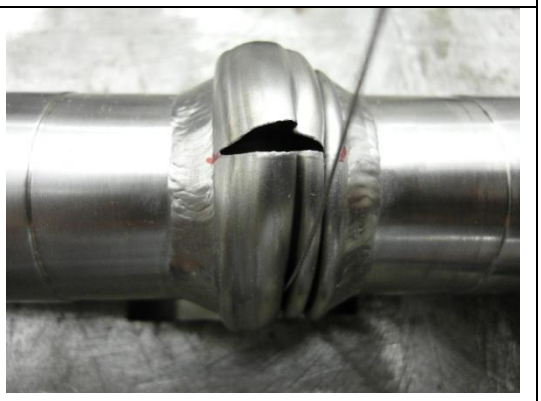
Sample 3	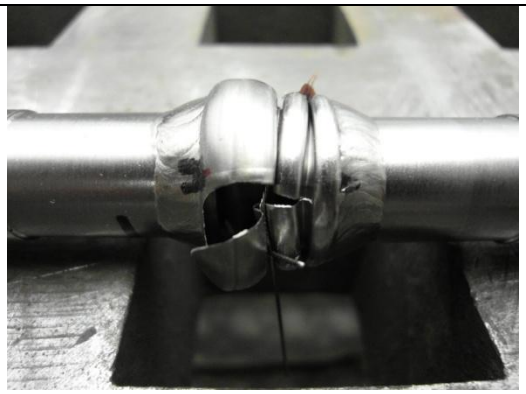	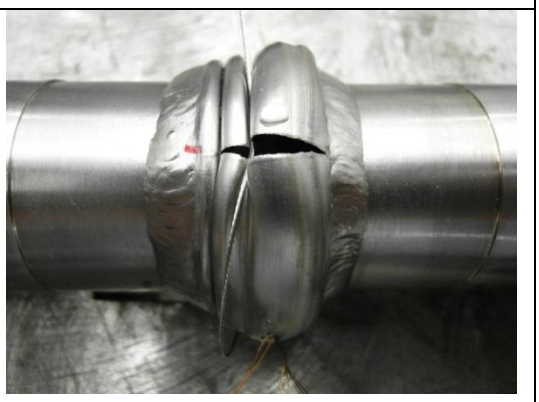

Figure 4-29. Fixed-end failed specimens.

4.1.5.2 Free-End Testing

The second three specimens of each size were tested using the fixture only to support one end of the specimen. The other end of the specimen was allowed to move freely. To reduce machining costs, the free-end specimens were constructed by cutting off the end tubes from the fixed-end specimens, and attaching them to new corrugated tube test sections. Due to the

difficulty of welding the thin corrugated tubes to the relatively thick end pieces, and because the pressure at failure was expected to be lower for the free specimens, for this series of tests the corrugated sections were attached to the end tubes by brazing.

Due to the difficulty in controlling the pressure using the hand pump, the water cylinder was removed from the pressurizing system, and hydraulic oil was pumped directly into the specimens. Also, the loading and unloading steps were eliminated, and the specimen was pressurized to bursting as smoothly as possible. Typical data plots for the free-end specimens are shown in Figure 4-30 and Figure 4-31.

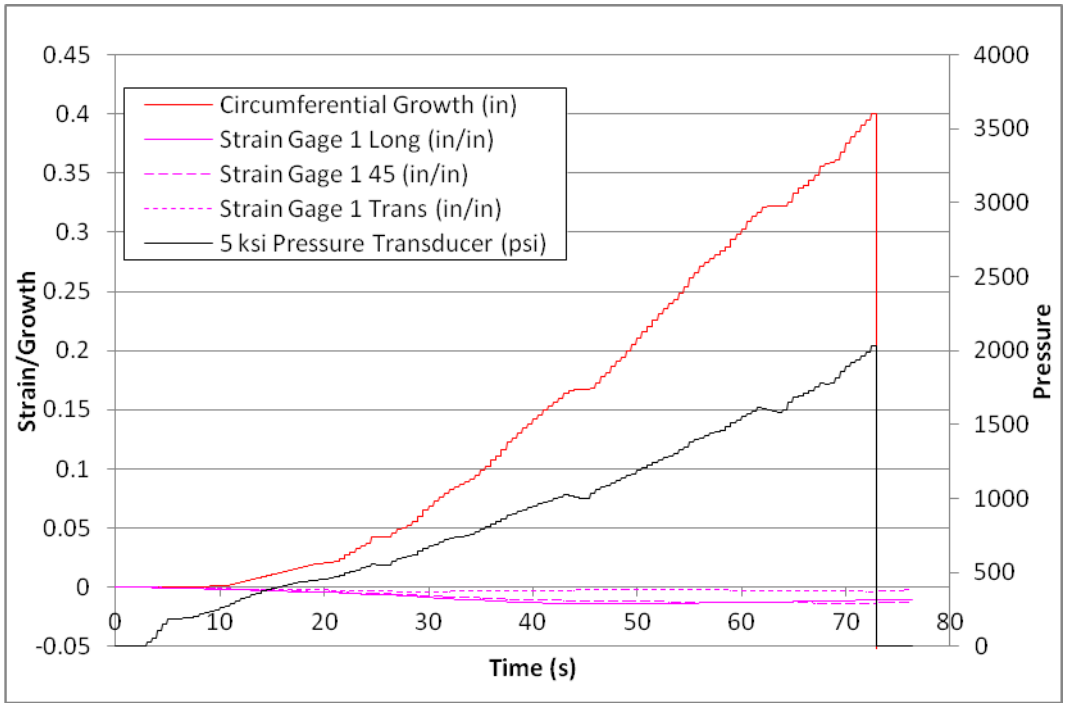

Figure 4-30. Free-end chart, DN 16 sample #4.

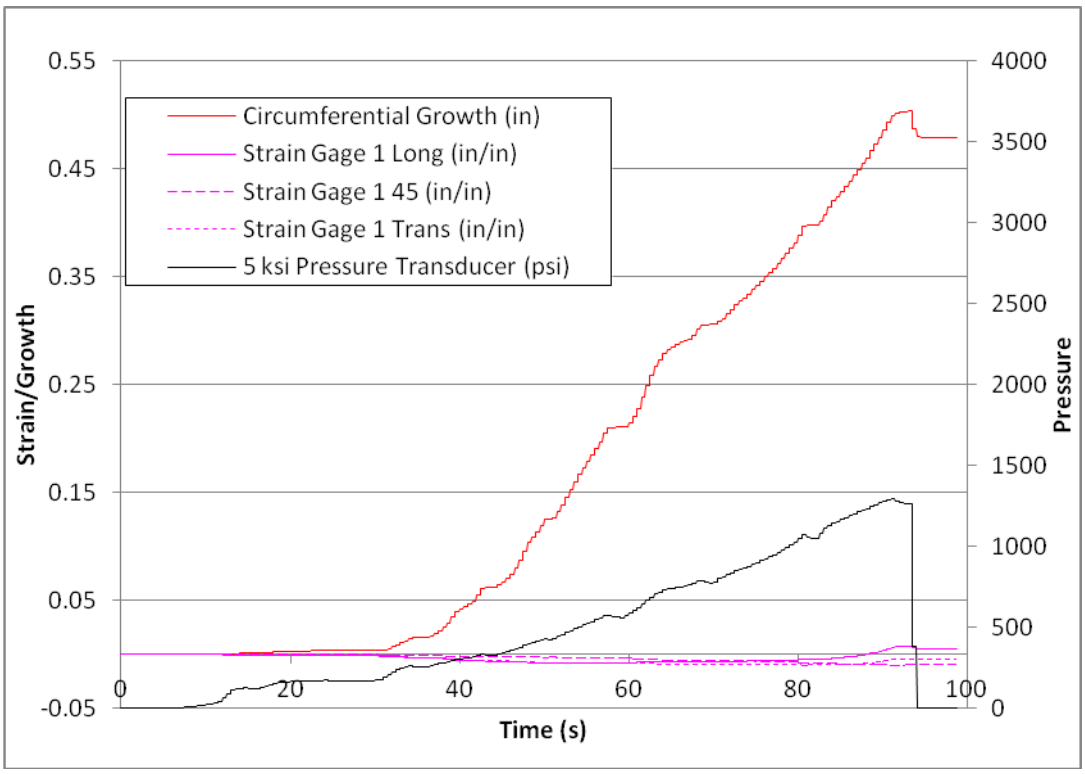

Figure 4-31. Free-end chart, DN 32 sample #4.

Despite the fact that the failure pressures were indeed generally lower than the fixed-end specimens, three of the free-end specimens failed at the braze joint instead of the corrugated tube. DN 16 specimens 4 and 6 failed by separation of the corrugated tube from the end tube entirely, and DN 32 specimen 6 failed by cracking of the brazed joint and subsequent leakage. Figure 4-32 shows photos of the failed specimens, or in the case of DN 16 specimens 4 and 6, photos of the specimens just prior to failure. In all cases, the tubing first deformed by the inversion of all convolutes, then subsequent bursting of the tube or failure of the brazed joint.

	DN 16	DN 32
Sample 4	 Specimen just prior to failure	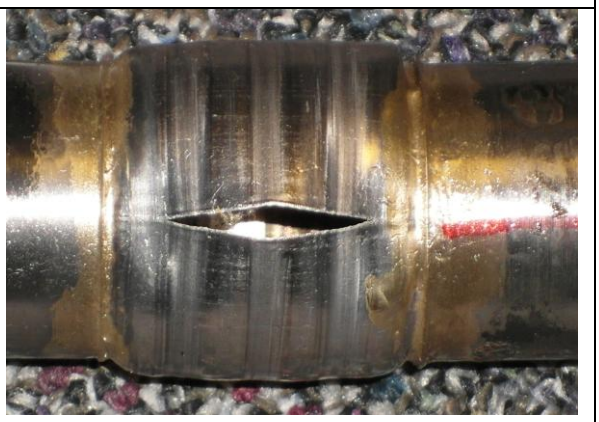
Sample 5	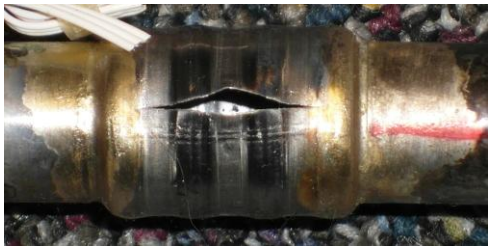	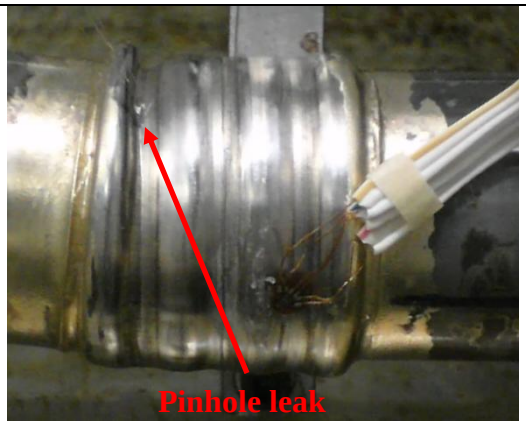 Pinhole leak
Sample 6	 Specimen just prior to failure	 Failure by leaking braze joint

Figure 4-32. Free-end failed specimens.

Again, due to the severe deformation of the convolutions at even low pressures, the strain gauge data collected were not useful except at very low pressures. Since the step load method was not used, no estimate of yield pressure is available.

4.1.5.3 Burst Test Results

Table 4-9 shows the results from the burst testing. In both sizes of tubing, the lowest burst pressures recorded (from the free-end specimens) exceeded the maximum operating pressures as rated by the tubing manufacturer of 116 psi (DN 16) and 43.5 psi (DN 32) by a factor of at least 20.

Table 4-9. Burst Test Results

End Condition	Size	Specimen ID	Peak Pressure (psi)	Failure Location
Constrained	DIN 16	1	3842	Tubing Weld
		2	3674	Tubing Base Metal
		3	3609	Tubing Weld
		Average	**3708**	
	DIN 32	1	1853	Tubing Weld
		2	1885	Tubing Weld
		3	1956	Tubing Weld
		Average	**1898**	
Free	DIN 16	4	2031[1]	Braze
		5	2365	Tubing Base Metal
		6	636[1]	Braze
		Average	**2365**	
	DIN 32	4	1295	Tubing Weld
		5	873	Tubing Base Metal
		6	1286[1]	Braze
		Average	**1084**	

[1] Not included in average.

4.2 INSULATION SYSTEM ASSESSMENT

The following sections summarize key results of the Cryostat-100 and 5-meter prototype testing as well as recommendations for future work. Complete analysis and discussion regarding this testing can be found in Appendices B, C, D and E.

4.2.1 CRYOSTAT 100 TESTING

4.2.1.1 Initial Cryostat-100 Testing

Thermal performance data were obtained for three MLI test articles under cryogenic-vacuum conditions: MLI Baseline, MLI Design 1, and MLI Design 2. With boundary temperatures of 78 K and 293 K, the cold vacuum pressure was in the range of 10^{-6} to 10^{-5} torr. Additional tests were made at degraded vacuum conditions up to 1 millitorr or more. Installation was performed in a layer by layer fashion for consistency in all test series. The heat flux and effective thermal conductivity values were directly calculated from the absolute boil-off flow rate measurements.

The MLI Design 1 with one pair of spacer rods was found to be superior to the MLI Design 2 with two pairs of spacer rods. The average values for heat flux and k-value are shown in Table 4-10.

Table 4-10. Average Heat Flux and k-values for MLI Test Articles

Test article	Heat flux (W/m^2)	k-value (mW/m-K)
Baseline MLI	0.95	0.028
Design 1	1.10	0.033
Design 2	1.42	0.045

The Design 1 thermal performance was approximately 15% higher than the baseline MLI, which is considered to be the ideal laboratory case. The thermal performance of Design 2 was nearly 30% higher than the Design 1. Note that all calculated heat flux values met the maximum allowable heat flux for the HTSDG cryostat of 5.08 W/m^2.

4.2.1.2 Follow-on Cryostat-100 Testing

Thermal performance data were obtained for three MLI test articles under cryogenic-vacuum conditions. The MLI system in this series was comprised of DAM reflectors and polyester net spacers in a blanket configuration. Three test articles, with 10, 15 and 20 MLI layers, were tested and compared with the original 10 layer baseline test article comprised of DAM reflectors and non-woven polyester fabric spacers. The high vacuum test data are of

primary importance and are shown here for comparison. Figure 4-33 compares the heat flux results while Figure 4-34 compares the k-value results. The cold and warm boundary temperatures were 78 K and 293 K, respectively.

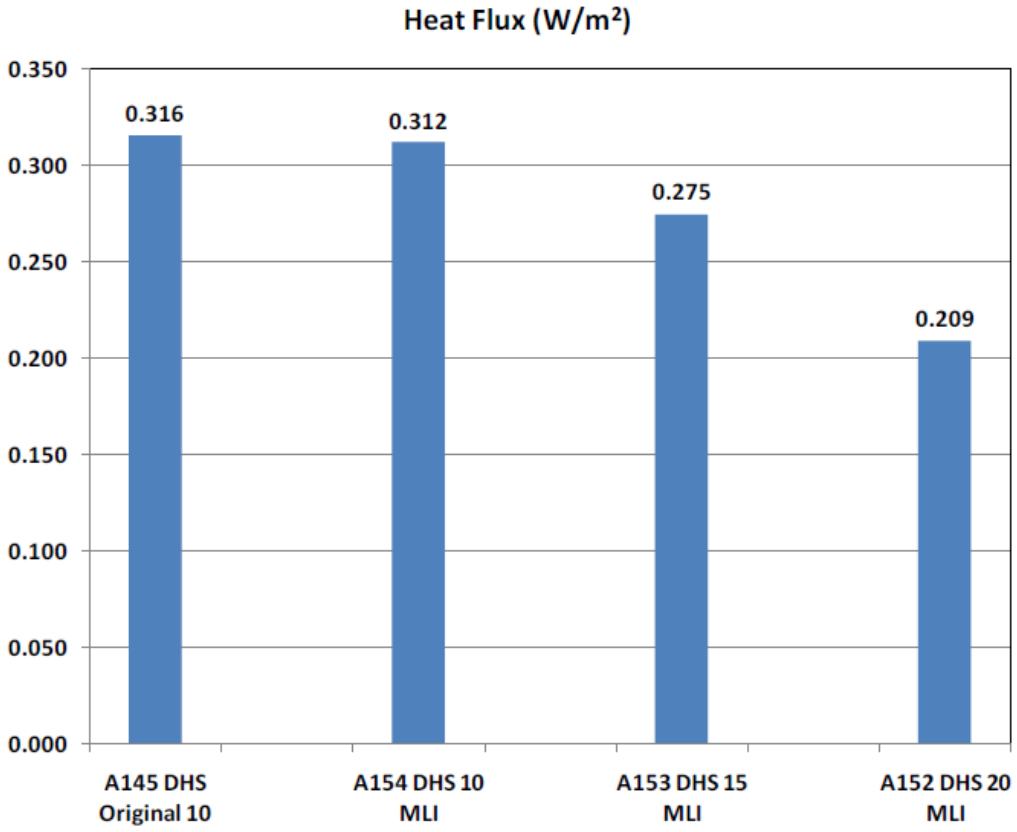

Figure 4-33. Summary of heat flux results for high vacuum test condition.

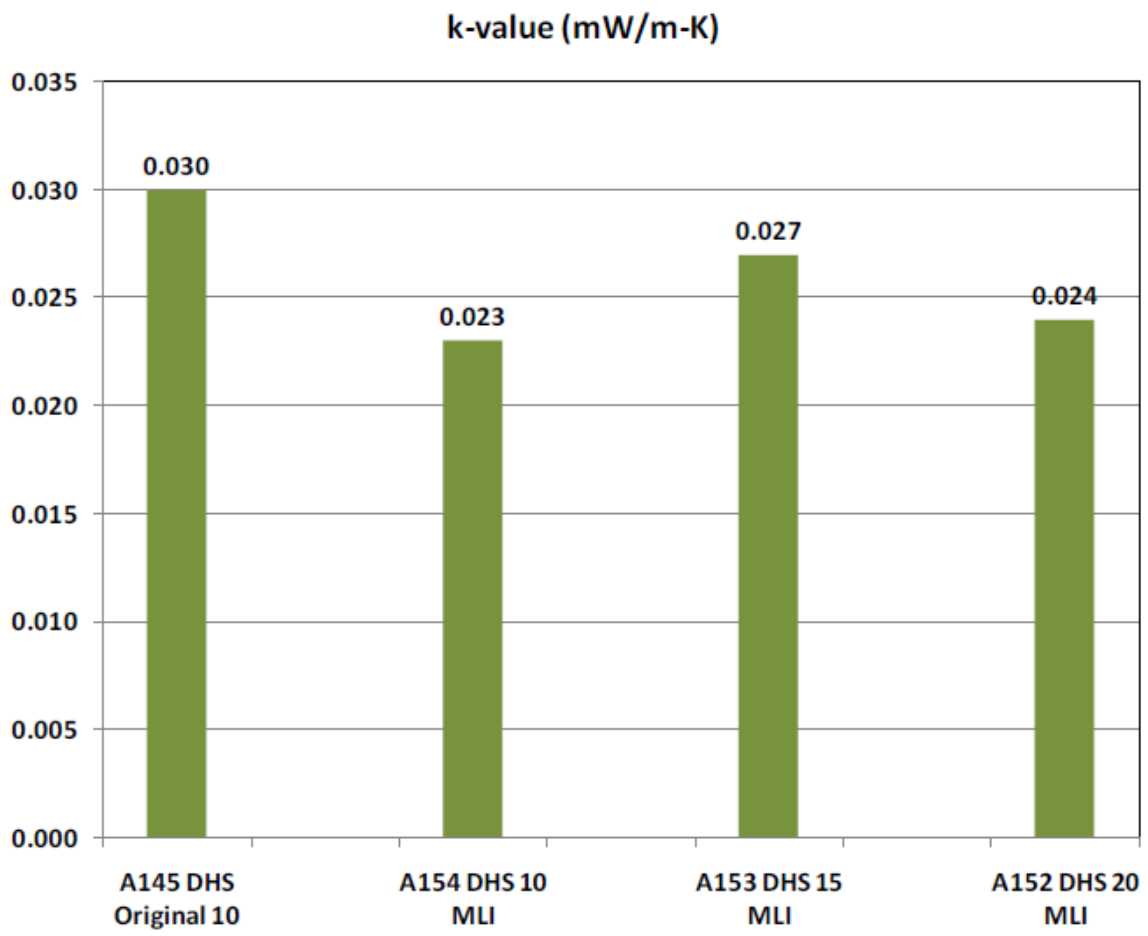

Figure 4-34. Summary of k-value results for high vacuum test condition.

The 10-layer test article showed a 1% lower heat flux compared to the original 10-layer baseline test article, but in significantly less space (thickness of 4.9 mm versus 6.5 mm). Compared to the 10-layer system of the new test article, the heat flux was reduced by 12% for the 15-layer system and 33% for the 20 layer system. The k-value was calculated to be the lowest for the new 10 layer system (0.023 mW/m-K) and was 23% lower compared to the original baseline system.

The new baseline combination of MLI materials, DAM and polyester net appears favorable compared to DAM and polyester fabric for a number of reasons, including: 1) lower thermal conductivity (k-value), 2) less sensitivity to variations in layer density, 3) more conformable to small complex surfaces, and 4) improved vacuum performance. The lower mass and open structure of the polyester net, in combination with the perforated DAM used for the 5-meter prototypes, should provide both improved evacuation from between the layers as well as

lower outgassing potential over the lifetime of the cryostat. The thinner profile and resulting increase in annular space gap could also provide additional thermal performance benefit for the long flexible cryostat in bent configurations. One drawback of the polyester net compared to the polyester fabric is that it does not have any tensile strength. The wrapping process will therefore fully rely on the load-carrying ability of the DAM material.

For the 1.75–inch class cryostat with its nominal annular gap of approximately 7 mm, the recommended number of layer pairs can be 10 or 12 depending on the wrapping process and methodology. Utilization of an increased layer density (effectively increasing the gap space) will provide additional tolerance in the wrapping process and facilitate assembly of the inner to outer tubes.

4.2.2 FABRICATION AND TESTING OF 5-METER PROTOTYPE CRYOSTATS

4.2.2.1 Thermal Performance Testing at KSC

Two 5-meter prototypes of flexible cryostat were successfully built. The prototypes were designated as Fluffy (low density MLI system) and Tiger (high density MLI system). Thermal and vacuum performance data were obtained for each prototype unit. Testing was performed in both effectively straight (gentle U-shape) and bent (S-shape) configurations. Complete thermal performance results are presented and discussed in Appendix B.

The overall summaries of thermal performance test results are given in Figure 4-35 and Figure 4-36. Figure 4-35 shows the heat leakage rate (W) of both test articles from the initial test (U-shape), after placement in the S-bend apparatus, and upon restoration to the initial state (U-shape). Figure 4-36 shows the heat leak per unit length (W/m) results for each test. Test results in the U-shape configuration were below the maximum heat leak target of 1.0 W/m and below the corresponding heat flux target of 5.8 W/m^2. Boil-off rates for the S-shape tests were from 90 to 100 % higher compared to the U-shape tests. These thermal performance results for these 10 layer MLI systems showed high sensitivity to mechanical bending, as expected. No permanent degradation in performance was found as the boil-off rates after the S-bending test series returned to their initial values within about 3%. These data indicate that the basic fabrication and installation processes of the cryostats should be robust enough to withstand the type of flexing that may occur when the cryostats are installed on vessels as part of a degaussing system. When

the flex lines were returned to the U-bend position, the heat loads returned to the original values (within the error of the test).

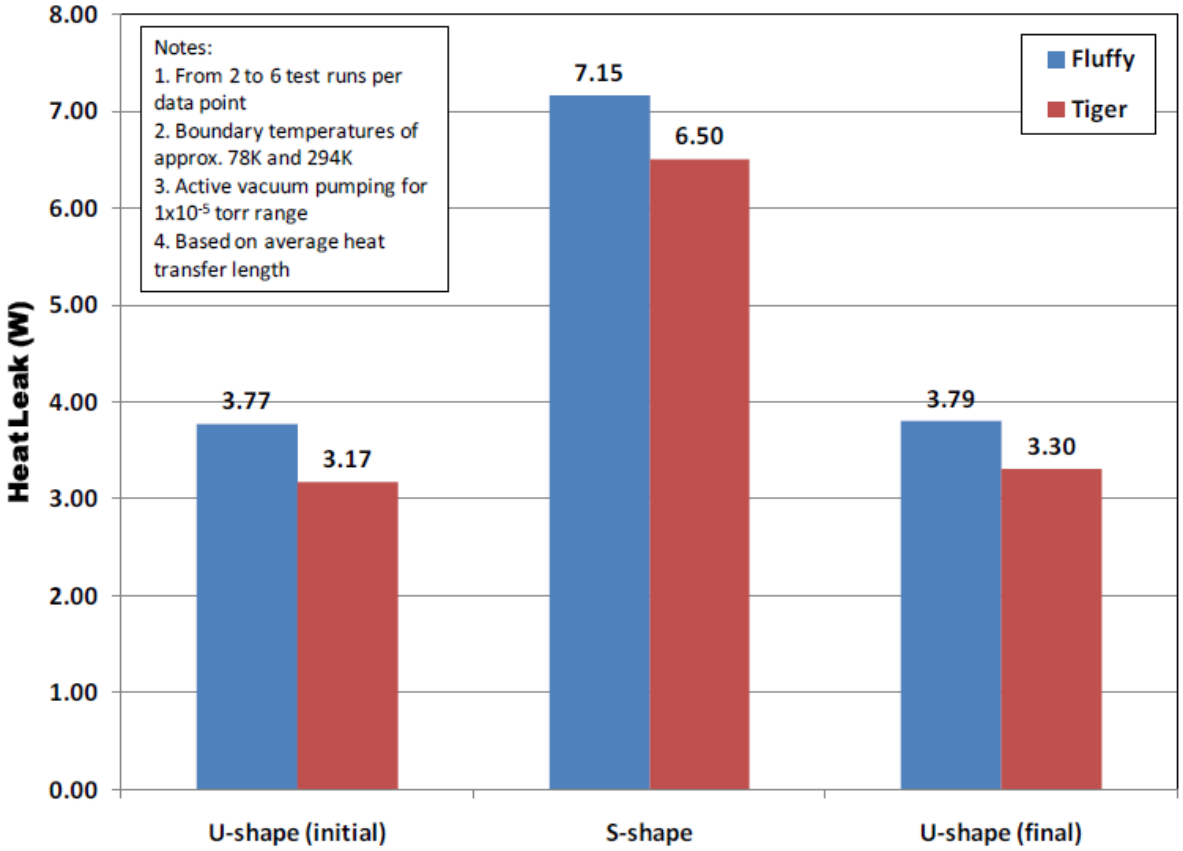

Figure 4-35. Thermal performance testing of 5-m prototypes by boil-off testing; average heat leakage rate (W) for straight (U) and bent (S) configurations (KSC).

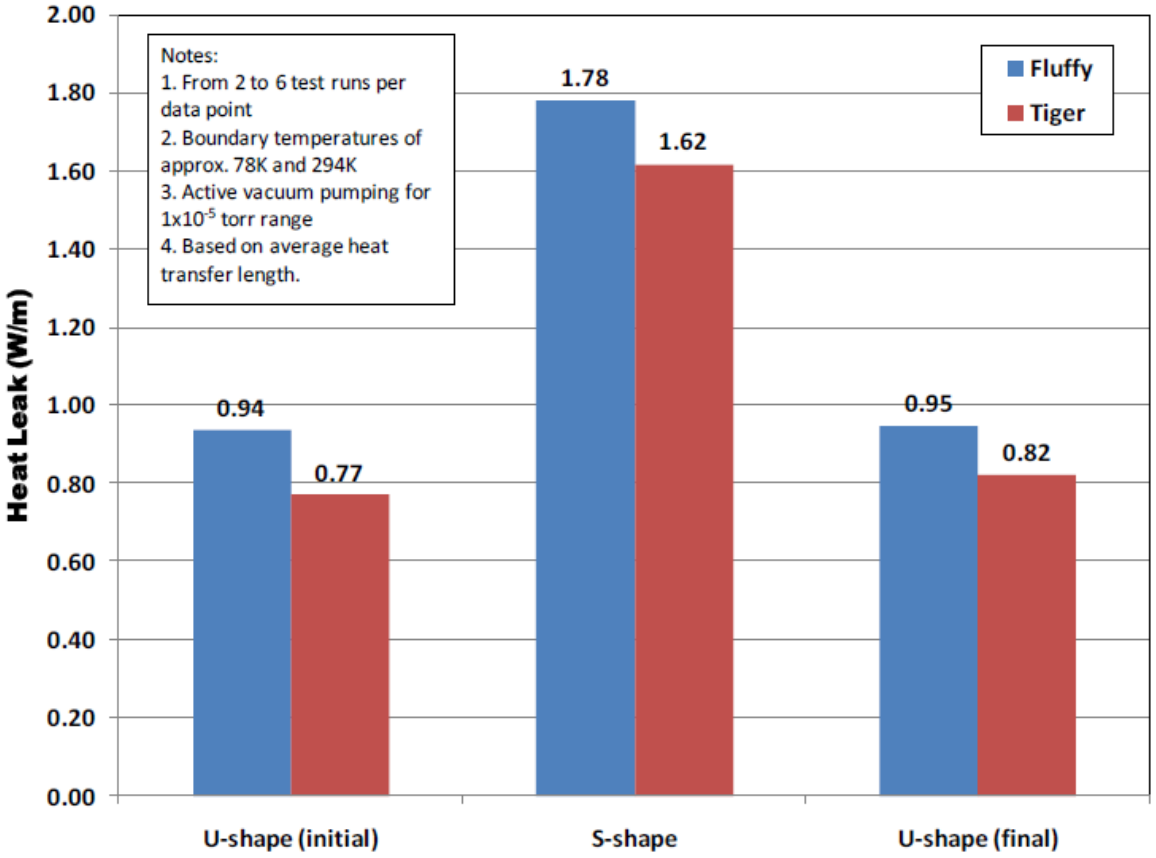

Figure 4-36. Thermal performance testing; average heat leak per unit length (W/m) for straight (U) and bent (S) configurations (KSC).

Tiger was consistently better than Fluffy in all thermal performance tests. In the U-shape tests, the Fluffy heat leakage rate was from 15 to 20% higher compared to Tiger. In the S-shape tests, the Fluffy heat leakage rate was approximately 10% higher compared to Tiger. The positive aspect of these results is that a tightly-wrapped MLI system composed of the perforated DAM and polyester netting and as installed with the Ultem spacer rods appears to work well without the need for exceptional pumping and heating or other difficult processes. Furthermore, the expectation was that the design of the MLI system could be modified to include additional layers within the available annular space gap to further boost the thermal performance. This was demonstrated by the follow-on Cryostat-100 test results presented in Section 4.2.1.2, Follow-on Cryostat-100 Testing.

4.2.2.2 Thermal Performance Testing at ORNL

Complete thermal performance results of flow-through (dynamic) testing completed at ORNL are presented and discussed in Appendix E. The testing at ORNL utilized calorimetric measurement based on a measurement of the temperature rise of flowing liquid nitrogen. As with the prototype testing at KSC, thermal performance testing at ORNL was performed for the test articles in both straight (gentle U-shape) and bent (S-shape) configurations. Table 4-11 provides the calculated heat leak for each test. Note that the tests shown in italics were found to have poor insulating vacuum during the test and therefore are not considered valid tests.

Table 4-11. Thermal Performance Testing; Heat Leak per Unit Length (W/m) for Straight (U) and Bent (S) Configurations (ORNL)

Test Article	**Configuration**	**Heat Leak[1] (W/m)**
Fluffy	*Straight*	*10.7*
	Straight/Pumped	2.7
	Straight/Pumped	3.3
	Bent	2.4
Tiger	Straight	1.9
	Bent	1.4
	Straight	*7.8*
[1] Assumes 10.6 W from end effects.		

The heat leak was found to range from 1.4 W/m to 3.3 W/m; these values are considerably higher than those reported by KSC. As documented in the ORNL report, the test apparatus and method differ significantly from that used for the KSC boil-off testing. As such, the heat leak values provided in the table had to be corrected to account for end effects associated with the end fittings utilized for testing. The relatively short length of the 5-meter prototypes made the end affect contributions a large fraction of the total heat load. In addition, based on the accuracy of the flow meter and the thermometers used during testing, a minimum average error of +/- 3 W was estimated for the measured heat loads. This further contributed to the difference in heat leak values calculated by KSC and ORNL.

The testing at ORNL demonstrated that evaluation of thermal performance using a flowing liquid nitrogen stream can be suitably performed. However, certain aspects of the test

set-up and instrumentation need to be improved to reduce measurement uncertainty. Recommendations regarding these improvements have been included in the ORNL report.

4.2.3 RECOMMENDATIONS FOR FUTURE WORK

Based on the information learned through this work, further optimization of the thermal performance must be approached through the design of the long length cryostat wrapping process. Key considerations of this process, from a thermal viewpoint, can be listed as follows:

- Tensile strength and tear resistance of materials
- Collation (number of layer pairs) and diameters of rolls of materials
- Placement and sequencing of rolls of materials
- Basic wrapping method—spiral (conventional) or longitudinal (novel)
- Integration of spacer rods.

Further laboratory work that could support this manufacturing process development effort is listed as follows:

- Perform MLI testing of spiral or longitudinal wrap (Cryostat-100)
- Perform MLI testing with compression effects (Cryostat-100)
- Re-build and test the pair of 5-meter prototypes to validate Cryostat-100 results for physical application.

In addition, the necessary proving out of a suitable vacuum bake-out process, long-life vacuum retention, and incorporation of the getter/adsorbent packages remains a critical underlying part of the manufacturing process for long-length flexible cryostat for HTSDG.

5.0 BENEFITS ANALYSIS

Although a U.S. manufacturing capability for long length flexible cryostats was not developed, the project did realize the following technical accomplishments:

1. A baseline cryostat insulation system was developed and validated via Cryostat-100 testing and thermal performance testing of two 5-meter long prototype cryostats. Prototype test results in the U-shape configuration were below the maximum heat leak target of 1.0 W/m and below the corresponding heat flux target of 5.8 W/m^2. Boil-off rates for the S-shape tests were from 90 to 100% higher compared to the U-shape tests,

which was less than the 200% maximum permissible increase in heat leak target across the bend.

2. The baseline combination of MLI materials, DAM and polyester net appears favorable compared to DAM and polyester fabric for several reasons, including: 1) lower thermal conductivity (k-value), 2) less sensitivity to variations in layer density, 3) more conformable to small complex surfaces, and 4) improved vacuum performance. For the 1.75-inch class cryostat, the number of MLI layers can be 10 or 12 depending on the wrapping process and methodology. For the 2.75-inch class cryostat, the number of layer pairs could be the same, or up to 18 layers if a further reduction in heat leak is desired.
3. Current technology available through W&S has been identified for forming, welding and corrugating stainless steel sheet of the desired thickness ranges for the manufacture of HTSDG cryostats. FEA analyses showed the W&S process is fully capable of producing corrugated tubing with sufficient residual strength to meet bending and pressure requirements. FEA analyses of the bending performance, in conjunction with fatigue testing of representative materials, also confirmed that the resulting corrugated tubing will have acceptable flexibility when using optimized profile designs.
4. Burst tests of commercially available corrugated tubing were well above the target 1,000 psi burst pressure. Lessons learned during testing of this tubing will improve upon future test specimen design and burst testing of actual HTSDG cryostats to demonstrate required performance metrics.

6.0 IMPLEMENTATION REPORT

As part of project tasking, a preliminary business case analysis (BCA) was done to assist Southwire in returning a Go/No-go decision with regard to committing the capital needed to upgrade their existing facility to manufacture long-length cryostat for the Navy. The complete BCA is provided as Appendix L. In summary, the analysis initially assumed a capital investment cost of $3,131,744 and that Southwire would obtain 100% of the expected market share of future Navy LCS orders for HTSDG cryostats. Results showed that Southwire would need to sell the cryostats at $850 per meter to ensure a positive rate of return after three years following implementation of production upgrades. However, if Southwire were willing to wait five years

to see a return on their investment, they could sell the cryostats at a price of $650 per meter. While these prices were less than the $900 per meter initially assumed for the Nexans cryostat, subsequent discussions with the Navy revealed that the baseline Nexans price had been more recently estimated at $400 per meter.

In light of this new information, the data were reassessed using lower estimates for capital expenditures, as well as more refined estimates regarding cryostat production costs. Southwire was able to reduce the capital expenditure estimate by allocating some of those costs to other products that would be manufactured on the same production line. The cryostat price was held static at $350 per meter to better compete with the revised $400 per meter Nexans price, and the expected market share of the LCS orders was reduced from 100% to 50% at Southwire's request. The results of this discounted payback analysis showed that even with a reduced capital expenditure of $1,750,000, the payback time was unattractive at almost 13 years. Like the previous analyses, the results of these additional scenarios forecast an unacceptable payback period for Southwire relative to the capital investment and the price per meter required for the cryostats in order to be competitive with the Nexans product. In light of this information, Southwire returned a No-go decision on July 5, 2011 for commitment to upgrade their production facility.

As a result of Southwire's No-go decision, a significant portion of the project work was not completed. However, the LCS Program Office is still interested in the establishment of a U.S. manufacturer for the HTSDG long-length cryostats. The technical work completed on the project has addressed the primary manufacturing issues associated with forming, welding and corrugating the stainless steel tubing that are the structural components of the cryostat. The completed thermal performance testing also made great gains in developing the insulation system for the cryostats. A follow-on project with another industry partner could easily leverage this work to its logical conclusion of a U.S. manufacturing capability for long-length cryostats.

The use of HTS cables for the LCS degaussing system is currently undergoing qualification trials using long-length cryostats manufactured by Nexans. This NMC project was developed as an upgrade for HTSDG cryostats focused on cost reduction and does not impact the availability of the HTSDG system to future LCS hulls.

7.0 CONCLUSIONS AND RECOMMENDATIONS

Although a U.S. manufacturing capability for long-length flexible cryostats was not developed, the project did realize numerous technical accomplishments as detailed in Section 5, Benefits Analysis. A follow-on project with another industry partner could easily leverage this work to its logical conclusion of a U.S. manufacturing capability for long-length cryostats. This project was developed as an upgrade for HTSDG cryostats focused on cost reduction and does not impact the availability of the HTSDG system to future LCS hulls.

In moving forward to establish a U.S. manufacturing capability, the following recommendations for future work are provided.

1. Further optimization of the thermal performance of the cryostat insulation system must be approached through the design of the long length cryostat wrapping process. Key considerations of this process, from a thermal viewpoint, include:
   - Tensile strength and tear resistance of materials
   - Collation (number of layer pairs) and diameters of rolls of materials
   - Placement and sequencing of rolls of materials
   - Basic wrapping method, spiral (conventional) or longitudinal (novel)
   - Integration of spacer rods.
2. Laboratory work to support manufacturing process development includes:
   - Perform MLI testing of spiral or longitudinal wrap (Cryostat-100)
   - Perform MLI testing with compression effects (Cryostat-100)
   - Re-build and test the pair of 5-meter prototypes to validate Cryostat-100 results for physical application.
3. A suitable vacuum bake-out process, long-life vacuum retention, and incorporation of the getter/adsorbent packages remains a critical underlying part of the manufacturing process that must be addressed for long-length flexible cryostat for HTSDG.
4. Down-selection of a suitable material for the outer jacket of the cryostat and determination of appropriate application methods are required.
5. Continue work with W&S to finalize the design of the corrugation tooling required to manufacture the identified cryostat profile geometries.

6. Perform bend fatigue and burst pressure testing on corrugated tubing samples from the final manufacturing process.
7. Complete cryostat performance testing in accordance with identified metrics.

8.0 REFERENCES

1. Huber, P., Fowler, B., "Development of Long Length, Flexible, Vacuum-Jacketed Cryostats, S2304, Project Plan," NMC TR No. 09-100, Concurrent Technologies Corporation, Johnstown, PA, 23 November 2009.

2. ASME B31.1, "Code for Pressure Piping (Power Piping)," The American Society of Mechanical Engineers, New York, New York, 07 December 2007.

3. ASME B31.3, "Code for Pressure Piping (Process Piping)," The American Society of Mechanical Engineers, New York, New York, 31 May 2007.

4. Standards of the Expansion Joint Manufacturers Association, Expansion Joint Manufacturers Association, Inc., Ninth Edition including 2009 Errata, www.ejma.org.

5. ASTM Standard E 8, 2001, "Standard Test Methods for Tension Testing of Metallic Materials," ASTM International, West Conshohocken, PA, www.astm.org.

6. ASTM E606-04e1, "Standard Practice for Strain-Controlled Fatigue Testing," ASTM International, West Conshohocken, PA.

7. "Effect of Static Pre-Strain on Low Cycle Fatigue Life of AISI 316L Stainless Steel," www.scientific.net/KEM.462-463.65.

8. "Tensile and Low Cycle Fatigue Properties of Solution Annealed Type 316L Stainless Steel Plate and TIG Weld Exposed to 5 dpa at Low Temperature (42 °C)," http://www.sciencedirect.com/science/article/pii/S0022311500003676.

9. "Evaluation of the Technical Basis for New Proposals of Fatigue Design of Nuclear Components," Swedish Radiation Safety Authority Report Number: 2011:04. ISSN: 2000-0456.

10. MMPDS-04: Metallic Materials Properties Development and Standardization, Washington, D.C.: Federal Aviation Administration, 2008.

9.0 APPENDICES

9.1 APPENDIX A – FINAL PROJECT SCHEDULE

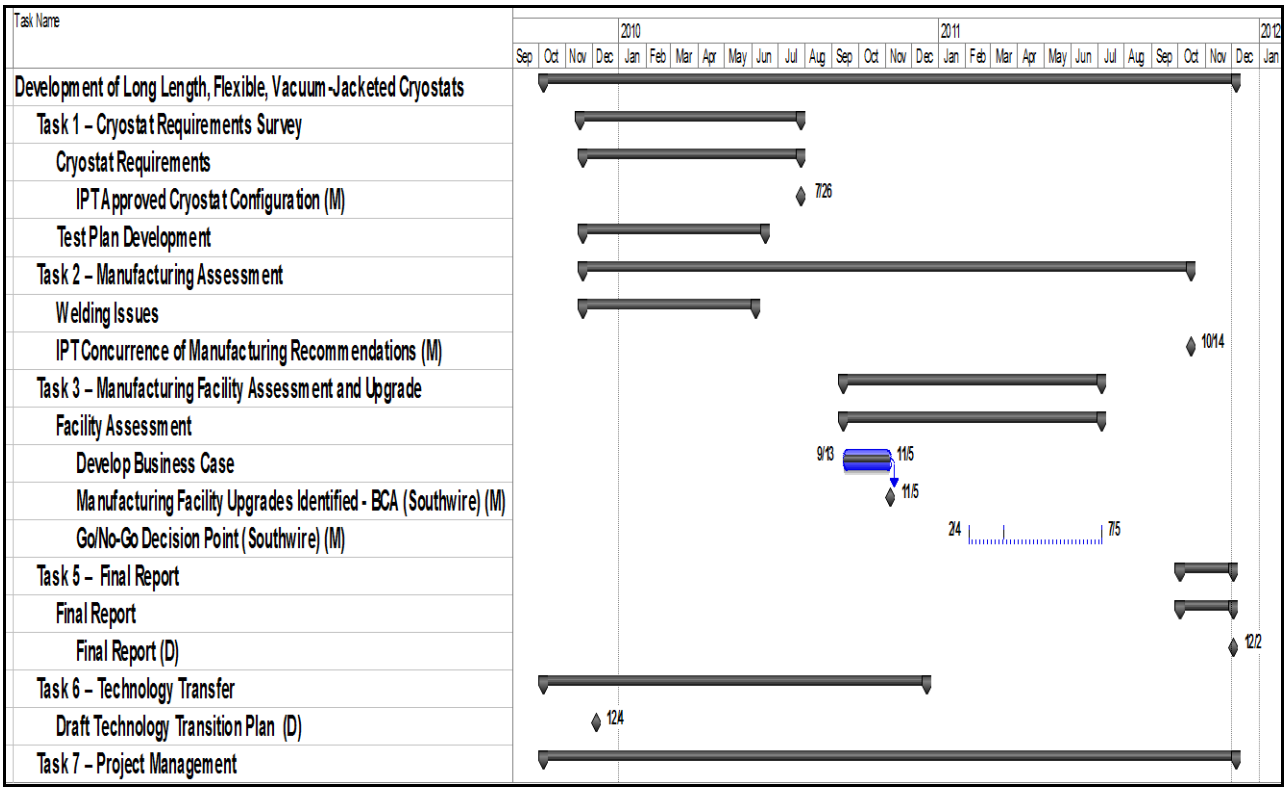

9.2 APPENDIX B – NASA KSC 5-METER PROTOYPE CRYOSTAT REPORT

Attached as separate document.

9.3 APPENDIX C – NASA KSC CRYOSTAT-100 TEST SUMMARY REPORT

Attached as separate document.

9.4 APPENDIX D – NASA KSC CRYOSTAT-100 TEST SUMMARY REPORT #2

Attached as separate document.

9.5 APPENDIX E – ORNL 5-METER PROTOTYPE CRYOSTAT TEST REPORT

Attached as separate document.

9.6 APPENDIX F – CORRUGATED TUBING SURVEY

Attached as separate document.

9.7 APPENDIX G – NUMERICAL ANALYSIS OF THE WEBER & SCHER FORMING PROCESS

Attached as separate document.

9.8 APPENDIX H – PRELIMINARY NUMERICAL STUDY TO DETERMINE KEY PROCESS PARAMETERS

Attached as separate document.

9.9 APPENDIX I – DEVELOPMENT OF THE CRYOSTAT CORRUGATION PROFILE DESIGN BOUNDS

Attached as separate document.

9.10 APPENDIX J – LCF SPECIMEN PREPARATION AND TEST MATRIX

Attached as separate document.

9.11 APPENDIX K – LCF TESTING REPORT

Attached as separate document.

9.12 APPENDIX L – SOUTHWIRE PRELIMINARY BUSINESS CASE ANALYSIS

Attached as separate document.

9.13 APPENDIX M – ELECTRONIC DISTRIBUTION

Names	Copies
External Distribution by Program Office	
Greg Woods, ONR	1
John Carney, ONR	1
Anthony Smith, NAVSEA	1
Brian Fitzpatrick, NSWCCD	1
Naval Research Laboratory	1
Defense Technical Information Center-OMI	1
Jacob Kephart, NSWCCD	1
David Knoll, Southwire	1
Jonathan Demko, ORNL	1
James Fesmire, NASA KSC	1
George Stimak, ONR	1
Sarah Mahmood, DHS	1
Debbie Haught, DOE	1
Internal Distribution by Program Office	
Daniel L. Winterscheidt, NMC Program Office, CTC	1
Cindra L. Shearman, Contracts Administrator, CTC*	1
Patricia Huber, CTC	1
Daniel George, CTC	1
Shawn Rhodes, CTC	1
John Ryan, CTC	1
Juan Valencia, CTC	1
Information Resource Center, CTC	1
Project File, CTC	1

* Unbound hard copy

REPORT DOCUMENTATION PAGE

Form Approved
OMB No. 0704-0188

1. AGENCY USE ONLY *(Leave blank)*	2. REPORT DATE 05 December 2011	3. REPORT TYPE AND DATES COVERED Final Report, 08-01-04-12/02/11

4. TITLE AND SUBTITLE
Development of Long Length, Flexible, Vacuum-Jacketed Cryostats, S2304, Final Report

5. FUNDING NUMBERS
N00014-06-D-0048

6. AUTHOR(S)
Patricia Huber, Daniel George, Shawn Rhodes, John Ryan, Dr. Juan Valencia

7. PERFORMING ORGANIZATION NAME(S) AND ADDRESS(ES)
Navy Metalworking Center
Operated by Concurrent Technologies Corporation
100 CTC Drive
Johnstown, PA 15904

8. PERFORMING ORGANIZATION REPORT NUMBER
TR.11-5725

9. SPONSORING/MONITORING AGENCY NAME(S) AND ADDRESS(ES)
Office of Naval Research
One Liberty Center
875 North Randolph St. Suite 1425
Arlington, Va 22203-1995

10. SPONSORING/MONITORING AGENCY REPORT NUMBER

10 SUPPLEMENTARY NOTES

12a. DISTRIBUTION/AVAILABILITY STATEMENT
Distribution Statement D: Distribution authorized to the Department of Defense and U.S. DoD contractors only; Critical Technology: 02 December 2011. Other Requests for this Document Shall be Referred to: Office of Naval Research Code 03T MT.

12b. DISTRIBUTION CODE

13. ABSTRACT *(Maximum 200 words)*

The objective of this project was to reduce cost and address cryostat configuration and manufacturing issues associated with fabricating long-length, flexible, vacuum-jacketed cryostats that meet Navy shipboard performance requirements. Ultimately, a U.S. manufacturing capability was to be developed by adapting processing techniques at an existing facility for manufacturing electrical conduit. The project was completed without meeting all the technical objectives for the project; a U.S. manufacturing capability was not developed. Southwire Company, the industry partner that was targeted as a U.S. supplier of these cryostats, returned a No-go decision to commit the capital needed to upgrade their manufacturing facility. However, the project did realize the following technical accomplishments: 1. A baseline cryostat insulation system was developed and validated via thermal performance testing, 2. The use of double aluminized Mylar® and polyester net for the reflector and spacer materials of the cryostat insulation system were shown to perform better than double aluminized Mylar® and polyester (non-woven) fabric. 3. Current technology available from an existing vendor has been identified for forming, welding and corrugating stainless steel sheet of the desired thickness ranges for the manufacture of HTSDG cryostats. Analyses have shown the technology will be able to produce corrugated tubing that meets application requirements, 4. Lessons learned during burst testing of commercially available corrugated tubing will improve upon future test specimen design and burst testing of actual HTSDG crostats to demonstrate required performance metrics. A follow-on project with another industry partner could easily leverage this work to its logical conclusion of a U.S. manufacturing capability for long-length cryostats. This project was developed as an upgrade for HTSDG cryostats focused on cost reduction and does not impact the availability of the HTSDG system to future LCS hulls.

14. SUBJECT TERMS
Degaussing, high temperature superconductors, superconductor, HTS, HTSDG, HTS DG, corrugated tubing, bellows, cryogenic piping, cryogenic, expansion joint, Expansion Joint Manufacturers Association, EJMA, Nexans, Southwire, cryostat.

15. NUMBER OF PAGES
320

16. PRICE CODE

17. SECURITY CLASSIFICATION OF REPORT	18. SECURITY CLASSIFICATION OF THIS PAGE	19. SECURITY CLASSIFICATION OF ABSTRACT	20. LIMITATION OF ABSTRACT
Unclassified	Unclassified	Unclassified	SAR

NSN 7540-01-280-5500

Standard Form 298 Rev. 12/00
Prescribed by ANSI ST. 239-18
880922